UNIVERSITY OF BIO-BIO
FACULTY OF SCIENCE
DEPARTMENT OF MATHEMATICS

TECHNICAL REPORT FOR PROJECT ANILLO ACT 210087 STATE OF THE ART AND PHYSICAL MODELS FOR THE DESALINATION PROCESS

BY

Nicolás Emilio Carro Aceituno

Project Director
Dr Ricardo Oyarzúa

Project Codirector
Dr. Verónica Anaya

Abril 2022
Concepción (Chile)

Summary

This document synthesises the basic aspects of two of the most promising desalination process, as well as the State of the Art (SoA) for the development of new technologies associated with the process energetic and productive efficiency and the different models used for Computational Fluid Dynamics (CFD) at the project Anillo ACT 210087.

Because the details and engineering aspects of each process are different, the present document is divided in various chapters corresponding to the different desalination methods and some of the common topics among the processes. The internal structure of each chapter will be similar: first, the process will be defined; second, the technical and physical-chemical aspects of the processs will be given, and finally the transport equations and boundary conditions for several models considered in this study will be presented.

Chapter 1

Transport Phenomena

This chapter condenses all the relevant equations of transport used to represent the desalination process along with the boundary conditions for each field. All of our derivations are balances of certain quantities over a generalized control volume such as the one shown in Figure 1.1.

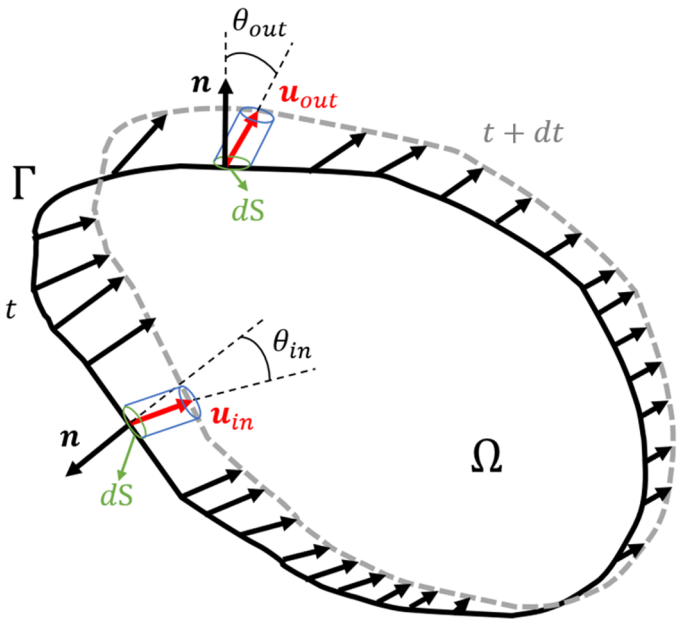

Figure 1.1: Graphical representation of an arbitrarily shaped control volume.

1.1 shows an arbitrarily fixed volume called Ω with an arbitrarily fixed control surface Γ evolving in time and space. The normal vectors $\boldsymbol{n}$ are defined as perpendicular and directed outward the control surface.

The governing equations of a system (let it be energy, mass, etc.) are focused on describing the evolution of its constituents (namely a single or collective of mass particles) along its time-space trajectory. This Lagrangian approach is computationally intensive for complex systems as it requires not only to store the coordinates and velocities of each system particle and evaluate its interactions, but also the coordinates of the discretization volumes that enclose each particle (a task not easily done for fluid systems). However we could, instead of focalizing in what happens to a certain system, describe what happens inside the volume that encloses the system, called the domain. This allows for an easier way of discretizing and evaluating numerically the equations involved in the system.

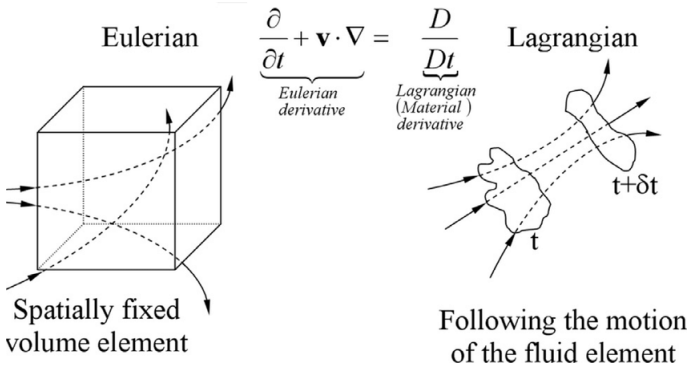

Figure 1.2: Comparison betwenn the Lagrangian and Eulerian approach. Source: Shadloo et al. (2016)

This method requires the conversion of the description of the properties from a particle centered analysis (Lagrangian approach) to a control volume analysis (Eulerian approach). In the following section, we present a theorem that allows us to accomplish such a task: Reynold's Transport Theorem.

1.1 Reynold's Transport Theorem (RTT)

Let us consider an extensive general property B (could be a scalar or vector) which characterizes the system under study, contained within a volume Ω and surface Γ as shown in Figure 1.1. The intensive property of B is $\beta = \beta(\boldsymbol{r}, t)$, i.e, the amount of the property B per unit mass in any small element of the control volume. If the density of any element in the control volume is $\rho = \rho(\boldsymbol{r}, t)$, then the relation between intensive and extensive property inside the control volume is:

$$\begin{aligned} B &= \int_\Omega \beta dm \\ &= \int_\Omega \beta\rho d\boldsymbol{r} \end{aligned} \tag{1.1}$$

Then,

$$\beta = \frac{dB}{dm} \tag{1.2}$$

The changes of B in the control volume then can occur from:

- A change of β within the control volume

$$\frac{d}{dt}\left(\int_\Omega \beta\rho d\boldsymbol{r}\right) \tag{1.3}$$

- A rate of β leaving the volume

$$\int_\Gamma \beta\rho u_{out}\cos\theta_{out} dS_{out} = \int_{\Gamma_{out}} \beta\rho\left(\boldsymbol{u}\cdot\boldsymbol{n}\right) dS \tag{1.4}$$

- A rate of β entering the volume

$$\int_\Gamma \beta\rho u_{in}\cos\theta_{in} dS_{in} = \int_{\Gamma_{in}} \beta\rho\left(-\boldsymbol{u}\cdot\boldsymbol{n}\right) dS \tag{1.5}$$

The minus sign appearing in the inlet term are due to the opposing definitions of $\boldsymbol{u}$ and $\boldsymbol{n}$ at the inlet: where a normal vector pointing outwards is positive, the entering velocity has the opposite direction. Then, if we take the limit where the change is infinitesimal $dt \to 0$, then the intantaneous change in B of the system is the change within, plus the leaving flow, minus the entering flow (as leaving flow has opposite direction of normal vector):

$$\frac{dB_{sys}}{dt} = \frac{d}{dt}\left(\int_\Omega \beta\rho d\boldsymbol{r}\right) + \int_{\Gamma_{out}} \beta\rho\left(\boldsymbol{u}\cdot\boldsymbol{n}\right) dS - \int_{\Gamma_{in}} \beta\rho\left(-\boldsymbol{u}\cdot\boldsymbol{n}\right) dS \tag{1.6}$$

If we consider that $\Gamma = \Gamma_{in} \cup \Gamma_{out}$, then we arrive at the final version of RTT for a fixed arbitrary control volume:

$$\frac{dB_{sys}}{dt} = \frac{d}{dt}\left(\int_{\Omega} \beta\rho d\boldsymbol{r}\right) + \int_{\Gamma} \beta\rho\left(\boldsymbol{u}\cdot\boldsymbol{n}\right) dS \tag{1.7}$$

For a volume moving at a velocity $\boldsymbol{u}_s = \boldsymbol{u}_s(\boldsymbol{r}, t)$, the RTT becomes

$$\frac{dB_{sys}}{dt} = \frac{d}{dt}\left(\int_{\Omega} \beta\rho d\boldsymbol{r}\right) + \int_{\Gamma} \beta\rho\left(\boldsymbol{u}_r\cdot\boldsymbol{n}\right) dS \tag{1.8}$$

where $\boldsymbol{u}_r = \boldsymbol{u} - \boldsymbol{u}_s$ is the relative velocity of the fluid with respect the volume reference.

1.2 Continuity Equation

1.2.1 Derivation

The continuity equation is the conservation of mass of a system over time. Then, if we define $B_{sys} = m$, $\beta = 1$. The conservation of mass implies that the change of the mass of the system is equal to the generation of mass minus its consumption, representing any reaction or process that generates or consumes mass (e.g. nuclear reactions, physical removal of mass, etc.). If we group both source terms per unit volume as a unique term S_m, it follows that:

$$\frac{dB_{sys}}{dt} = \int_{\Omega} S_m d\boldsymbol{r} \tag{1.9}$$

Then, replacing equation 1.8 in equation 1.2.1, we arrive at:

$$\frac{d}{dt}\left(\int_{\Omega} \rho d\boldsymbol{r}\right) + \int_{\Gamma} \rho\left(\boldsymbol{u}_r\cdot\boldsymbol{n}\right) dS = \int_{\Omega} S_m d\boldsymbol{r} \tag{1.10}$$

Applying the Gauss divergence theorem to the surface integral in equation 1.10, we arrive at

$$\frac{d}{dt}\left(\int_{\Omega} \rho d\boldsymbol{r}\right) + \int_{\Omega} \operatorname{div}\left(\rho\boldsymbol{u}_r\right) d\boldsymbol{r} = \int_{\Omega} S_m d\boldsymbol{r} \tag{1.11}$$

If we consider a fixed and stationary ($\boldsymbol{u}_r = \boldsymbol{u}$) control volume, the equation con be written as:

$$\int_{\Omega} \rho_t d\boldsymbol{r} + \int_{\Omega} \operatorname{div}\left(\rho\boldsymbol{u}\right) d\boldsymbol{r} = \int_{\Omega} S_m d\boldsymbol{r} \tag{1.12}$$

Where $\rho_t = \frac{d\rho}{dt}$. Finally, grouping the integrals into one and recognizing that for the equation to be valid the whole integrand must be zero, we arrive at the continuity equation:

$$\rho_t + \operatorname{div}\left(\rho\boldsymbol{u}\right) = S_m \tag{1.13}$$

If there is no nuclear reactions occuring or any physical removal of mass (that isn't convective), $S_m = 0$. Then, we have the classic continuity equation:

$$\rho_t + \operatorname{div}\left(\rho\boldsymbol{u}\right) = 0 \tag{1.14}$$

1.2.2 Formulations

Considering the general case where the medium density is defined as dependent on the field variables P (pressure), T (temperature) and C_i (concentration of each of the i species in the fluid) $\rho_* = \rho_*\left(t, T, P, C_i\right)$, the formulation is:

$$\rho_{*,t} + \operatorname{div}\left(\rho_*\boldsymbol{u}_*\right) = 0 \qquad *\ in\,\Omega_* \tag{1.15}$$

For a isotropic porous medium (a domain which is porous, and its porosity ε_* is constant and the same in all directions), the velocity $\boldsymbol{u}$ is replaced by an apparent velocity $\boldsymbol{u}_*/\varepsilon_*$, giving place to:

$$\rho_{*,t} + \operatorname{div}\left(\rho_*\frac{\boldsymbol{u}_*}{\varepsilon_*}\right) = 0 \qquad *\ in\,\Omega_* \tag{1.16}$$

If we consider the steady state (i.e., the calculated fields like density don't change with time anymore, or $\rho_t = 0$), equation 1.15 reduces to:

$$\operatorname{div}(\rho_* \boldsymbol{u}_*) = 0 \qquad * \; in \, \Omega_* \tag{1.17}$$

And equation 1.16 reduces to:

$$\operatorname{div}\left(\rho_* \frac{\boldsymbol{u}_*}{\varepsilon_*}\right) = 0 \qquad * \; in \, \Omega_* \tag{1.18}$$

If we further consider that the fluid is incompressible (i.e. the density is independent of other fields and has a constant value), then equation 1.17 reduces to:

$$\operatorname{div}(\boldsymbol{u}_*) = 0 \qquad * \; in \, \Omega_* \tag{1.19}$$

For a medium with constant porosity and incompressible fluid, equation 1.19 also reduces to equation 1.18.

1.3 Momentum Equation

For the momentum equation we start with Newton's Second Law, which is essentially a balance of forces acting over a system. Mathematically, for a system of momentum $(m\boldsymbol{u})_{sys}$ and forces acting over it F_i, $i = 1, ..., \infty$, we have:

$$\frac{d}{dt}(m\boldsymbol{u})_{sys} = \sum_i \boldsymbol{F}_i \tag{1.20}$$

Here, the forces acting over the system can be of different nature, e.g. gravitational, electromagnetic, etc. If we consider that the extensive quantity is the momentum $B = m\boldsymbol{u}$ (and therefore $\beta = \boldsymbol{u}$) a fixed and stationary control volume, applying the RTT yields

$$\int_\Omega (\rho \boldsymbol{u})_t \, d\boldsymbol{r} + \int_\Gamma \rho \boldsymbol{u} \, (\boldsymbol{u} \cdot \boldsymbol{n}) \, dS = \sum_i \boldsymbol{F}_i \tag{1.21}$$

Applying the asociative product rule, we can rewrite the previous expression as:

$$\int_\Omega (\rho \boldsymbol{u})_t \, d\boldsymbol{r} + \int_\Gamma (\rho \boldsymbol{u} \otimes \boldsymbol{u}) \cdot \boldsymbol{n} dS = \sum_i \boldsymbol{F}_i \tag{1.22}$$

Using the divergence theorem on the surface integral and combining the terms in the left hand side, we arrive at:

$$\int_\Omega \left((\rho \boldsymbol{u})_t + \operatorname{div}(\rho \boldsymbol{u} \otimes \boldsymbol{u}) \right) d\boldsymbol{r} = \sum_i \boldsymbol{F}_i \tag{1.23}$$

Which is the momentum balance for a fixed and stationary control volume. The different equations of momentum depend on the terms considered in the right hand side of the equation.

1.3.1 Derivation: Navier-Stokes

The Navier-Stokes equations are used to model the behavior of a fluid subject to two main forces: viscous momentum diffusion, external pressures exerted over the volume, and gravitational forces. We can include said forces as an integral over the surface of the domain:

$$\sum_i \boldsymbol{F}_i = \sum_i \int_\Gamma \frac{\partial \boldsymbol{F}_i}{\partial \boldsymbol{S}} \cdot \boldsymbol{n} dS + \sum_j \int_\Omega \frac{\partial \boldsymbol{F}_j}{\partial \boldsymbol{r}} d\boldsymbol{r} \tag{1.24}$$

Where the first term at the right hand side of equation 1.24 sums all forces that act on the control volume surface Γ, the second term sums all forces acting on the whole control volume due to external fields being applied (e.g. gravity or magnetic), $\frac{\partial \boldsymbol{F}_i}{\partial \boldsymbol{S}}$ is the force per unit area tensor applied to the control volume boundary Γ, and $\frac{\partial \boldsymbol{F}_j}{\partial \boldsymbol{r}}$ is the force per unite volume vector due to external fiedls applied to the fluid in Ω. This term has two components, a normal hydrostatic pressure term representing

external pressures applied to the volume, and a viscous stress tensor $\boldsymbol{\tau}$ responsible to represent the momentum losses due to the molecular friction of the fluid:

$$\frac{\partial \boldsymbol{F}_i}{\partial \boldsymbol{S}} = -P\boldsymbol{I} - \boldsymbol{\tau} \tag{1.25}$$

In the cases studied in this work, the only present field is gravity, so we have:

$$\frac{\partial \boldsymbol{F}_j}{\partial \boldsymbol{r}} = \rho \boldsymbol{g} \tag{1.26}$$

Replacing equations 1.24 and 1.26 in equation 1.24, we arrive at:

$$\sum_i \boldsymbol{F}_i = \int_\Gamma (-p\boldsymbol{I} - \boldsymbol{\tau}) \cdot \boldsymbol{n} dS + \int_\Omega \rho \boldsymbol{g} d\boldsymbol{r} \tag{1.27}$$

Once more, we apply the divergence theorem to the surface integral, and we merge the resulting volume integrals:

$$\begin{aligned} \sum_i \boldsymbol{F}_i &= \int_\Omega \left(\operatorname{div}(-p\boldsymbol{I} - \boldsymbol{\tau}) + \rho \boldsymbol{g}\right) d\boldsymbol{r} \\ &= \int_\Omega \left(-\nabla p + \operatorname{div}(-\boldsymbol{\tau}) + \rho \boldsymbol{g}\right) d\boldsymbol{r} \end{aligned} \tag{1.28}$$

Now we can merge expressions 1.23 and 1.28, arriving at

$$\int_\Omega \left((\rho \boldsymbol{u})_t + \operatorname{div}(\rho \boldsymbol{u} \otimes \boldsymbol{u}) + \nabla P - \operatorname{div}(-\boldsymbol{\tau}) - \rho \boldsymbol{g}\right) d\boldsymbol{r} = 0 \tag{1.29}$$

As the integral equal to zero requires that its integrand is zero, we arrive at Cauchy's equation:

$$(\rho \boldsymbol{u})_t + \operatorname{div}(\rho \boldsymbol{u} \otimes \boldsymbol{u}) = -\nabla P - \operatorname{div}(\boldsymbol{\tau}) + \rho \boldsymbol{g} \tag{1.30}$$

The last step is to use a relationship between tensor and the velocity and/or its moments. For a Newtonian fluid where there is a linear relation between the stress tensor and the velocity gradients:

$$\boldsymbol{\tau} = -\mu\left(\nabla \boldsymbol{u} + \nabla \boldsymbol{u}^T\right) + \left(\frac{2}{3}\mu - \kappa\right) \operatorname{div}(\boldsymbol{u}) \boldsymbol{I} \tag{1.31}$$

Applying the Stokes hypothesis, $\frac{2}{3}\mu - \kappa = 0$:

$$\boldsymbol{\tau} = \mu\left(\nabla \boldsymbol{u} + \nabla \boldsymbol{u}^T\right) \tag{1.32}$$

Then, the Navier-Stokes equation is:

$$(\rho \boldsymbol{u})_t + \operatorname{div}(\rho \boldsymbol{u} \otimes \boldsymbol{u}) = -\nabla P + \operatorname{div}\left(\mu\left(\nabla \boldsymbol{u} + \nabla \boldsymbol{u}^T\right)\right) + \rho \boldsymbol{g} \tag{1.33}$$

If the fluid is incompressible, the system reduces to:

$$\boldsymbol{u}_t + \operatorname{div}(\boldsymbol{u} \otimes \boldsymbol{u}) = -\nabla\left(\frac{P}{\rho}\right) + \operatorname{div}\left(\frac{\mu}{\rho}\left(\nabla \boldsymbol{u} + \nabla \boldsymbol{u}^T\right)\right) + \boldsymbol{g} \tag{1.34}$$

If we define the gauge pressure as $p = P - \rho g$, we can rewrite the equation as:

$$\boldsymbol{u}_t + \operatorname{div}(\boldsymbol{u} \otimes \boldsymbol{u}) = -\nabla\left(\frac{p}{\rho}\right) + \operatorname{div}\left(\frac{\mu}{\rho}\left(\nabla \boldsymbol{u} + \nabla \boldsymbol{u}^T\right)\right) \tag{1.35}$$

1.3.2 Derivation: Darcy-Forchheimer

The Darcy-Forchheimer equation is the inclusion of both Darcy's law and Forchheimer equation in the Navier-Stokes equations to model the pressure drop in an isotropic porous meida:

$$\nabla p_{darcy} = -\frac{\mu}{K}\boldsymbol{u} \tag{1.36}$$

$$\nabla p_{forchheimer} = -\frac{C_{frc}}{\sqrt{K}}|\boldsymbol{u}|\boldsymbol{u} \tag{1.37}$$

Considering that the total pressure drop on the volume is the sum of the porous media pressure p, the Darcy pressure p_{darcy} and the Forchheimer pressure $p_{forchheimer}$ contributions:

$$\nabla p_{total} = \nabla p + \nabla p_{darcy} + \nabla p_{forchheimer} \tag{1.38}$$

Also, the true velocity for the transient, convective and diffusive terms need to account the porosity ε of the medium. Replacing both of these assumptions, we arrive at:

$$\left(\rho\frac{\boldsymbol{u}}{\varepsilon}\right)_t + \operatorname{div}\left(\rho\frac{\boldsymbol{u}}{\varepsilon}\otimes\frac{\boldsymbol{u}}{\varepsilon}\right) = -\nabla P + \operatorname{div}\left(\mu\left(\nabla\frac{\boldsymbol{u}}{\varepsilon} + \nabla\frac{\boldsymbol{u}}{\varepsilon}^T\right)\right) - \frac{\mu}{K}\boldsymbol{u} - \frac{C_{frc}}{\sqrt{K}}|\boldsymbol{u}|\boldsymbol{u} + \rho\boldsymbol{g} \tag{1.39}$$

Note that the true velocity isn't used on the Darcy and Forchheimer terms, since these expressions already account the porosity of the medium. If we consider an incompressible fluid and the definition of the gauge pressure, we arrive at:

$$\left(\frac{\boldsymbol{u}}{\varepsilon}\right)_t + \operatorname{div}\left(\frac{\boldsymbol{u}}{\varepsilon}\otimes\frac{\boldsymbol{u}}{\varepsilon}\right) = -\nabla\left(\frac{p}{\rho}\right) + \operatorname{div}\left(\frac{\mu}{\rho}\left(\nabla\frac{\boldsymbol{u}}{\varepsilon} + \nabla\frac{\boldsymbol{u}}{\varepsilon}^T\right)\right) - \frac{\mu}{\rho K}\boldsymbol{u} - \frac{C_{frc}}{\rho\sqrt{K}}|\boldsymbol{u}|\boldsymbol{u} \tag{1.40}$$

1.4 Momentum: Boundary Conditions

1.4.1 No-slip boundary

The no slip-condition often is applied when the boundary is a wall in contact with the fluid. The physical meaning of this Dirichlet-type condition is the following: as the fluid molecules and the wall molecules interact, when the attractive forces between them outweigh the tangential stress applied by the fluid flow, the fluid molecules tend to "stick" to the wall, therefore diminishing its velocity to zero. The boundary is written as:

$$\boldsymbol{u}_* = \boldsymbol{0} \qquad in\ \Gamma_* \tag{1.41}$$

This condition holds for walls whose material is wetted by the fluid that flows on them.

1.4.2 Slip boundary

In some cases, the no-slip condition doesn't hold for all surfaces, as the pore presence (Beavers & Joseph, 1967) and the hydrophobicty of the surface tends to form a molecular floating film that reduces the shear stress of the fluid on the wall. Therefore the fluid slips on the surface, as if it were gliding across an icy surface.

Then, the boundary condition is given by:

$$\boldsymbol{u}_* = \boldsymbol{L}_{slip}\cdot(\boldsymbol{n}\cdot\nabla\boldsymbol{u}) \qquad in\ \Gamma_* \tag{1.42}$$

Where $\boldsymbol{L}_{slip}$ is the slip length vector for each coordinate, that can be interpreted as a displacement length of the zero velocity from the wall.

1.4.3 Set velocity profile boundary

For a fluid entering a domain, one can specify a value (or the complete inlet profile) if it is known. This corresponds then to a Dirichlet type boundary condition, and its written as:

$$\boldsymbol{u}_* = \boldsymbol{U}(\boldsymbol{r}, t) \qquad in\ \Gamma_* \tag{1.43}$$

Where $\boldsymbol{U}$ is the know velocity vector field at the boundary.

1.4.4 Set pressure boundary

Given an specified outlet pressure P_{out}, if we make a force balance on the boundary surface to obtain the pressure at the boundary,

$$\left(-P_*\boldsymbol{I} + \mu\left(\nabla \boldsymbol{u}_* + \nabla \boldsymbol{u}_*^T\right) - \frac{2}{3}\mu\left(\operatorname{div} \boldsymbol{u}_*\right)\boldsymbol{I}\right)\cdot \boldsymbol{n} = -P_{out}\boldsymbol{n} \qquad in\ \Gamma_* \tag{1.44}$$

Note that the above formulation is valid for single-phase flows. For incompressible flows, the previous expression reduces to:

$$\left(-P_*\boldsymbol{I} + \mu\left(\nabla \boldsymbol{u}_* + \nabla \boldsymbol{u}_*^T\right)\right)\cdot \boldsymbol{n} = -P_{out}\boldsymbol{n} \qquad in\ \Gamma_* \tag{1.45}$$

1.4.5 Reverse osmosis membrane boundary

When considering the membrane as a surface, a widely used model is the solution-diffussion model, which considers the water to "dissolve" in the membrane helped by the hydrogen bonds between water molecules and the membrane material, whilst blocking the passage of bigger salt ions. Lets consider the domain which contains the salt water as Ω, and the domain which contains the pure water as Ω_p.
Mathematically, the permeate flow for this model is expressed as an interface condition:

$$\boldsymbol{u}_f \cdot \boldsymbol{n} = \boldsymbol{u}_p \cdot \boldsymbol{n} \tag{1.46}$$
$$\boldsymbol{u}_f \cdot \boldsymbol{n} = A(p_f - p_p - iR(T_f C_f - T_p C_p)) \tag{1.47}$$

Where A is the membrane's water permeability, i is the number of ions that the salt dissociates into, R is the real gas constant, and C refers to the molar concentration of salt. If the experiment is conducted isothermically, then the condition can be written as

$$\boldsymbol{u}_f \cdot \boldsymbol{n} = \boldsymbol{u}_p \cdot \boldsymbol{n} \tag{1.48}$$
$$\boldsymbol{u}_f \cdot \boldsymbol{n} = A(p_f - p_p - iRT(C_f - C_p)) \tag{1.49}$$

As in reverse osmosis the pressures are high, the pressures changes inside either channel are low in comparison. Then, if we consider that the effect of this pressure change on the permeate flux is negligible, we can further simplify the expression as:

$$\boldsymbol{u}_f \cdot \boldsymbol{n} = \boldsymbol{u}_p \cdot \boldsymbol{n} \tag{1.50}$$
$$\boldsymbol{u}_f \cdot \boldsymbol{n} = A(\Delta p - iRT(C_f - C_p)) \tag{1.51}$$

Where $\Delta p = p_{f,in} - p_{p,in}$ is the transmembrane pressure. One last approximation is to neglect the permeate effects on the permeate flux, as $C_p \sim 0$. Additionally, we have to specify the tangential component of the velocity to give it closure (Kucera, 2015):

$$\boldsymbol{u}_f \cdot \boldsymbol{n} = A(\Delta p - iRTC_f) \tag{1.52}$$
$$\boldsymbol{u}_f \cdot \boldsymbol{t} = 0 \tag{1.53}$$

1.4.6 Porous membrane interface boundary

1.5 Turbulence Equations

Turbulence is a phenomena in which the fluid flow acts random and irregular. Of course, this chaotic nature makes it a naturally unsteady process. To locate at which velocity the system will experience turbulence, Reynolds (1883) INSERT introduced its number Re that upon reaching a critical value would indicate the transition of laminar to turbulent flow.
Richardson (1922) INSERT described turbulence as an erratic process in which, at a high enough velocity, turbulent swirls ("eddies") of all sizes begin to destabilize between them, and break down to the smallest scale possible to them, forming an eddie breakdown cascade downstream. Each eddy would have its own length, velocity and time scales, and the energy transfer would occur from the larger to the smaller eddies, until at the smallest eddy scale possible, energy would be dissipated as internal energy. Kolmogorov (1941) INSERT quantified the scale values at which the energy

dissipation would occur, assuming that anisotropy is lost along the eddy breakdown and the smaller eddies can be considered statistically isotropic. Additionaly, the forces dominating in this scale are considered mainly viscous, characterized by a molecular kinematic viscosity ν and an energy dissipation rate ϵ. Then, Kolmogorov's length, velocity and time scales η, u_η and τ_η are, respectively:

$$\eta = \left(\frac{\nu^3}{\epsilon}\right)^{1/4} \tag{1.54}$$

$$u_\eta = (\nu\epsilon)^{1/4} \tag{1.55}$$

$$\tau_\eta = \left(\frac{\nu}{\epsilon}\right)^{1/2} \tag{1.56}$$

On the other side of the scale spectrum, Kolmogorov assumed that at high enough Re there is a range of scales where the eddy breakdown is inviscidm and transfer energy to smaller eddies at a constant rate that is proportional to the larger scales. In this section, we will explain the reason why turbulence models are often used instead of the Navier-Stokes exact treatment of the equations as well as derive the set of equations for this, to then present the boundary conditions normally used for the turbulent equations.
The previous momentum equations are valid for all velocity ranges. However, there are two disadvantages that prevents us of using these:

- As the turbulence phenomena has a minimum scale length at which energy dissipates, even for large systems whose scales are kilometers, the scale is in the order of millimeters. Therefore, to model the turbulent scale at an adequate resolution, taking into account small length scales is needed.
- The iterative procedure requires that the time step advances at a reasonable pace, relying on the Courant number (Co) as an indicator:

$$Co = \sum_i \frac{U_i \Delta t}{\Delta x_i} \tag{1.57}$$

  Where U_i is the flow velocity in the i direction, Δt is the time step, and Δx_i is the characteristic length time of the cell in the i direction. The ideal condition is $Co \sim 1$, but as seen in the equation, to model higher velocities requires smaller time steps, which requires more computational effort.

Taking into account the previous indications to model turbulence using Navier-Stokes equation results in an unreal number of volume elements to be tracked over a huge amount of time steps, which is computationally unfeasible. There are different ways to solve this, but in this report we only use the Reynolds Averaged Navier-Stokes (RANS) equations, more specifically, a second-order approximation of these, called the $\kappa - \epsilon$ model.

1.5.1 Derivation: $\kappa - \epsilon$ model

The first step into deriving the equations is to obtain the main expression for the RANS model. As its name suggests, it stems from averaging the Navier-Stokes and Continuity equations, and its main equation is due to the decomposition of the velocity and pressure into two parts: a time-averaged mean term $\bar{\boldsymbol{u}}, \bar{P}$, and a fluctuating term $\boldsymbol{u}'$. This separation is known as Reynolds Decomposition:

$$\boldsymbol{u} = \bar{\boldsymbol{u}} + \boldsymbol{u}' \tag{1.58}$$

If we define the time average $\langle \boldsymbol{u} \rangle_t$ as

$$\bar{\boldsymbol{u}} = \langle \boldsymbol{u} \rangle_t = \lim_{T\to\infty} \frac{1}{T} \int_t^{t+T} \boldsymbol{u}(\boldsymbol{x}, t) dt \tag{1.59}$$

then

$$\bar{\boldsymbol{u}} = \bar{\bar{\boldsymbol{u}}} \rightarrow \bar{\boldsymbol{u}'} = \boldsymbol{0} \tag{1.60}$$

INSERT FIGURE
The thermophysical properties (density and viscosity) can also be decomposed into average and

fluctuating terms. However, additional closure relations for each new fluctuating term would be required. However, for weakly compressible fluids we can consider that its value is the average (i.e., the fluctuations in density and viscosity due to local turbulence are negligible):

$$\rho(\boldsymbol{x},t) = \bar{\rho}(\boldsymbol{x},t) \tag{1.61}$$
$$\mu(\boldsymbol{x},t) = \bar{\mu}(\boldsymbol{x},t) \tag{1.62}$$

From now on, we will use the symbol without the bar for both properties. Now, if we take Equation 1.14 and use it together with Equation 1.58, time-average it and rearrange it:

$$\begin{aligned}\rho_t + \operatorname{div}\left(\rho(\bar{\boldsymbol{u}} + \boldsymbol{u}')\right) = 0 &\rightarrow \bar{\rho}_t + \overline{\operatorname{div}\left(\rho(\bar{\boldsymbol{u}} + \boldsymbol{u}')\right)} = 0 \\ &\rightarrow \rho_t + \operatorname{div}\left(\rho(\overline{\bar{\boldsymbol{u}}} + \overline{\boldsymbol{u}'})\right) = 0 \\ &\rightarrow \rho_t + \operatorname{div}\left(\rho\bar{\boldsymbol{u}}\right) = 0\end{aligned} \tag{1.63}$$

In the second line of the equation, the distributive property of the divergence and in the third line, the properties in equation 1.60 were used. As it can be seen, the continuity equation mantains the same form as its original counterpart. In the case of the Navier-Stokes equations, we proceed in a similar way: we time average Equation 1.33, and obtain:

$$\overline{(\rho\boldsymbol{u})}_t + \operatorname{div}\overline{(\rho\boldsymbol{u}\otimes\boldsymbol{u})} = -\overline{\nabla P} + \operatorname{div}\overline{(\mu\left(\nabla\boldsymbol{u} + \nabla\boldsymbol{u}^T\right))} + \rho\boldsymbol{g} \tag{1.64}$$

Let's see each term:

$$\begin{aligned}\overline{(\rho\boldsymbol{u})}_t &= \overline{\left(\rho(\bar{\boldsymbol{u}} + \bar{\boldsymbol{u}'})\right)_t} \\ &= \left(\rho(\bar{\bar{\boldsymbol{u}}} + \bar{\boldsymbol{u}'})\right)_t \\ &= \left(\rho\bar{\boldsymbol{u}}\right)_t\end{aligned} \tag{1.65}$$

$$\begin{aligned}\operatorname{div}\overline{(\rho\boldsymbol{u}\otimes\boldsymbol{u})} &= \operatorname{div}\left(\overline{\rho(\boldsymbol{u}\otimes\boldsymbol{u})}\right) \\ &= \operatorname{div}\left(\rho(\overline{\bar{\boldsymbol{u}}\otimes\bar{\boldsymbol{u}}} + \overline{\bar{\boldsymbol{u}}\otimes\boldsymbol{u}'} + \overline{\boldsymbol{u}'\otimes\bar{\boldsymbol{u}}} + \overline{\boldsymbol{u}'\otimes\boldsymbol{u}'})\right) \\ &= \operatorname{div}\left(\rho(\bar{\boldsymbol{u}}\otimes\bar{\boldsymbol{u}} + \bar{\bar{\boldsymbol{u}}}\otimes\overline{\boldsymbol{u}'} + \overline{\boldsymbol{u}'}\otimes\bar{\bar{\boldsymbol{u}}} + \overline{\boldsymbol{u}'\otimes\boldsymbol{u}'})\right) \\ &= \operatorname{div}\left(\rho(\bar{\boldsymbol{u}}\otimes\bar{\boldsymbol{u}})\right) + \operatorname{div}\left(\rho(\overline{\boldsymbol{u}'\otimes\boldsymbol{u}'})\right)\end{aligned} \tag{1.66}$$

$$\begin{aligned}\operatorname{div}\overline{(\mu\left(\nabla\boldsymbol{u} + \nabla\boldsymbol{u}^T\right))} &= \operatorname{div}\left(\mu\overline{(\nabla\boldsymbol{u} + \nabla\boldsymbol{u}^T)}\right) \\ &= \operatorname{div}\left(\mu\left(\overline{\nabla\boldsymbol{u}} + \overline{\nabla\boldsymbol{u}}^T\right)\right) \\ &= \operatorname{div}\left(\mu\left(\nabla\bar{\boldsymbol{u}} + \nabla\bar{\boldsymbol{u}}^T\right)\right)\end{aligned} \tag{1.67}$$

$$-\overline{\nabla P} = -\nabla\overline{P} \tag{1.68}$$

Replacing the above expressions on Equation 1.64,

$$\left(\rho\bar{\boldsymbol{u}}\right)_t + \operatorname{div}\left(\rho(\bar{\boldsymbol{u}}\otimes\bar{\boldsymbol{u}})\right) + \operatorname{div}\left(\rho(\overline{\boldsymbol{u}'\otimes\boldsymbol{u}'})\right) = -\nabla\overline{P} + \operatorname{div}\left(\mu\left(\nabla\bar{\boldsymbol{u}} + \nabla\bar{\boldsymbol{u}}^T\right)\right) + \rho\boldsymbol{g} \tag{1.69}$$

Equation 1.69 is the formal equation of RANS. As it can be seen, it is almost the same as Equation 1.33 but an additional advective term appears due to the Reynolds decomposition. This extra term represents the turbulent advection. A common approximation to this term is separate its contributions into an isotropic advective term dependent on the turbulent kinetic energy κ, and a deviatronic term that still needs to be taken care of:

$$\begin{aligned}\bar{\boldsymbol{u}}\otimes\bar{\boldsymbol{u}} &= \frac{2}{3}\kappa\boldsymbol{I} + \boldsymbol{R}_{dev} \\ \boldsymbol{R}_{dev} &= \bar{\boldsymbol{u}}\otimes\bar{\boldsymbol{u}} - \frac{2}{3}\kappa\boldsymbol{I}\end{aligned} \tag{1.70}$$

A common way of treating the deviatronic term is to assume that it behaves similar to the Newtonian fluid viscous term, but with an associated turbulent viscosity μ_t. This is known as the Bousinnesq hypothesis:

$$\rho\boldsymbol{R}_{dev} = -\mu_t(\nabla\bar{\boldsymbol{u}} + \nabla\bar{\boldsymbol{u}}^T) \tag{1.71}$$

Inserting Equation 1.71 in Equation 1.69,

$$(\rho\bar{\boldsymbol{u}})_t + \operatorname{div}(\rho(\bar{\boldsymbol{u}} \otimes \bar{\boldsymbol{u}})) = -\nabla\overline{P} + \operatorname{div}\left((\mu + \mu_t)\left(\nabla\overline{\boldsymbol{u}} + \nabla\overline{\boldsymbol{u}}^T\right)\right) + \frac{2}{3}\rho\kappa\boldsymbol{I} + \rho\boldsymbol{g} \tag{1.72}$$

Defining the pressure here as $\bar{P}_{tr} = \bar{P} + \frac{2}{3}\kappa$, we arrive at the RANS equation:

$$(\rho\bar{\boldsymbol{u}})_t + \operatorname{div}(\rho(\bar{\boldsymbol{u}} \otimes \bar{\boldsymbol{u}})) = -\nabla\overline{P}_{tr} + \operatorname{div}\left((\mu + \mu_t(\kappa,\epsilon))\left(\nabla\overline{\boldsymbol{u}} + \nabla\overline{\boldsymbol{u}}^T\right)\right) + \rho\boldsymbol{g} \tag{1.73}$$

$$\mu_t(\kappa,\epsilon) = \rho C_\mu \frac{\kappa^2}{\epsilon} \tag{1.74}$$

In Equation 1.73, the dependence of μ_t is established: according to the model, the dependence is on both the turbulent kinetic energy κ (not to be confused with the kinetic energy κ used in the following section), and the turbulent dissipative energy ϵ, both defined as

$$\kappa = \frac{1}{2}\overline{\boldsymbol{u}' \cdot \boldsymbol{u}'} \tag{1.75}$$

$$\epsilon = \nu\overline{|\nabla\boldsymbol{u}'|^2} \tag{1.76}$$

Both definitions introduce new variables that need additional equations to be solved. For the $\kappa - \epsilon$ model, this involves two additional partial differential equations, one for each new variable. Normally the procedure to derive the respective equations, we start with the partial differential equations of the variables $\kappa = \frac{1}{2}\boldsymbol{u} \cdot \boldsymbol{u}$ and $\epsilon = \nu|\nabla\boldsymbol{u}|^2$ (which can be derived from the Navier-Stokes equations, as will be demonstrated for κ in the following section) and proceed exactly like it was done with the RANS equation: time average the equations, and separate the mean and variable terms.
Since the averaging procedure generates a new variable that needs to be known for the system to have closure, this process can be repeated as many times as desired, but this model focuses on the first two orders of approximation, closing the expression for the ϵ differential equation. The goal of this chapter is not to derive these equations as there are long and tedious to obtain. The final expression for both differential equations that close the model are:

$$(\rho\kappa)_t + \bar{\boldsymbol{u}} \cdot \nabla(\rho\kappa) = \operatorname{div}\left(\left(\mu + \frac{\mu_t(\kappa,\epsilon)}{\sigma_k}\right)\nabla\kappa\right) + P_\kappa - \rho\epsilon \tag{1.77}$$

$$(\rho\epsilon)_t + \bar{\boldsymbol{u}} \cdot \nabla(\rho\epsilon) = \operatorname{div}\left(\left(\mu + \frac{\mu_t(\kappa,\epsilon)}{\sigma_k}\right)\nabla\epsilon\right) + \frac{C_1\epsilon}{\kappa}P_\kappa - \frac{C_2}{\kappa^2}\rho\epsilon^2 \tag{1.78}$$

$$P_\kappa = \mu_t(\kappa,\epsilon)\left(\nabla\overline{\boldsymbol{u}} : (\nabla\overline{\boldsymbol{u}} + \nabla\overline{\boldsymbol{u}}^t) - \frac{2}{3}(\operatorname{div}(\bar{\boldsymbol{u}}))^2\right) - \frac{2}{3}\rho\kappa\operatorname{div}(\bar{\boldsymbol{u}}) \tag{1.79}$$

1.6 Turbulence: Boundary Conditions

1.6.1 Inlet boundary

For the inlet, the boundary conditions are Dirichlet-type functions:

$$a \tag{1.80}$$

$$a \tag{1.81}$$

Normally, depending on the type of inlet flow, there are different functions. In the case of a developed tubulent flow on a pipe, the functions are:

1.6.2 Free-flow boundary

When a fluid has developed its flow enough, the change in dissipative and kinetic energy due to turbulence remains constant. Then, the boundary conditions can be written as a von-Neumann type boundary:

$$\nabla\kappa \cdot \boldsymbol{n} = 0 \tag{1.82}$$

$$\nabla\epsilon \cdot \boldsymbol{n} = 0 \tag{1.83}$$

Where k is the thermal conductivity.

1.6.3 Wall boundary

law of the wall

1.7 Heat Equation

1.7.1 Derivation

The heat equation starts with the conservation of energy for a system. From the first law of thermodynamics for a system, we have:

$$dE_{sys} = dW + dQ \tag{1.84}$$

Where E_{sys} is the energy of the system, W is the work done over the system at the boundaries, and Q is the heat that enters the system through the boundaries. Taking the time derivative of the system,

$$\frac{dE_{sys}}{dt} = \frac{dW}{dt} + \frac{dQ}{dt} = \dot{W} + \dot{Q} \tag{1.85}$$

Identifying the observed variable as $B = E$ with its respective intensive variable $\beta = e = dE/dm$ or energy per unit mass, we can apply RTT to the left side of the equation, arriving at the balance for the specific volume of Figure 1:

$$\frac{d}{dt}\left(\int_{\Omega} e\rho d\boldsymbol{r}\right) + \int_{\Gamma} e\rho\left(\boldsymbol{u}\cdot\boldsymbol{n}\right)dS = \dot{W} + \dot{Q} \tag{1.86}$$

The energy is composed of several contributions:

$$e = e_{internal} + e_{kinetic} + e_{potential} + e_{other} \tag{1.87}$$

Considering only the three first terms in the previous equation and replacing the corresponding expressions for each contribution,

$$e = \hat{u} + \frac{1}{2}(\boldsymbol{u}\cdot\boldsymbol{u}) + \boldsymbol{g}\cdot\boldsymbol{r} = \hat{u} + \kappa + e_p \tag{1.88}$$

For the work done on the fluid, we have two contributions for a fluid moving in a system without mechanical parts impulsating them: the work done by pressure forces over Γ and the work due to viscous stresses over Γ, denoted $\dot{W}_p$ and $\dot{W}_v$:

$$\dot{W} = \dot{W}_p + \dot{W}_v \tag{1.89}$$

Taking the work differential for $\dot{W}_p$,

$$\begin{aligned} d\dot{W}_p &= \boldsymbol{F}\cdot\frac{d\boldsymbol{x}}{dt} \\ &= -Pd\boldsymbol{S}\cdot\boldsymbol{u} \\ &= -P(\boldsymbol{u}\cdot\boldsymbol{n})dS \\ &= -P(\boldsymbol{u}\cdot\boldsymbol{n})dS \end{aligned} \tag{1.90}$$

In the first equation, the definition of work is used. In the second equation, the differential relation between the pressure and the force is applied. Integrating the expression over Γ,

$$\dot{W}_p = -\int_{\Gamma} P(\boldsymbol{u}\cdot\boldsymbol{n})dS \tag{1.91}$$

The viscous stress $\dot{W}_v$ we have the following relation:

$$\dot{W}_v = -\int_{\Gamma} (\boldsymbol{\tau}\cdot\boldsymbol{u})\cdot\boldsymbol{n}dS \tag{1.92}$$

In case of the transported heat at Γ, we first write it in terms of the heat flux per unit area $\boldsymbol{q}$

$$\begin{aligned} \dot{Q} &= \int_{\Gamma} -\boldsymbol{q}\cdot d\boldsymbol{S} \\ &= -\int_{\Gamma} \boldsymbol{q}\cdot\boldsymbol{n}dS \end{aligned} \tag{1.93}$$

Then, if the fluid (or solid) in the system has a linear dependence between $\boldsymbol{q}$ and ∇T, we can use Fourier's Law:

$$\boldsymbol{q} = -k\nabla T \tag{1.94}$$

Then, we can replace the obtained expressions on the energy balance:

$$\frac{d}{dt}\left(\int_\Omega e\rho d\boldsymbol{r}\right) + \int_\Gamma e\rho\left(\boldsymbol{u}\cdot\boldsymbol{n}\right)dS = -\int_\Gamma P(\boldsymbol{u}\cdot\boldsymbol{n})dS - \int_\Gamma(\boldsymbol{\tau}\cdot\boldsymbol{u})\cdot\boldsymbol{n}dS - \int_\Gamma \boldsymbol{q}\cdot\boldsymbol{n}dS \tag{1.95}$$

Using the divergence theorem on the surface integrals,

$$\frac{d}{dt}\left(\int_\Omega e\rho d\boldsymbol{r}\right) + \int_\Omega \mathrm{div}\left(\rho e\boldsymbol{u}\right)d\boldsymbol{r} = -\int_\Omega \mathrm{div}\left(P\boldsymbol{u}\right)d\boldsymbol{r} - \int_\Omega \mathrm{div}(\boldsymbol{\tau}\cdot\boldsymbol{u})d\boldsymbol{r} - \int_\Omega \mathrm{div}\left(-k\nabla T\right)d\boldsymbol{r} \tag{1.96}$$

Considering a fixed control volume and using the divergence theorem on the surface integrals,

$$\begin{aligned}&\int_\Omega (e\rho)_t d\boldsymbol{r} + \int_\Omega \mathrm{div}\left(\rho e\boldsymbol{u}\right)d\boldsymbol{r}\\ &= -\int_\Omega \mathrm{div}\left(P\boldsymbol{u}\right)d\boldsymbol{r} - \int_\Omega \mathrm{div}(\boldsymbol{\tau}\cdot\boldsymbol{u})d\boldsymbol{r} - \int_\Omega \mathrm{div}\left(-k\nabla T\right)d\boldsymbol{r}\end{aligned} \tag{1.97}$$

Replacing e in the equations, we arrive at,

$$\begin{aligned}&\int_\Omega ((\hat{u}+\kappa+e_p)\rho)_t d\boldsymbol{r} + \int_\Omega \mathrm{div}\left(\rho(\hat{u}+\kappa+e_p)\boldsymbol{u}\right)d\boldsymbol{r}\\ &= -\int_\Omega \mathrm{div}\left(P\boldsymbol{u}\right)d\boldsymbol{r} - \int_\Omega \mathrm{div}(\boldsymbol{\tau}\cdot\boldsymbol{u})d\boldsymbol{r} - \int_\Omega \mathrm{div}\left(-k\nabla T\right)d\boldsymbol{r}\end{aligned} \tag{1.98}$$

Separating the kinetic and potential energy terms, we obtain

$$\begin{aligned}&\int_\Omega (\hat{u}\rho)_t d\boldsymbol{r} + \int_\Omega \mathrm{div}\left(\rho\hat{u}\boldsymbol{u}\right)d\boldsymbol{r} + \int_\Omega \mathrm{div}\left(P\boldsymbol{u}\right)d\boldsymbol{r}\\ &= -\int_\Omega \mathrm{div}(\boldsymbol{\tau})d\boldsymbol{r} - \int_\Omega \mathrm{div}\left(-k\nabla T\right)d\boldsymbol{r} - \int_\Omega \left((\rho\kappa)_t + \mathrm{div}\left(\rho\kappa\boldsymbol{u}\right)\right)d\boldsymbol{r} - \int_\Omega \left((\rho e_p)_t + \mathrm{div}\left(\rho e_p\boldsymbol{u}\right)\right)d\boldsymbol{r}\end{aligned} \tag{1.99}$$

Here, we introduce two definitions: the enthalpy $\hat{h}$ and the energy source term S_κ:

$$\begin{aligned}\hat{h} &= \hat{u} + \frac{P}{\rho}\\ S_e &= (\rho\kappa)_t + \mathrm{div}\left(\rho\kappa\boldsymbol{u}\right) + (\rho e_p)_t + \mathrm{div}\left(\rho e_p\boldsymbol{u}\right)\\ &= (\rho\kappa)_t + \mathrm{div}\left(\rho\kappa\boldsymbol{u}\right) + \rho_t e_p + \rho e_{p,t} + \rho\boldsymbol{u}\nabla(e_p) + e_p\mathrm{div}(\rho\boldsymbol{u})\\ &= (\rho\kappa)_t + \mathrm{div}\left(\rho\kappa\boldsymbol{u}\right) + (\rho_t + \mathrm{div}(\rho\boldsymbol{u}))e_p + \rho e_{p,t} + \rho\boldsymbol{u}\cdot\nabla(e_p)\\ &= (\rho\kappa)_t + \mathrm{div}\left(\rho\kappa\boldsymbol{u}\right) + \rho(\boldsymbol{g}\cdot\boldsymbol{r})_t + \rho\boldsymbol{u}\cdot\nabla(\boldsymbol{g}\cdot\boldsymbol{r})\\ &= (\rho\kappa)_t + \mathrm{div}\left(\rho\kappa\boldsymbol{u}\right) + \rho\boldsymbol{g}\cdot\boldsymbol{u} + \rho\boldsymbol{u}\cdot\boldsymbol{g}\end{aligned} \tag{1.100}$$

Replacing the definitions, we arrive at:

$$\begin{aligned}&\int_\Omega (\hat{u}\rho)_t d\boldsymbol{r} + \int_\Omega \mathrm{div}\left(\rho\boldsymbol{u}\hat{h}\right)d\boldsymbol{r}\\ &= -\int_\Omega \mathrm{div}(\boldsymbol{\tau}\cdot\boldsymbol{u})d\boldsymbol{r} + \int_\Omega \mathrm{div}\left(k\nabla T\right)d\boldsymbol{r} - \int_\Omega S_e d\boldsymbol{r}\end{aligned} \tag{1.101}$$

Or,

$$(\hat{u}\rho)_t + \mathrm{div}\left(\rho\boldsymbol{u}\hat{h}\right) = -\mathrm{div}(\boldsymbol{\tau}\cdot\boldsymbol{u}) + \mathrm{div}\left(k\nabla T\right) - S_e \tag{1.102}$$

To obtain an expression for S_e, we need an equation that describes the evolution of the new variable κ. This equation can be derived from the momentum balance as we will show. First, lets us recast the equation into a different form for mathematical convenience:

$$\rho_t\boldsymbol{u} + \rho\boldsymbol{u}_t + \mathrm{div}\left(\rho\boldsymbol{u}\right)\boldsymbol{u} + \left(\rho\boldsymbol{u}\cdot\nabla\right)\boldsymbol{u} = -\nabla P - \mathrm{div}\left(\boldsymbol{\tau}\right) + \rho\boldsymbol{g} \tag{1.103}$$

The only operation done was to expand the transient and the advective terms. Grouping similar terms, we arrive at:

$$\left(\rho_t + \operatorname{div}\left(\rho \boldsymbol{u}\right)\right)\boldsymbol{u} + \rho \boldsymbol{u}_t + \left(\rho \boldsymbol{u} \cdot \nabla\right)\boldsymbol{u} = -\nabla P - \operatorname{div}\left(\boldsymbol{\tau}\right) + \rho \boldsymbol{g} \tag{1.104}$$

As the first term in parenthesis is zero due to the continuity equation, we arrive at the equivalent form of the momentum equation:

$$\rho \boldsymbol{u}_t + \left(\rho \boldsymbol{u} \cdot \nabla\right)\boldsymbol{u} = -\nabla P - \operatorname{div}\left(\boldsymbol{\tau}\right) + \rho \boldsymbol{g} \tag{1.105}$$

If we multiply the whole equation by $\boldsymbol{u}$, we have:

$$\boldsymbol{u} \cdot \rho \boldsymbol{u}_t + \boldsymbol{u} \cdot \left(\rho \boldsymbol{u} \cdot \nabla\right)\boldsymbol{u} = -\boldsymbol{u} \cdot \nabla P - \boldsymbol{u} \cdot \operatorname{div}\left(\boldsymbol{\tau}\right) + \boldsymbol{u} \cdot \rho \boldsymbol{g} \tag{1.106}$$

Noting that:

$$\begin{aligned}
(\rho\kappa)_t &= \left(\rho \frac{(\boldsymbol{u} \cdot \boldsymbol{u})}{2}\right)_t \\
&= \frac{1}{2}\left(\rho(\boldsymbol{u} \cdot \boldsymbol{u})_t + \rho_t(\boldsymbol{u} \cdot \boldsymbol{u})\right) \\
&= \frac{1}{2}\left(2\rho \boldsymbol{u} \cdot \boldsymbol{u}_t + \rho_t(\boldsymbol{u} \cdot \boldsymbol{u})\right) \\
&= \rho \boldsymbol{u} \cdot \boldsymbol{u}_t + \rho_t \left(\frac{\boldsymbol{u} \cdot \boldsymbol{u}}{2}\right) \\
&= \rho \boldsymbol{u} \cdot \boldsymbol{u}_t + \rho_t \kappa \\
&= \rho \boldsymbol{u} \cdot \boldsymbol{u}_t + (-\operatorname{div}(\rho \boldsymbol{u}))\kappa \\
\rightarrow \rho \boldsymbol{u} \cdot \boldsymbol{u}_t &= (\rho\kappa)_t + \operatorname{div}(\rho \boldsymbol{u})\kappa
\end{aligned} \tag{1.107}$$

As well as:

$$\begin{aligned}
(\rho \boldsymbol{u} \cdot \nabla)(\boldsymbol{u} \cdot \boldsymbol{u}) &= [(\rho \boldsymbol{u} \cdot \nabla)\boldsymbol{u}] \cdot \boldsymbol{u} + \boldsymbol{u} \cdot [(\rho \boldsymbol{u} \cdot \nabla)\boldsymbol{u}] \\
&= 2\boldsymbol{u} \cdot (\rho \boldsymbol{u} \cdot \nabla)\boldsymbol{u} \\
\rightarrow \boldsymbol{u} \cdot (\rho \boldsymbol{u} \cdot \nabla)\boldsymbol{u} &= (\rho \boldsymbol{u} \cdot \nabla)\left(\frac{\boldsymbol{u} \cdot \boldsymbol{u}}{2}\right) = (\rho \boldsymbol{u} \cdot \nabla)\kappa
\end{aligned} \tag{1.108}$$

Then, we can write the momentum balance as:

$$(\rho\kappa)_t + \operatorname{div}(\rho \boldsymbol{u})\kappa + (\rho \boldsymbol{u} \cdot \nabla)\kappa = -\boldsymbol{u} \cdot \nabla P - \boldsymbol{u} \cdot \operatorname{div}\left(\boldsymbol{\tau}\right) + \boldsymbol{u} \cdot \rho \boldsymbol{g} \tag{1.109}$$

Or

$$(\rho\kappa)_t + \operatorname{div}(\rho \boldsymbol{u}\kappa) = -\boldsymbol{u} \cdot \nabla P - \boldsymbol{u} \cdot \operatorname{div}\left(\boldsymbol{\tau}\right) + \boldsymbol{u} \cdot \rho \boldsymbol{g} \tag{1.110}$$

We can also state that:

$$\begin{aligned}
\operatorname{div}(\boldsymbol{\tau} \cdot \boldsymbol{u}) &= \boldsymbol{\tau} : \nabla \boldsymbol{u} + \boldsymbol{u} \cdot \operatorname{div}(\boldsymbol{\tau}) \\
&= \Phi + \boldsymbol{u} \cdot \operatorname{div}(\boldsymbol{\tau}) \\
&= \Phi - (\rho\kappa)_t - \operatorname{div}(\rho \boldsymbol{u}\kappa) - \boldsymbol{u} \cdot \nabla P + \boldsymbol{u} \cdot \rho \boldsymbol{g} \\
&= \Phi - S_e - \boldsymbol{u} \cdot \nabla P
\end{aligned} \tag{1.111}$$

Where Φ is defined as the viscous dissipation function. Finally, we obtain the general heat equation:

$$(\hat{u}\rho)_t + \operatorname{div}\left(\rho \boldsymbol{u}\hat{h}\right) = \boldsymbol{u} \cdot \nabla P + \operatorname{div}\left(k \nabla T\right) - \Phi \tag{1.112}$$

We can further replace the internal energy with the enthalpy definition, and obtain a expression only dependent on the enthalpy:

$$(\hat{h}\rho)_t + \operatorname{div}\left(\rho \boldsymbol{u}\hat{h}\right) = P_t + \boldsymbol{u} \cdot \nabla P + \operatorname{div}\left(k \nabla T\right) - \Phi \tag{1.113}$$

If we consider the system to be in steady state, the equation reduces to:

$$\operatorname{div}\left(\rho \boldsymbol{u}\hat{h}\right) = \boldsymbol{u} \cdot \nabla P + \operatorname{div}\left(k \nabla T\right) - \Phi \tag{1.114}$$

$$\operatorname{div}\left(\rho \boldsymbol{u}\hat{h}\right) = \boldsymbol{u}\cdot\nabla P + \operatorname{div}\left(k\nabla T\right) - \Phi \tag{1.115}$$

Furthermore, we can express the enthalpy of a fluid in terms of its temperature and density with respect a reference state as:

$$\hat{h} - \hat{h}_0 = \int_{T_0}^{T} \hat{C}_p dT + \int_{p_0}^{p} \left(\frac{\partial \ln \rho}{\partial \ln T}\right)_p dp \tag{1.116}$$

For an ideal gas (or incompressible fluid), the expression can be written as:

$$\hat{h} - \hat{h}_0 = \int_{T_0}^{T} \hat{C}_p dT + \frac{p - p_0}{\rho} \tag{1.117}$$

Replacing the previous expression in the heat balance, and remembering that for an incompressible fluid $\operatorname{div}(\boldsymbol{u}) = 0$, we arrive at:

$$\rho\boldsymbol{u}\cdot\nabla\left(\int_{T_0}^{T}\hat{C}_p dT\right) = \operatorname{div}\left(k\nabla T\right) - \Phi$$

$$\rho\boldsymbol{u}\left(\hat{C}_p(T) - \hat{C}_p(T_0)\right)\cdot\nabla T = \operatorname{div}\left(k\nabla T\right) - \Phi \tag{1.118}$$

As the reference temperature is chosen such as $\hat{C}_p(T_0) = 0$, we arrive at:

$$\rho\boldsymbol{u}\hat{C}_p(T)\cdot\nabla T = \operatorname{div}\left(k\nabla T\right) - \Phi \tag{1.119}$$

For fluids that don't have high velocity gradients, we can make the assumption that $\Phi = 0$, we obtain the classic heat equation in its convection-difussion format:

$$\rho\hat{C}_p(T)\boldsymbol{u}\cdot\nabla T = \operatorname{div}\left(k\nabla T\right) \tag{1.120}$$

1.8 Heat: Boundary Conditions

1.8.1 Set temperature boundary

If we have a boundary in contact with an element at a constant temperature (e.g., evaporating water or a block of ice) or we have a temperature whose dependence in time and space is known beforehand, then the condition describing it is a Dirichlet type boundary:

$$T_* = T_D(\boldsymbol{r}, t) \tag{1.121}$$

1.8.2 Outflow boundary

When a fluid has developed its flow enough, the conductive heat along the flow is almost zero, i.e. the heat transport is only carried out by convection. Then, if the diffusive flux obeys Fourier's Law, the boundary condition can be written as a von-Neumann type boundary:

$$-k\nabla T_*\cdot\boldsymbol{n} = 0 \tag{1.122}$$

Where k is the thermal conductivity.

1.8.3 Heat source boundary

If the boundary has a heating (or cooling) element that provides (or extracts) heat at a known rate, the boundary condition for the surface in contact with the element is:

$$(\rho_*\hat{C}_{p*}T_*\boldsymbol{u}_* - k\nabla T_*)\cdot\boldsymbol{n} = q_D(\boldsymbol{r}, t) \tag{1.123}$$

1.8.4 Insulated wall boundary

If the wall is fully insulated, there is no convertive or diffusive heat flux traversing the boundary, so the boundary can be written as a Robin type condition:

$$(\rho_*\hat{C}_{p,*}T_*\boldsymbol{u}_* - k\nabla T_*)\cdot\boldsymbol{n} = 0 \tag{1.124}$$

If the wall is impermeable to the fluid and the no-slip condition for the velocity is applied, then equation 1.124 reduces to equation 1.122.

1.8.5 Continuity of temperature at an interface

In the case of two domains in contact, if the boundary is not physical (i.e., the boundary is an imaginary surface) a possibility is that the temperature across it is the same for both domains. If both sides of the boundary are denoted by T_{*+} and T_{*-},

$$T_{*+} = T_{*-} \tag{1.125}$$

1.8.6 Heat balance at an interface

In the case of two domains in contact, if the boundary is physical (i.e., the boundary is an obstacle between both domains) the heat between boundaries must be conserved. If the heat at both sides of the boundary are denoted by $\boldsymbol{q}_{*+}$ and $\boldsymbol{q}_{*-}$, then (Incropera & DeWitt, 1999)

$$\boldsymbol{q}_{*+} \cdot \boldsymbol{n} = \boldsymbol{q}_{*-} \cdot \boldsymbol{n} \tag{1.126}$$

1.9 Species Transport Equation

1.9.1 Derivation

In this case, the observed extensive quantity is the mass $B = m_i$ of a certain species i. The fundamental law governing the system is the conservation of species i. Taking as reference Figure 1, the law is given by the following equation:

$$accumulation\,in\,\Omega = enters\,at\,\Gamma - leaves\,at\,\Gamma + generates\,at\,\Omega - consumes\,at\,\Omega \tag{1.127}$$

Which can be written in mathematical notation as:

$$\frac{dm_{i,sys}}{dt} = -\sum_{j,i\neq j}^{c} \int_{\Gamma} \frac{\partial \dot{m}_{ij}}{\partial \boldsymbol{S}} \cdot \boldsymbol{n} dS + \sum_{j}^{rxn} \int_{\Omega} \frac{\partial \dot{m}_{ij}}{\partial \boldsymbol{r}} d\boldsymbol{r} \tag{1.128}$$

Where the first summation is done over al components of the fluid except component i, and the second summation is done over all reactions occuring at the system. Therefore, $\frac{\partial \dot{m}_{ij}}{\partial \boldsymbol{S}}$ refers to the flux of i leaving the volume through Γ due to the component j, and $\frac{\partial \dot{m}_{ij}}{\partial \boldsymbol{r}}$ is the reaction rate of component i in the reaction j.
If we define the mass fraction of the component as $w_i = m_i/m$, then we can define the intensive property as $\beta = w_i$, so the RTT for the observed variable is:

$$\frac{dm_{i,sys}}{dt} = \frac{d}{dt} \int_{\Omega} w_i \rho d\boldsymbol{r} + \int_{\Gamma} \rho w_i (\boldsymbol{u} \cdot \boldsymbol{n}) dS \tag{1.129}$$

For a fixed volume and applying the divergence theorem,

$$\frac{dm_{i,sys}}{dt} = \int_{\Omega} (w_i \rho)_t d\boldsymbol{r} + \int_{\Omega} \mathrm{div}(\rho \boldsymbol{u} w_i) d\boldsymbol{r} \tag{1.130}$$

Replacing this in the component balance,

$$\int_{\Omega} (w_i \rho)_t d\boldsymbol{r} + \int_{\Omega} \mathrm{div}(\rho \boldsymbol{u} w_i) d\boldsymbol{r} = -\sum_{j,i\neq j}^{c} \int_{\Gamma} \frac{\partial \dot{m}_{ij}}{\partial \boldsymbol{S}} \cdot \boldsymbol{n} dS + \sum_{j}^{rxn} \int_{\Omega} \frac{\partial \dot{m}_{ij}}{\partial \boldsymbol{r}} d\boldsymbol{r} \tag{1.131}$$

We can apply the divergence theorem to the first term in the right hand side as well as reordering the summation with the integral to get:

$$\int_{\Omega} (w_i \rho)_t d\boldsymbol{r} + \int_{\Omega} \mathrm{div}(\rho \boldsymbol{u} w_i) d\boldsymbol{r} = -\int_{\Omega} \sum_{j,i\neq j}^{c} \mathrm{div} \left(\frac{\partial \dot{m}_{ij}}{\partial \boldsymbol{S}} \right) d\boldsymbol{r} + \int_{\Omega} \sum_{j}^{rxn} \frac{\partial \dot{m}_{ij}}{\partial \boldsymbol{r}} d\boldsymbol{r} \tag{1.132}$$

If there is no reaction occuring in the system, then $\frac{\partial \dot{m}_{ij}}{\partial \boldsymbol{r}} = 0$, and the system reduces to:

$$\int_{\Omega} (w_i \rho)_t d\boldsymbol{r} + \int_{\Omega} \mathrm{div}(\rho \boldsymbol{u} w_i) d\boldsymbol{r} = -\int_{\Omega} \sum_{j,i\neq j}^{c} \mathrm{div} \left(\frac{\partial \dot{m}_{ij}}{\partial \boldsymbol{S}} \right) d\boldsymbol{r} \tag{1.133}$$

Furthermore, if the only form of transport through the boundaries is through molecular diffusion, and the relation between the mass flux and the mass concentration gradient is linear, the flux is modelled by Fick's law:

$$\frac{\partial \dot{m}_{ij}}{\partial \boldsymbol{S}} = \boldsymbol{J}_{ij} = -D_{ij}\nabla\left(C_i\right) = -D_{ij}\nabla\left(\rho w_i\right) \tag{1.134}$$

Replacing this expression in the component balance, we have:

$$\int_\Omega (w_i\rho)_t d\boldsymbol{r} + \int_\Omega \operatorname{div}(\rho \boldsymbol{u} w_i) d\boldsymbol{r} = \int_\Omega \sum_{j,i\neq j}^{c} \operatorname{div}\left(D_{ij}\nabla\left(\rho w_i\right)\right) d\boldsymbol{r} \tag{1.135}$$

Finally, we obtain the differential balance of the system:

$$(w_i\rho)_t + \operatorname{div}(\rho \boldsymbol{u} w_i) = \sum_{j,i\neq j}^{c} \operatorname{div}\left(D_{ij}\nabla\left(\rho w_i\right)\right) \tag{1.136}$$

If we write it in terms of the mass concentration, we obtain the equivalent equation, best known as the Convection-Diffusion equation:

$$(C_i)_t + \operatorname{div}(\boldsymbol{u} C_i) = \sum_{j,i\neq j}^{c} \operatorname{div}\left(D_{ij}\nabla C_i\right) \tag{1.137}$$

1.10 Species Transport: Boundary Conditions

1.10.1 Set concentration boundary

If the concentration at the boundary is known or fixed, the Dirichlet type boundary can be written as:

$$C_* = C_D(\boldsymbol{r}, t) \tag{1.138}$$

1.10.2 Outflow boundary

When a fluid has developed its flow enough, the diffussion of the species along the flow is almost zero, i.e. the species transport is only carried out by convection. Then, if the diffusive flux obeys Fick's Law, the boundary condition can be written as a von-Neumann type boundary:

$$-D\nabla C_* \cdot \boldsymbol{n} = 0 \tag{1.139}$$

Where D is the diffussion coefficient of the species in the medium.

1.10.3 Concentration source boundary

If the boundary has an heat at a known rate, the boundary condition for the surface in contact with the element is:

$$(C_*\boldsymbol{u}_* - D\nabla C_*) \cdot \boldsymbol{n} = S_D(\boldsymbol{r}, t) \tag{1.140}$$

Where S_D is the source term of the species.

1.10.4 Wall boundary

If the species cannot penetrate the boundary, i.e. there is no convertive or diffusive flux traversing the boundary, it can be written as a Robin type condition:

$$(C_*\boldsymbol{u}_* - D\nabla C_*) \cdot \boldsymbol{n} = 0 \tag{1.141}$$

1.10.5 Continuity of concentration at an interface

In the case of two domains in contact, if the boundary is not physical (i.e., the boundary is an imaginary surface) a possibility is that the concentration across it is the same for both domains. If both sides of the boundary are denoted by C_{*+} and C_{*-}, then (Bird, 1960)

$$C_{*+} = C_{*-} \tag{1.142}$$

1.10.6 Reverse osmosis membrane boundary (non-porous)

As the membranes are not perfect, some degree of salt penetration is present. This is accounted for with a Robin type boundary condition. Lets consider the domain which contains the salt water as Ω, and the domain which contains the pure water as Ω_p.
Mathematically, the salt flow for this model is expressed as an interface condition:

$$(C_f \boldsymbol{u}_f - D_f \nabla C_f) \cdot \boldsymbol{n} = (C_p \boldsymbol{u}_p - D_p \nabla C_p) \cdot \boldsymbol{n} \tag{1.143}$$

$$(C_f \boldsymbol{u}_f - D_f \nabla C_f) \cdot \boldsymbol{n} = B(C_f - C_p) \tag{1.144}$$

Where B is the membrane's salt permeability, and C refers to the molar concentration of salt. If we neglect the permeate effects on the permeate flux (as $C_p \sim 0$), the boundary can be written as:

$$(C_f \boldsymbol{u}_f - D_f \nabla C_f) \cdot \boldsymbol{n} = B C_f \tag{1.145}$$

1.10.7 Liquid-vapor thermodynamic equilibrium boundary

If there is an interface, product of a vapor-liquid equilibrium between two phases contained in their respective domains, the concentration of a species will be given by the thermodynamic relationship of thermodynamic equilibrium, namely, the equality of the chemical potential of said species in both fluids. In membrane distillation, there is salt water in the feed domain Ω_f and water vapor + air in the membrane domain Ω_m. Then, the equilibrium boundary condition is:

$$T_f = T_m \tag{1.146}$$

$$C_m = \frac{C_f \gamma(C_{S,f}) p^0(T_f)}{\rho_f R T_f} \tag{1.147}$$

Where C is the molar concentration of the water, C_S is the molar concentration of salt, ρ is the molar density and γ is the activity coefficient of the salt solution at the interface point. It is worth noting that the equilibrium condition comes accompanied by the equality of temperature condition for the heat balance.

Chapter 2

Thermophysical and Transport Properties

Once we have defined our problem, the system of equations need closure expressions for all thermodynamic and transport properties involved, e.g., density, viscosity, thermal conductivity, etc. The following chapter is dedicated to give expressions to the substances present in the literature for each relevant property, as well as some simplifications to the available formulas, taking the precaution that they don't inccur in a large error from real data.

2.1 Seawater

2.1.1 Composition

It is well known that seawater is a complex mixture of various salt ions such as chloride, sodium, potassium, carbonate, etc. However, due to the various geophysical characteristics and mineral composition in different regions of the world, the percentage of salts present in each region may vary. This caused variations in the property measurements reported by different oceanographers (Mangi, Makhija, Raza, Khahro, & Jhatial, 2021). The need for a practical and unified way of correlating the global salt content with the thermophysical properties for industrial design paved the way to define a standard salinity scale where an arbitrary salt ion composition is used (called artificial seawater) to measure the properties (Lewis & Perkin, 1978). Salinity is defined as the mass of salt per kilogram of seawater:

$$S[g/kg] = \frac{\sum_i mass\,of\,salt\,i}{total\,seawater\,mass} = \frac{\sum_i m_{s,i}}{m_{sw}} \tag{2.1}$$

With the previous equation, we can relate the salinity with the molar concentration of the salt in solution, $C_{s,i}[mol/m^3]$:

$$S[g/kg] = \frac{\sum_i MW_{s,i}C_{s,i}}{\rho_{sw}} \tag{2.2}$$

Where $MW_{s,i}[g/mol]$ is the molar weight of the solute i and $\rho_{sw}[kg/m^3]$ is the mass density of the seawater. Analysis from equation 2.2 together with the fact that most seawater density expressions are polynomials in terms of S suggests that obtaining ρ_{sw} in terms of the concentrations $C_{s,i}$ ends up in a nonlinear equation to be solved through an iterative process. In this work we will use various approximations of seawater composition, as the desalination process needs to account the different salts present in the seawater, so a focus on the effects of each species present on the performance of the system is also needed. For this reason, when working with either simpler representations of seawater (e.g. sodium chloride + water, sodium chloride + calcium carbonate + water, etc.) or the fully represented seawater, we will refer to the molar fraction of salts and its salinity definition as stated by (Millero, Feistel, Wright, & McDougall, 2008), whose molar fraction is presented in Table **??** If available, for simpler compositions we will use available property correlations. In case there isn't a formula to represent the target pseudo-seawater studied, the equations of state for standard seawater will be used, by considering the salinity of the solution as the mere sum of all the forming salts.

Table 2.1: Dry composition molar fractions X_i of seawater with salinity $S = 35 g/kg$ and $T = 25°C$. From (Millero et al., 2008)

Component i	$10^7\, X_i$
Na^+	4188071.5
Mg^{2+}	471677.6
Ca^{2+}	91822.9
K^+	91158.8
Sr^{2+}	809.6
Cl^-	4874838.9
SO_4^{2-}	252152.4
HCO_3^-	15340.4
Br^-	7520.1
CO_3^{2-}	2133.6
$B(OH)_4^-$	899.8
F^-	610.2
OH^-	71.2
$B(OH)_3$	2806.5
CO_2	86.5
Sum	10000000

2.1.2 Density

When considering seawater as an incompressible fluid, the density of seawater or pure water at normal temperature ($25°C$) and pressure ($1\, atm$) is often used (Lin, Lei, Wang, Wang, & Huang, 2022). In our work, for the models which use this assumption, the value

$$\rho[kg/m^3] = 1027.2 \tag{2.3}$$

will be used. For a simple mixture of sodium chloride and water at normal temperature and pressure, we will use the linear relation proposed by (Geraldes, Semião, & De Pinho, 2001) :

$$\rho[kg/m^3] = 997.1 + 694\omega_{NaCl} \tag{2.4}$$

Where $\omega_{NaCl}[kg\, Nacl/kg]$ is the mass fraction of NaCl in the solution. If we write this expression in terms of molar concentration $C_{NaCl}[mol\, NaCl/m^3]$, we obtain

$$\rho[kg/m^3] = \frac{997.1}{1 + 11875.4 C_{NaCl}} \tag{2.5}$$

In the case of more complex mixtures imitating seawater and a more complex dependence, the correlation due to (Nayar, Sharqawy, Banchik, et al., 2016) is used. This last equation has been used in a wide array of not only salinities but also pressures and temperatures. For this correlation, the units are $T[°C], S[g/kg], P[MPa]$.

$$\rho(T,S,P)[kg/m^3] = \rho(T,S,P_0) F_P(T,P) \tag{2.6}$$

$$\begin{aligned}\rho(T,S,P_0) = {} & a_1 + a_2 T + a_3 T^2 + a_4 T^3 + a_5 T^4 + \frac{b_1}{1000} S + \frac{b_2}{1000} ST \\ & + \frac{b_3}{1000} ST^2 + \frac{b_4}{1000} ST^3 + \frac{b_5}{10^4} S^2 T^2\end{aligned} \tag{2.7}$$

$$\begin{aligned}F_P(T,P) = {} & \exp\left((P-P_0)(c_1 + c_2 T + c_3 T^2 + c_4 T^3 + c_5 T^4 + c_6 T^5 + S(d_1 + d_2 T + d_3 T^2))\right) \\ & \times \exp\left(\frac{(P^2 - P_0^2)}{2}(c_7 + c_8 T + c_9 T^3 + d_4 S)\right)\end{aligned} \tag{2.8}$$

The constants for the equation are shown in Table 2.2 We derived a simpler polynomial expression that, although it doesn't have the low error that its original counterpart, it may simplify the treatment when performing the finite element analysis (FEA). One of the simplifications also considered is the independence of pressure, as in the working conditions its effect is negligible. The resulting expression is:

$$\rho[kg/m^3](T[°C], S[g/kg]) = a_1 + a_2 T + (a_3 + a_4 T) S \tag{2.9}$$

Table 2.2: Constants used for the correlation of Nayar et al. (2016).

Constant	Value	Constant	Value
a_1	9.999×10^2	c_3	5.6931×10^{-8}
a_2	2.034×10^{-2}	c_4	-3.7263×10^{-10}
a_3	-6.162×10^{-3}	c_5	1.4465×10^{-12}
a_4	2.261×10^{-5}	c_6	-1.7058×10^{-15}
a_5	-4.657×10^{-8}	c_7	-1.3389×10^{-6}
b_1	8.020×10^2	c_8	4.8603×10^{-9}
b_2	-2.001	c_9	-6.8039×10^{-13}
b_3	1.677×10^{-2}	d_1	-1.1077×10^{-6}
b_4	-3.060×10^{-5}	d_2	5.5584×10^{-9}
b_5	-1.613×10^{-5}	d_3	-4.2539×10^{-11}
c_1	5.0792×10^{-4}	d_4	8.3702×10^{-9}
c_2	-3.4168×10^{-6}		

Table 2.3: Constants used for the simplified correlation.

Constant	Value	Constant	Value
a_1	1.00268×10^3	a_3	-2.45805×10^{-1}
a_2	8.04725×10^{-1}	a_4	-2.4225×10^{-4}

2.1.3 Vapor pressure

Important for the membrane distillation boundary conditions, the vapor pressure of saltwater is not directly parametrized, but rather expressed in terms of the pure water vapor pressure p^0. A commonly used equation is Antoine's equation:

$$\log_{10} P[bar](T[^\circ C]) = a_1 + \frac{a_2}{T[^\circ C] + a_3} \tag{2.10}$$

A simpler polynomial expression that can be used is:

Table 2.4: Constants used for Antoine's equation for water. Source: NIST

Constant	Value	Constant	Value
a_1	4.6543	a_3	2.08302×10^2
a_2	-1.435264×10^3		

$$P[Pa](T[^\circ C]) = a_1 + a_2 T + a_3 T^2 + a_4 T^3 \tag{2.11}$$

2.1.4 Dynamic viscosity

When considering constant viscosity of seawater as an approximation, the value of Ma et al. (2004) is used INSERT REF:

$$\mu[Pa \cdot s] = 8.9 \times 10^{-4} \tag{2.12}$$

For a simple mixture of sodium chloride and water at normal pressure, we will use the linear relation proposed by (Geraldes et al., 2001):

$$\mu[Pa \cdot s](\omega_{NaCl}[kg/kg]) = 8.9 \times 10^{-4}(1 + 3.52\omega_{NaCl}) \tag{2.13}$$

As done with the density, we write this expression in terms of molar concentration $C_{NaCl}[mol/m^3]$ and obtain

$$\mu[Pa \cdot s](C_{nacl}) = 8.9 \times 10^{-4}(1 + 60.2327\rho C_{NaCl}) \tag{2.14}$$

In the case of adding the temperature dependence, the correlation due to Lou et al. (2019) INSERT REF is used.

$$\mu[Pa \cdot s](T[^\circ C], S[g/kg]) = a_1 + a_2 T + a_3 T^2 + (a_4 + a_5 T + a_6 T^2)S \tag{2.15}$$

Table 2.5: Constants used for the simplified correlation.

Constant	Value	Constant	Value
a_1	1.00268×10^3	a_3	-2.45805×10^{-1}
a_2	8.04725×10^{-1}	a_4	-2.4225×10^{-4}

Table 2.6: Constants used for the correlation of Lou et al. (2019).

Constant	Value	Constant	Value
a_1	1.00268×10^3	a_4	-2.45805×10^{-1}
a_2	8.04725×10^{-1}	a_5	-2.4225×10^{-4}
a_3	8.04725×10^{-1}	a_6	-2.4225×10^{-4}

2.1.5 Thermal Conductivity

When considering constant thermal conductivity as an approximation, the following value is used INSERT REF:

$$k[W/(m \cdot K)] = 0.6 \tag{2.16}$$

In the case of more complex mixtures imitating seawater and a more complex dependence, the correlation due to Nayar et al. (2016) INSERT REF is used. This last equation has been used in a wide array of not only salinities but also pressures and temperatures.

$$k(S,T,P)[W/(m \cdot K)] = \frac{k_w(T,P)}{1 + 0.00022S[g/kg]} \tag{2.17}$$

$$k_w(T,P) = k_{w0}(T)(1 + P^*(a_1 + a_2T^* + a_3T^{*2} + a_4T^{*3} + a_5T^{*4})) \tag{2.18}$$

$$k_{w0}(T) = b_1T^{*-0.194} + b_2T^{*-4.717} + b_3T^{*-6.385} + b_4T^{*-2.134} \tag{2.19}$$

$$T^* = \frac{T[^\circ C] + 273.15}{300} \tag{2.20}$$

$$P^* = \frac{0.00001P[Pa] - 0.1}{139.9} \tag{2.21}$$

Table 2.7: Constants used for the correlation of equation INSERT REF.

Constant	Value	Constant	Value
a_1	21.942	b_1	0.797015
a_2	-77.387	b_2	-0.251242
a_3	102.81	b_3	0.096437
a_4	-60.727	b_4	-0.032696
a_5	13.464		

We derived a simpler polynomial expression that, although it doesn't have the low error that its original counterpart, it may simplify the treatment when performing the finite element analysis (FEA):

$$k[W/(m \cdot K)](T[^\circ C], S[g/kg]) = a_1 + a_2T + (a_3 + a_4T)S \tag{2.22}$$

2.1.6 Specific Heat Capacity

When considering constant heat capacity as an approximation, the following value is used INSERT REF:

$$C_p[J/(kg \cdot K)] = 4184 \tag{2.23}$$

In the case of more complex mixtures imitating seawater and a more complex dependence, the correlation due to Nayar et al. (2016) INSERT REF is used. This last equation has been used in a

Table 2.8: Constants used for the simplified correlation.

Constant	Value	Constant	Value
a_1	5.66824×10^{-1}	a_3	-4.06568×10^{-6}
a_2	1.55991×10^{-3}	a_4	-5.75784×10^{-8}

wide array of not only salinities but also pressures and temperatures.

$$\begin{aligned} C_p[J/(kg \cdot K)](S[g/kg], T[^\circ C], P[Mpa]) &= C_{p0}(T,P) + (P - P_0)(a_1 + a_2 T + a_3 T^2 + a_4 T^3 \\ &\quad + S(a_5 + a_6 T + a_7 T^2 + a_8 T^3)) \qquad (2.24) \\ C_{p0}(T,P) &= A_{cp}(S) + B_{cp}(S)(T + 273.15) \\ &\quad + C_{cp}(S)(T + 273.15)^2 + D_{cp}(S)(T + 273.15)^2 \qquad (2.25) \\ A_{cp}(S) &= a_9 + a_{10} S + a_{11} S^2 \qquad (2.26) \\ B_{cp}(S) &= a_{12} + a_{13} S + a_{14} S^2 \qquad (2.27) \\ C_{cp}(S) &= a_{15} + a_{16} S + a_{17} S^2 \qquad (2.28) \\ D_{cp}(S) &= a_{18} + a_{19} S + a_{20} S^2 \qquad (2.29) \end{aligned}$$

Table 2.9: Constants used for the correlation of equation INSERT REF.

Constant	Value	Constant	Value
a_1	-3.118	a_{11}	4.04×10^{-1}
a_2	1.57×10^{-2}	a_{12}	-6.913
a_3	5.1014×10^{-5}	a_{13}	7.351×10^{-1}
a_4	-1.0302×10^{-6}	a_{14}	3.15×10^{-3}
a_5	1.07×10^{-2}	a_{15}	9.6×10^{-3}
a_6	-3.9716×10^{-5}	a_{16}	-1.927×10^{-3}
a_7	3.2088×10^{-8}	a_{17}	8.23×10^{-6}
a_8	1.0119×10^{-9}	a_{18}	2.5×10^{-6}
a_9	5.328×10^{3}	a_{19}	1.666×10^{-6}
a_{10}	-9.76×10^{1}	a_{20}	-7.125×10^{-9}

We derived a simpler polynomial expression that may simplify the treatment when performing the finite element analysis (FEA):

$$\begin{aligned} C_p(S[g/kg], T[^\circ C], P[Mpa]) &= A_{cp}(T) + B_{cp}(T) S + C_{cp}(T) S^2 \qquad (2.30) \\ A_{cp}(T) &= a_1 + a_2 T \qquad (2.31) \\ B_{cp}(T) &= a_3 + a_4 T \qquad (2.32) \\ C_{cp}(T) &= a_5 + a_6 T \qquad (2.33) \end{aligned}$$

Table 2.10: Constants used for the simplified correlation.

Constant	Value	Constant	Value
a_1	4.2005×10^{3}	a_4	3.05487×10^{-2}
a_2	-5.2148×10^{-1}	a_5	1.7322
a_3	-6.3697	a_6	6.1565×10^{-3}

2.1.7 Diffusivity

When considering constant diffusivity as an approximation, the following value is used INSERT REF:

$$D[m^2/s] = 1.6 \times 10^{-9} \qquad (2.34)$$

For a simple mixture of sodium chloride and water at normal temperature and pressure, we will use the linear relation proposed by Geraldes et al. INSERT:

$$D[m^2/s] = \begin{cases} 1.6 \times 10^{-9}(1 - 14\omega_{nacl}) & if\, \omega_{nacl} \leq 0.006 \\ 1.45 \times 10^{-9} & if\, \omega_{nacl} > 0.006 \end{cases} \tag{2.35}$$

In the case of temperature dependence for the sodium chloride and water mixture, the correlation due to Lou et al. (2019) INSERT REF is used.

$$D(T[^\circ C]) = 1.7872 \times 10^{-13}(T + 273.15)\frac{\lambda_{Na}\lambda_{Cl}}{\lambda_{Na} + \lambda_{Cl}} \tag{2.36}$$

$$\lambda_{Na} = 50.11(1 + 0.02(T - 25)) \tag{2.37}$$

$$\lambda_{Cl} = 76.35(1 + 0.02(T - 25)) \tag{2.38}$$

2.2 Humid air

2.2.1 Composition

Inside the membrane distillation systems and inside its porous membranes, the fluid is a mixture of (already present) air and water vapor. The air is in itself a mixture of various gases, and therefore it would require a complex expression dependent on the concentration of each species. However, in the process of membrane distillation, the air is an inert product and doesn't change its dry composition (i.e. the composition of the species that aren't water), so we can use special expressions developed for standard dry air, and consider the dry air as a unique fluid. Finally, we can use them along a mixing rule for water to obtain the properties of the humid air at the desired conditions of pressure, temperature and water concentration (or humidity).

For the sake of completeness, in each property the pure component full expressions are presented along with the mixing rule for the humid air properties. Then, for simplification of the analysis, simpler correlations and mixing rules will be presented.

2.2.2 Density

A mixture of air and water is a compressible gas, so its density is dependent on temperature, pressure and water concentration. There are complex equations of state that can model this mixture with high precision (INSERT EOSs), but the additional steps in the calculations needed increase greatly the amount of simulation time. For this reason, at membrane distillation working conditions ($25 - 100^\circ C$ and $\sim 1\, atm$), a good approximation is to consider it as an ideal gas mixture INSERT PERFILOV, whose expression is:

$$\rho(P, T) = \frac{P}{RT} \tag{2.39}$$

Where P is the absolute pressure, T is the absolute temperature and R is the real gas constant.

2.2.3 Vapor pressure

Any fluid that starts to experience a dynamic equilibrium between its liquid and vapor phases has a unique pressure associated with it (at fixed temperature and concentration conditions). Important for the membrane distillation boundary conditions, the vapor pressure of saltwater is not directly parametrized, but rather expressed in terms of the pure water vapor pressure p^0, given by expressions 2.10 and 2.11.

2.2.4 Dynamic viscosity

There is no true unique way of considering a constant viscosity, which can oscillate greatly for minor temperature and humidity values INSERT KESTIN AND WHITELAW. For a more complex and precise treatment, the expression and mixing rules of INSERT PERFILOV is used. For this correlation,

the units are $T[^\circ C]$, $C_i[mol\, i/m^3]$, $P[Pa]$.

$$\mu[Pa \cdot s](P,T,C_i) = \sum_{i=1}^{c} \frac{\mu_i(T)}{1 + \frac{1}{y_i(P,T,C_i)} \sum_{j=1,j\neq i}^{c} y_j(P,T,C_j)\phi_{ij}(T)} \tag{2.40}$$

$$\phi_{ij}(T) = \frac{\left[1 + \left(\frac{\mu_i(T)}{\mu_j(T)}\right)^{0.5} \left(\frac{PM_i}{PM_j}\right)^{0.25}\right]^2}{\sqrt{8}\left(1 + \frac{PM_i}{PM_j}\right)} \tag{2.41}$$

A simpler expression can be obtained if we represent the pure component viscosities by temperature polynomials, and use a simple linear mixing rule. This expression has given better results than expected, with errors no higher than 7% at the middle of the humidity range (Melling et al. (1997) INSERT REF):

$$\mu[Pa \cdot s](P,T,C_i) = \sum_{i=1}^{c} \mu_i(T) y_i(P,T,C_i) \tag{2.42}$$

In both of the previous expressions, the viscosity for the pure component i and the molar fraction of component i in the gas mixture y_i are given by:

$$\mu_i[Pa \cdot s](T[^\circ C]) = a_i + b_i T \tag{2.43}$$

$$y_i(P,T,C_i) = \frac{C_i}{\rho(P,T)} \tag{2.44}$$

The density of the mixture is given by equation 2.39.

Table 2.11: Constants used for the correlation of equation INSERT REF.

Component	a_i	b_i
$H_2O\,(v)$	8.8859×10^{-6}	3.0983×10^{-8}
$dry\, air$	4.4894×10^{-6}	4.6960×10^{-8}

2.2.5 Thermal Conductivity

The previous mixing rule is also used for the thermal conductivity:

$$k[W/(m \cdot K)](P,T,C_i) = \sum_{i=1}^{c} \frac{k_i(T)}{1 + \frac{1}{y_i(P,T,C_i)} \sum_{j=1,j\neq i}^{c} y_j(P,T,C_j)\phi_{ij}(T)} \tag{2.45}$$

$$\phi_{ij}(T) = \frac{\left[1 + \left(\frac{\mu_i(T)}{\mu_j(T)}\right)^{0.5} \left(\frac{PM_i}{PM_j}\right)^{0.25}\right]^2}{\sqrt{8}\left(1 + \frac{PM_i}{PM_j}\right)} \tag{2.46}$$

A simpler expression can be obtained by using a simple linear mixing rule. This expression has given better results than expected, with errors with maximum error of 7% (Melling et al. (1997) INSERT REF):

$$k[Pa \cdot s](P,T,C_i) = \sum_{i=1}^{c} k_i(T) y_i(P,T,C_i) \tag{2.47}$$

Similar to the polynomials for the pure viscosities, for the thermal conductivity we have:

$$k_i[Pa \cdot s](T[^\circ C]) = a_i + b_i T \tag{2.48}$$

Table 2.12: Constants used for the correlation of equation INSERT REF.

Component	a_i	b_i
$H_2O\,(v)$	1.65198×10^{-2}	7.75356×10^{-5}
$dry\,air$	4.4464×10^{-3}	7.25141×10^{-5}

2.2.6 Specific Heat Capacity

An expression can be obtained if we represent the pure component heat capacities by temperature polynomials and use a simple linear mixing rule (Melling et al. (1997) INSERT REF):

$$C_p(P[Pa], T[K], C_i[mol/m^3])[kJ/(kg \cdot K)] = \sum_{i=1}^{c} C_{p,i}(T) y_i(P, T, C_i) \tag{2.49}$$

$$C_{p,i}(T) = a_i + b_i T + c_i T^2 + d_i T^3 \tag{2.50}$$

$$y_i(P, T, C_i) = \frac{C_i}{\rho(P, T)} \tag{2.51}$$

Table 2.13: Constants used for the correlation of equation INSERT REF.

Component	a_i	b_i	c_i	d_i
$H_2O\,(v)$	6.564117	$-2.6905819 \times 10^{-2}$	5.1820718×10^{-5}	$-3.2682964 \times 10^{-8}$
$dry\,air$	1.0653697	$-4.4730851 \times 10^{-4}$	9.8719042×10^{-7}	$-4.6376809 \times 10^{-10}$

2.2.7 Diffusivity (Molecular)

In porous media, one of the needed properties is the molecular diffusivity of water vapor in air. A constant value isn't really possible, and the full expression due to Karanikola et al. (2016) INSERT REF is:

$$D[m^2/s](P[Pa], T[K]) = \frac{0.926}{10^3 P[Pa]} \left(\frac{T^{2.5}}{T + 245} \right) \tag{2.52}$$

2.3 Membrane Materials

Although a membrane module has many other important characteristics associated with them, in this section we focus only in the thermophysical and structural properties of the membranes. As each manufacturer has its own uniques (and probably patented) formular to synthesise the membranes, these properties are different from membrane to membrane. For this reason, we inform specific values for different membranes, as well as ranges for certain materials. In the case of reverse osmosis membranes, the properties are listed in Table INSERT.

Table 2.14: Relevant properties for reverse osmosis membranes.

Membrane	Water Permeability $\left[\frac{m}{s\,Pa}\right]$	NaCl Permeability $\left[\frac{m}{s}\right]$	*Source*
SW30HRLE-400i	3.90×10^{-12}	-	INSERT REF
SW30XLE-400i	4.86×10^{-12}	-	INSERT REF
SW30ULE-400i	6.08×10^{-12}	-	INSERT REF
BW30-400	9.56×10^{-12}	5.58×10^{-8}	INSERT REF
ESPA2RO	1.75×10^{-11}	2.11×10^{-7}	INSERT REF
CDNF501	1.4×10^{-11}	-	INSERT REF
General range	$3.75 - 5.28 \times 10^{-12}$	$5.56 - 8.33 \times 10^{-9}$	INSERT REF

For membrane distillation membranes, the properties are given in Table INSERT.

Table 2.15: Relevant properties for membrane distillation membranes.

Membrane	$d\,[m]$	$k\left[\frac{W}{m\,K}\right]$	$C_p\left[\frac{J}{kg\,K}\right]$	ϵ	$d_p[m]$	*Source*
PDVF-HFP	1.3×10^{-4}	0.2662	1325	0.80	1.0×10^{-7}	INSERT REF
GE Osmonics	1.5×10^{-4}	0.28	1500	0.82	4.5×10^{-7}	INSERT REF
MS-3010	1.6×10^{-4}	0.28	1500	0.82	4.5×10^{-7}	INSERT REF
MS-3020	1.6×10^{-4}	0.28	1500	0.82	2.2×10^{-7}	INSERT REF
MS-4010	1.4×10^{-4}	0.28	1500	0.82	4.5×10^{-7}	INSERT REF
MS-2000	3.0×10^{-5}	0.28	1500	0.82	2.2×10^{-7}	INSERT REF
Sartorius 11807	6.5×10^{-5}	0.28	1500	0.62	2.0×10^{-7}	INSERT REF
Millipore Hydrophobic PVDF	1.25×10^{-4}	0.22	1500	0.62	2.0×10^{-7}	INSERT REF
Millipore Superhydrophobic PVDF 1	1.1×10^{-4}	0.45	1500	0.62	2.0×10^{-7}	INSERT REF
Millipore Hydrophobic PTFE/PP	$0.30/1.30 \times 10^{-4}$	0.45	1500/1700	0.62	2.0×10^{-7}	INSERT REF
Millipore Superhydrophobic PVDF 2	1.15×10^{-4}	0.65	1500	0.62	2.0×10^{-7}	INSERT REF

Chapter 3

Reverse Osmosis

3.1 Definition

Let us initially consider a normal diffusion process, illustrated in 3.1. The container of these solutions is open to the atmosphere, so they are initially at the same pressure. The difference in concentrations on both sides of the membrane generates a concentration gradient across it.

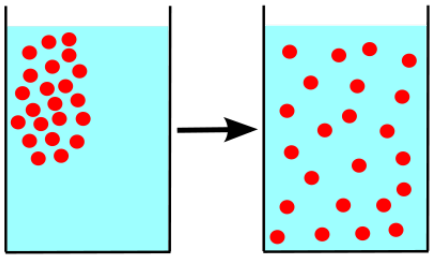

Figure 3.1: Graphical representation of molecular diffusion.

In the absence of barriers that prevent the movement of salt ions to the less concentrated side, said concentration gradient would produce a flow of ions (dissolved salt), whose direction will be in the opposite direction of the concentration gradient (that is, the flow will go from the least concentrated solution to the most concentrated). The volumetric flow per unit area (or flux $\boldsymbol{J}_s$) of solute moving by diffusion is described by Fick's law:

$$\boldsymbol{J}_s = -D\nabla c_s \tag{3.1}$$

Where $\boldsymbol{J}_s$is the ion diffusive flux, D is the diffusivity of salt in the solution, and c_s is the salt concentration.

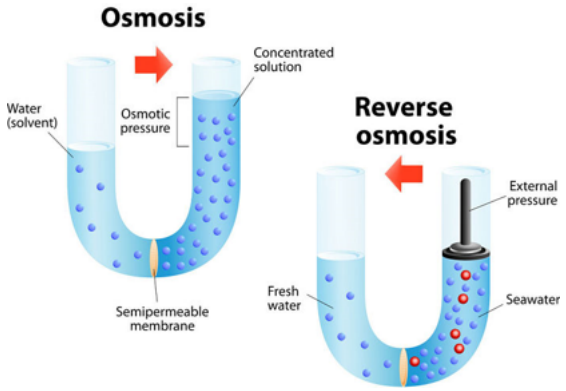

Figure 3.2: Graphical representation of reverse osmosis.

Now let us consider the situation in fig. 3.2: between the two aqueous solutions of different concentrations, a semi-permeable membrane is interposed, which only allows the passage of the solvent (in the case of seawater, it allows the water to pass but not the salt ions). Since the solute cannot migrate from one side to another, the solvent is forced to move across the membrane to reach equilibrium in the system. Similar to the previous case, the flux of solvent through the membrane is favored by the concentration gradient between both solutions.

As the system evolves and the solvent from the dilute side migrates to the concentrated side, the more dilute solution side will be lower than the more concentrated side. Hydrostatically, this height difference involves a pressure difference through the relationship $P = \rho gh + P_0$, where P is the fluids absolute pressure, ρ is the fluid density, g is the gravitational acceleration modulus, h is the fluids height with respect a reference point where $P = P_0$, and P_0 is the atmospheric pressure. The pressure difference between both columns of liquid once the process has equilibrated (that is, once the process has been allowed to stand for a long enough time so that it "does not change" over time) is known as osmotic pressure.

The reverse osmosis principle is based on the idea that the previous osmosis process can be reversed if an external pressure (greater than the osmotic pressure) is applied to the concentrated solution. This energy "forces" the concentrated solution to pass through the membrane and increase the amount of the diluted solution, while the solutes are rejected by the membrane. Applying this principle to the desalination process, we can force high-pressure salt water through the membranes, collecting diluted (or virtually salt-free) water on the other side of the membrane.

3.2 Process description

Reverse osmosis is the most widely used process to desalinate water industrially, due to its low operating cost and relatively low energy consumption compared to other methods. While its use in the world accounts for 84% of the world's desalination plants, producing 69% of the desalinated water in the world (Skuse et al., 2021), in Chile the largest desalination plants such as the desalination plant Minera Escondida Spa work by reverse osmosis. However, this technology is not exempt from technical problems, such as constant fouling of the membranes (fouling), efficiency losses over time, etc. Below we will see in more detail all the components that make up a generic desalination plant.

3.2.1 Flow Diagram

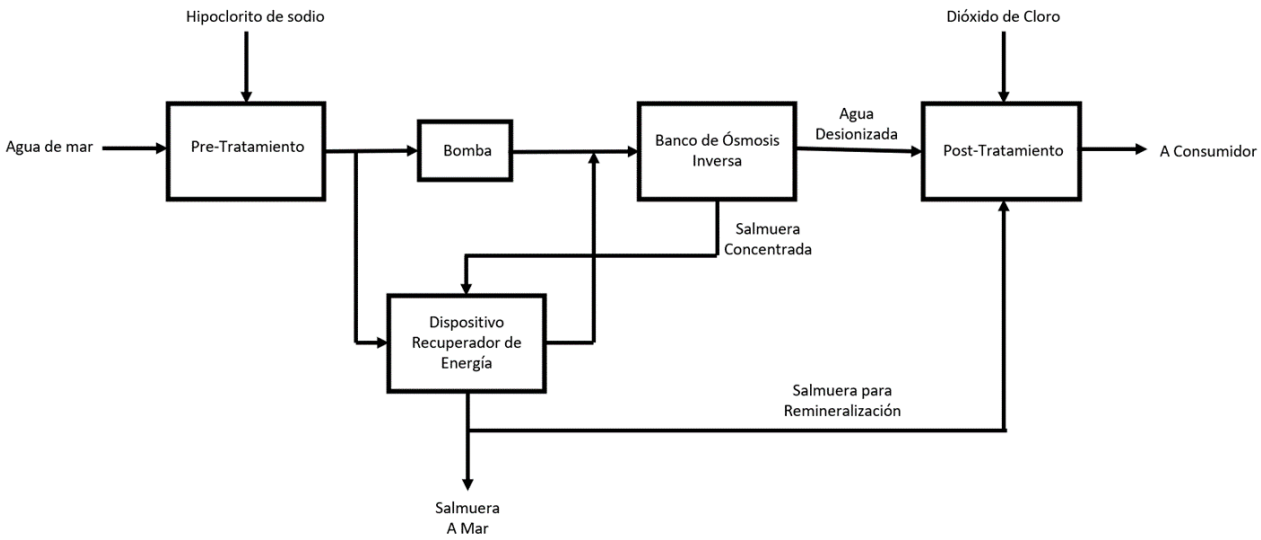

Figure 3.3: Block diagram of a Sea Water Reverse Osmosis (SWRO) desalination plant.

The desalination process can be broken down into three parts: pre-treatment, reverse osmosis, and post-water treatment. Depending on the quality and type of water supplied to the plant (brackish water, gray water, sea water, etc.) and the requirements that the water must have at the outlet

(irrigation water, drinking water, deionized water, etc.), the pre- and post treatment sub-stages will change, respectively. The stages for the desalination of seawater to produce drinking water are:

1. Sea water (with salinity $S = 35 - 40\, g\, salt/kg$ and temperature $T = 15 - 40°C$) enters the pre-treatment, which largely removes and/or eradicates organic matter, bacteria, viruses and macroscopic particles, in order to reduce the rate of fouling in the reverse osmosis membranes. Sodium hypochlorite is generally added to prevent bacterial proliferation, flocculants are used to precipitate colloidal particles, conventional filtration to remove particulates and sand, and occasionally filtration methods with larger pore sizes than reverse osmosis membranes such as ultrafiltration or nanofiltration are used, which they do not require a high pressure to work and prevent the passage of practically all contaminating agents in the water except dissolved salts.

2. Part of the pre-treated stream is fed to a high pressure pump, which is responsible for raising the pressure from 1 bar to $50 - 70\, bar$. The other fraction of water passes through an energy recovery device, exchanging pressures with a downstream stream, and finally rejoining the high pressure pre-treated water stream. As the full pressure cannot be totally recovered from the energy recovery device, a booster pump increases the missing pressure difference of the recycled current.

3. High pressure water stops at the reverse osmosis banks. Here, the main stream is divided into several sub-streams, each fed to a pressure vessel containing the osmosis filter bank. Each bank contains 7-8 osmosis filters (cartridges) connected in series. Finally, the pre-treated water is separated into a stream of desalinated water (permeate) and another stream of concentrated brine. On average, the pressure drop between the inlet and outlet of a vessel is $1 - 2\, bar$ (Jeong et al., 2021).

4. The permeate stream consisting of practically deionized water is subjected to a post-treatment process, where a small flow of concentrated brine is reincorporated until it reaches the appropriate concentration (deionized water is not suitable for human consumption), together with a amount of chlorine dioxide to disinfect the water and preserve it until consumption.

5. The high pressure concentrated brine stream is introduced to the energy recovery device (or pressure exchanger), where the high pressure concentrated brine stream exchanges its pressure with the pre-treated water fraction separated in step 2. Then, the stream of concentrated brine now at low pressure is discharged into the sea, while the stream of pre-treated water now at high pressure joins with the other fraction of pre-treated water.

Step 5 is fundamental in the technical-economic feasibility of the reverse osmosis process. As the main factor in the operating cost of the plant is the energy used in the high pressure pump, step 5 decreases the amount of energy that has to be supplied to the pre-treated water stream for the process to work, by recovering energy from the concentrated brine that would otherwise be lost. It is thanks to this energy integration that the osmosis process remains among the most economical desalination processes (Skuse et al., 2021).

3.2.2 Operating configurations

Strictly speaking, there are two ways to build desalination modules: as "dead-end" filtration or as "cross-flow" filtration. The graphic summary of these configurations is shown in the figure 3.4.

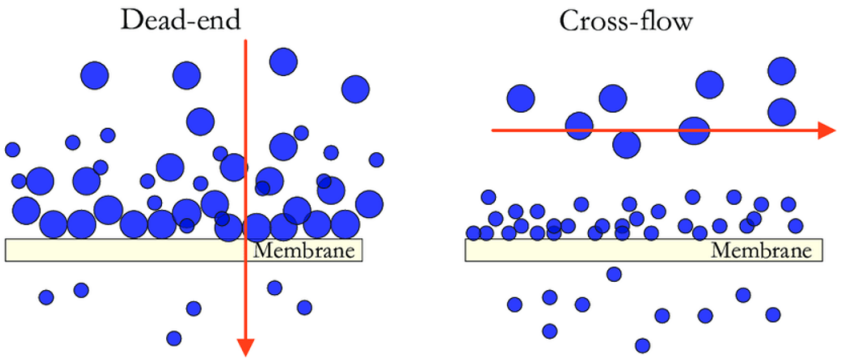

Figure 3.4: Filter configurations.

On one hand, in the dead-end filtration, the flow of water to be desalinated is supplied permendicularly to the surface. This configuration guarantees a higher filtration rate compared to the other method, but in exchange the membrane fouling rate increases drastically. This configuration is usually used for flat plate filters in experimental facilities, which seek to study the properties of the membranes or the effect of their operation due to the change in operating conditions. On the other hand, in cross-flow filtration, the flow is kept parallel to the membrane. Although this configuration produces less permeate than the previous method, the feed flow allows impurities and fouling substances that remain close to the membrane to be eliminated, thus postponing its fouling. This configuration is usually used for hollow-fiber, concentric tube, and spiral-wound filters, as this method is favored for continuous permeate production.

3.2.3 Cartridge Types

3.2.3.1 Plate and frame module

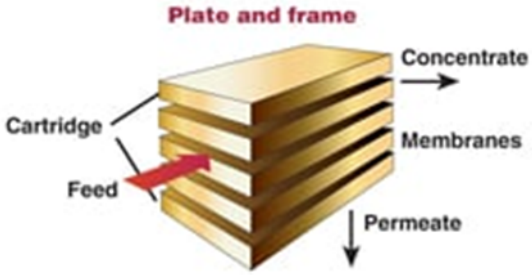

In a plate and frame filter, the membranes are spread over frames and are arranged parallel to each other. The feed enters from the sides, and the permeate exits perpendicular to the plates. These configurations take up a considerable amount of space and infrastructure due to their low specific area, but they are easier to clean (Kucera, 2010). Additionally, these modules tend to foul more easily due to the presence of dead volumes in areas where the volumetric flow is not high enough to remove accumulated deposits.

As stated before, this form is favored for experimental configurations, usually with a dead-end flow and for filtering flows with a high rate of suspended solids, and consider a packing area of the order of less than $45 - 150\ ft^2/ft^3$.

3.2.3.2 Concentric tube module

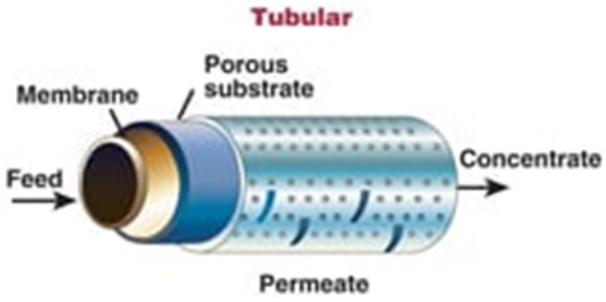

In the concentric tube filter, a tube (usually with diameters between 1.3 and 2.6 cm) with several holes is presented, which is wrapped in a membrane. As the feed progresses through the tube, the permeate filters through the membrane, collecting on the outside of the tube, while concentrated brine exits the other end of the tube.

This configuration is not optimal for specific tube area, with packing areas in the range of $6 - 120\, ft^2/ft^3$. Similar to plate modules, they require a lot of infrastructure to install, but they are easy to clean.

The arrangement of these filters is made in a shell and tube configuration, as shown in fig.3.5.

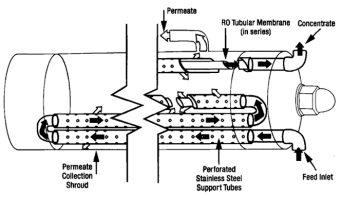

Figure 3.5: Configuraciones de los filtros de tubo en una carcasa.

3.2.3.3 Hollow fiber module

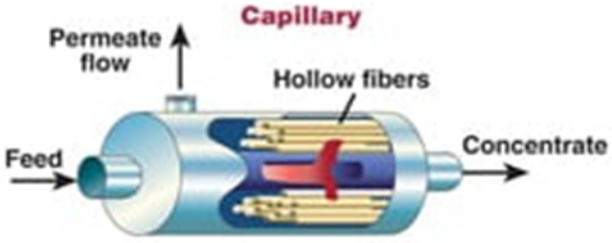

This configuration consists of a metal casing, inside which a multitude of membranes in the form of hollow fibers are placed, whose ends are tied to the caps of the casing and isolated from the power supply, as shown in the figure 3.6.

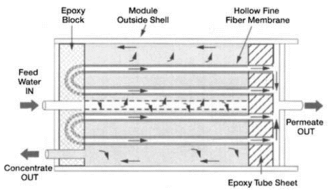

Figure 3.6: Transversal cut of a hollow fiber module.

The inner diameter of these fibers is in the order of $42\mu m$, while the outer diameter is about $85\,\mu m$. As fluid enters the casing, the hollow fibers filter water and produce permeate within it, joining the

permeate stream. This configuration has one of the highest specific areas of all the configurations ($150 - 1500\, ft^2/ft^3$), but it is especially susceptible to fouling in addition to having many dead volumes and resistance to passage. of fluids due to the resistance offered by the fibers, being more difficult to wash than other types of membrane. That is why its application is recommended for cases where the water is of better quality (less quantity of suspended solids).

3.2.3.4 Spiral-wound module

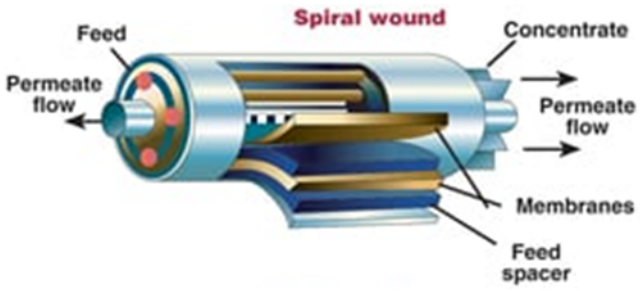

This module is similar to that of the concentric tube, with the difference that, instead of a layer of membrane on the orada tube, several layers of membranes and spacers alternate with each other to form several millimetric feeding compartments (thickness between $0.71 - 0.86\, mm$) and permeate located between the membranes, forming a spiral in cross section with a length of $50\, in$ and a diameter of $8\, in$.

As the feed enters the external part of the module in the feed spacers, the permeate filters through the membrane and settles in the spaces generated by the permeate spacers. As the fluid has nowhere to go, the permeate runs through the spiral until it is deposited in the central tube, while the concentrated brine leaves through the outside of the other side of the module.

These modules have a specific area of $150 - 380\ ft^2/ft^3$, higher than the tubular module and lower than the hollow fiber module, but the ease of construction and large area packaging make it one of the most used modules in the industry. However, there are spaces and dead volumes within each module, which not even cleaning with high speed water flows allows a complete distribution of anti-fouling agents.

The caps that are placed at the ends of the module prevent the occurrence of the "telescope effect", which occurs when the various layers of membranes and spacers slide past each other due to the differential pressure difference between them. This effect generates a conical bulge at the end of the membrane, hence its name, and is operationally undesirable, as it allows the feed water to pass next to the permeate water.

3.2.4 Advantages and disadvantages

Table 3.1: Advantages and disadvantages of the reverse osmosis desalination when compared to other desalination system.

Advantages	Disadvantages
Low investment cost	Very sensitive to fouling and scaling
Highly studied method	High operating costs
Requires less energy than thermic methods	Requires high pressures to operate
Lowest water desalination cost	Quicker membrane degradation due to antifouling/scaling treatment
	Requires water pre-treatment

3.2.5 Membranes

The type of membranes required for the process depends directly onthe transport mechanism across the membrane, as well as the chemical nature of the solutes in the seawater. The main mechanisms

of mattertransport through a membrane are presented in fig. 3.7. The type of mechanism used by the fluid to be transported through the membrane depends on the size of the pores in the membrane, or even the absence of them. In order of the pore size range where each mechanism occurs, they are:

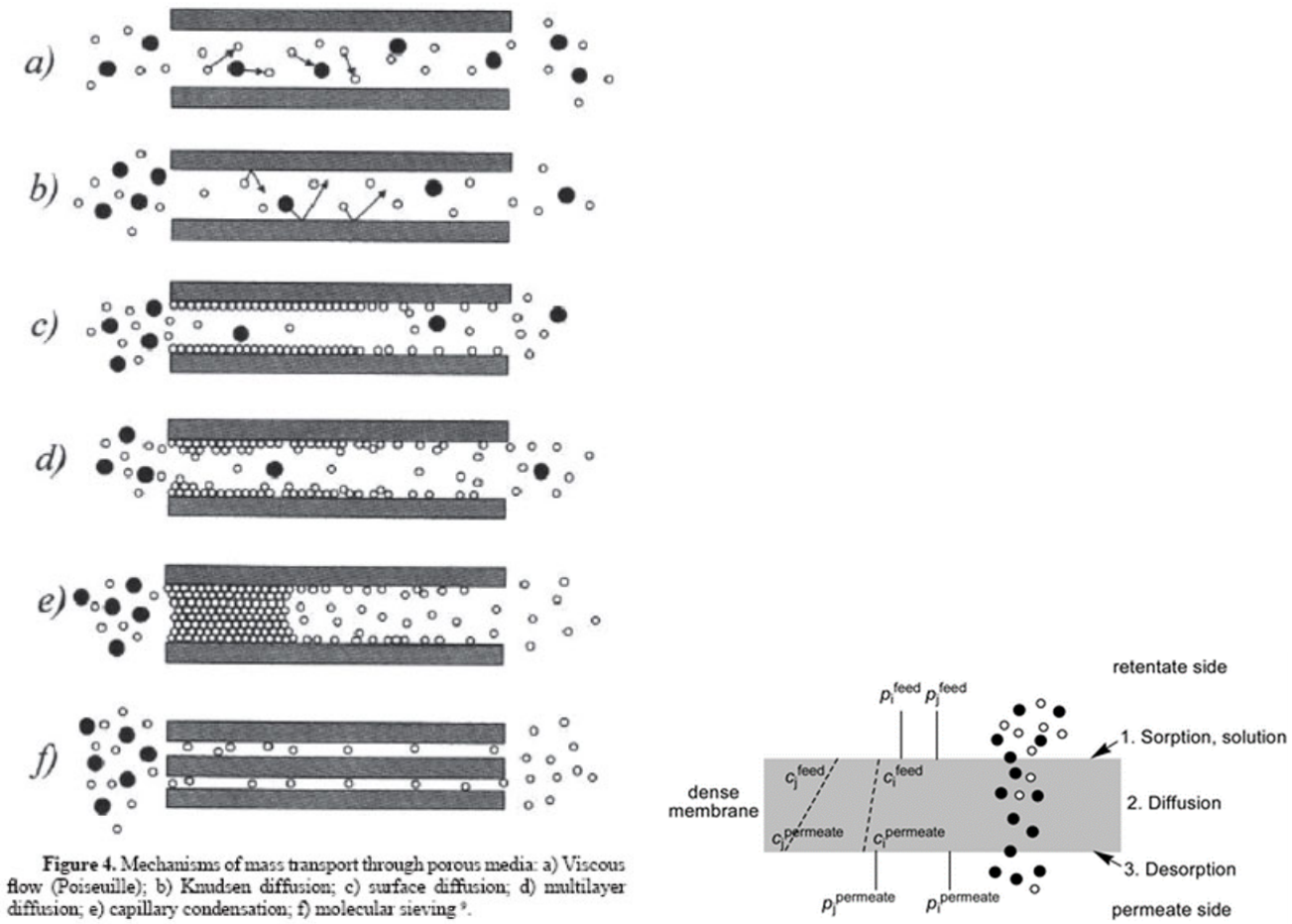

Figure 4. Mechanisms of mass transport through porous media: a) Viscous flow (Poiseuille); b) Knudsen diffusion; c) surface diffusion; d) multilayer diffusion; e) capillary condensation; f) molecular sieving [9].

Figure 3.7: Types of mass transport mechanisms though a membrane.

- Viscous flow (or Poseuille flow): Occurs when a membrane has pores large enough to allow fluid molecules to collide in greater quantity than the molecules collide with the membrane walls. Indeed, intermolecular friction is the cause of the shear stresses that are experimentally measured macroscopically and thus give meaning to viscosity as a transport property. Also, there must be a pressure difference on both sides of the membrane to act as the driving force. The fluid that moves by this mechanism can be represented by momentum balances such as the Navier-Stokes equation or the Darcy equation, although usually to simplify the analysis the incompressible Navier-Stokes equation is solved in one dimension for coordinates cylindrical (from here comes the name of Poiseuille flow, in analogy with the incompressible flow in a cylindrical tube), allowing to arrive at a simplified expression.

- Surface Diffusion (and multilayer diffusion): In the event that the membrane material is hydrophilic and porous, the water molecules are adsorbed on its surface, forming a thin layer. This layer continues its way through the pores, crossing the membrane. When the adsorbed layer is several water molecules thick, it is known as multilayer diffusion.

- Capillary Condensation: When the membrane material is hydrophilic and porous, and there is a temperature gradient (and therefore a vapor pressure difference) between both sides, the permeate can also condense inside the pore and evaporate towards the side with lower vapor pressure.

- Knudsen Diffusion: If the pores of the membrane are very narrow, when entering the pores, the

fluid molecules collide more frequently with the pore walls than they collide with each other. Therefore, the transport process resembles molecular self-diffusion (when a fluid diffuses into itself).

- Molecular Sieve: When the radius of the pores is the size of the fluid molecule (in the case of water, $2 - 3\,\mathring{A}$) the membrane acts as a sieve, allowing only the molecules of the fluid to pass through. fluid while preventing the passage of solute. Although this configuration has 100% salt rejection, the permeate flow produced is low.

- Solution - Diffusion: When the membrane is non-porous and hydrophilic, water adsorbs on the membrane surface, then "dissolves" through the membrane and diffuses through it.

To date there is no consensus among experts whether the mechanism of water transport through a reverse osmosis membrane is by molecular diffusion through the membrane, or if it is viscous transport through pores (Ismail et al.). Discussions about the validity of well-established transport models have recently been challenged (Song et al.). However, revealing the true transport mechanism in the membrane would involve an analysis with specialized equipment (atomic force microscopes, etc.) which is beyond the objectives of this project. Therefore, we will assume that the transport mechanism is the one accepted by the majority of the community: the permeate diffuses through the membrane by solution - molecular diffusion.

To achieve optimal transport through the solution-diffusion mechanism, the membrane must be as dense as possible and not have pores, in addition to being hydrophilic to allow the initial adsorption of water (polar molecule) on its surface for its subsequent dissolution in the membrane. The presence of pores in the membrane allows the passage of food (salt water) through the membrane, impairing its rejection rate.

As the reverse osmosis mechanism uses very high pressure gradients, the membrane must be tough enough to resist this applied force, which toughness increases with the thickness of the membrane. However, the membrane must be as thin as possible to minimize the resistance to mass transport (remembering Fick's law for diffusion in a medium and taking it to the infinitesimal limit, we have: $J = -D\frac{\Delta c}{\Delta x}$ Therefore, the smaller the thickness Δx, the larger the flux J). As can be seen, these characteristics have opposite effects on the permeate flux and induce the manufacturer to optimize both amounts to achieve the desired specifications in a membrane. However, two types of membrane with similar characteristics have been developed to alleviate these effects: asymmetric membranes and composite membranes. Both membranes have a very thin and dense active layer where solution-diffusion occurs, and also have a thick and very porous substrate layer that acts as a support for the active layer, without hindering permeate transport (and thus, the "bottleneck" of matter transport is the active layer).

Asymmetric membranes are membranes made from a single material, and both layers are achieved by drying the membrane under different conditions. On the contrary, composite membranes are prepared by depositing a thin, dense layer on a substrate layer that is chemically fixed to the membrane. The most used materials to prepare them are cellulose acetate and polyamide.

The most influential physicochemical properties of a reverse osmosis membrane in the fluid dynamics of desalination are:

- The active and support layer thickness
- Pore size distribution
- Pore tortuosity
- Water permeability
- Solute permeability

The scientific branch that studies the synthesis of membranes is another of the fundamental pillars in desalination technology, but the focus of this project is to study the optimization of the fluid dynamic conditions of the desalination modules throughout the process. Therefore, we will not delve further into this topic, since it is beyond the scope of this work.

Chapter 4

Membrane Distillation

While reverse osmosis plants are a resourceful way of desalinate water in a cost effective way, it has two main drawbacks: its membranes propensity to foul due to the high operating pressures, and the imposibility of desalinate brine to really high concentrations, due to increasing high pressure head requirements (and therefore, energy requirements). With the increasing environmental regulations on several regions, concentrated brine effluent disposal will be of paramount importance in the following decades. Among the various proposed solutions, a different membrane based desalination method suits these needs: membrane distillation. Recognized not only to be a more energy efficient thermal desalination process than its thermal-based relatives (e.g. multiple effect flash), but also its capability to integrate to renewable energy sources and to take advantage of low heat industrial currents via energy integration (INSERT REFERENCE). As there are different configurations for membrane distillation depending on how to generate the low vapor pressure side on the module configuration, in this chapter we will briefly explain all the main configurations, and focus on Direct Contact Membrane Distillation (DCMD), as is the most studied configuration, has the highest permeate flux production, and is the easiest to implement experimentally (and industrially).

4.1 Definition

True to its name, membrane distillation is a thermal process that consist in distill pure water from the brine trough evaporation in the liquid-vapor interface formed on the membrane pores, as shown in figure INSERT. Unlike reverse osmosis, the driving force in this process is vapor pressure difference: in the feed side, the fluid is at higher temperature than the permeate side, and thus, the water vapor pressure on the feed side is higher than the permeate's, so water vapor forms in the feed-membrane interface, and transports itself to the permeate-membrane interface, where it is transported away or condensed. INSERT FIGURE As the vapor pressure is a property that is independent of concentration, membrane distillation can work with higher salinities than reverse osmosis without compromising its permeate flux. This quality makes it suitable as a Zero Liquid Discharge (ZLD) technology (INSERT REFERENCE). This process isn't new: the original process was patented in the 70s by INSERT NAME, but since membrane distillation membranes have less permeability and the method itself uses more than five times (at least) the energy used by reverse osmosis, it hadn't been widely studied until recently (INSERT REFERENCE). As the membraneDue to its circumstantial and environmental advantages with respect to reverse osmosis, we will study this process as the other mechanisms of viable desalination

4.2 Process description

Membrane distillation has only recently been increasing in popularity among scholars INSERT REFENRECE. The versatility of this method coupled with its ability to use renewable energy sources make it a useful method to complement or even replace reverse osmosis systems in certain situation. Still, many problems are to be tackled: membrane distillation membranes are still susceptible to fouling (though less than reverse osmosis ones), the energy consumed is many times more than pressure based systems (altough less than other thermal methods), and the MD membranes have lower permeate flux than RO. However, with the continuous researcher efforts to improve MD membranes and reduce the

half century gap that RO has, the prospects of a competitive method are promising. As mentioned earlier, membrane distillation systems are not unique: depending on the permeate side carrier, not only its characteristics but also the equipment and process steps change. A graphical representation of the main MD configurations is shown on the following figure.

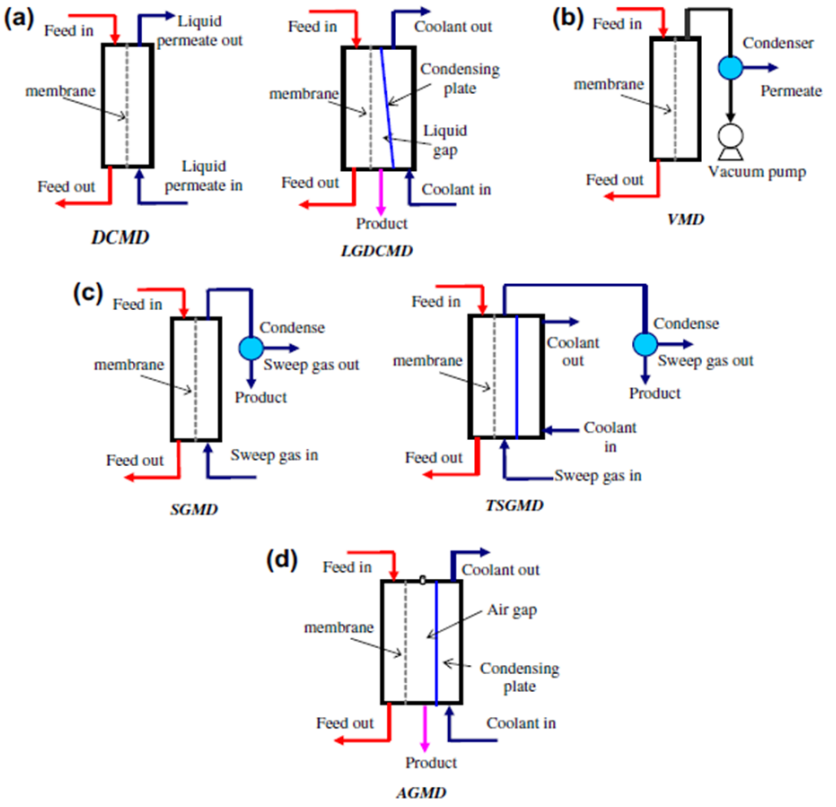

Figure 4.1: Different MD configurations.

- In Direct Contact Membrane Distillation (DCMD), the permeate side is filled with pure water at a colder temperature than the feed side ($15 - 20°$) that fills the pores at the substrate side of the membrane, reducing the distance that the vapor needs to travel to condense, therefore increasing the permeate flux. The permeate flow is then re-cooled in a heat exchanger, and part of it is removed as the product.
- In Sweeping Gas Membrane Distillation (SGMD), the permeate side is filled with flowing cold air that humidifies as the vapor passes though to the pemeate side. THe humid air is then pased through a condenser where the vapour turns into pure liquid water, and the dry air is recirculated into the module. This configuration is more cumbersome to set up, but the use of air diminishes the heat losses from conduction on the membrane, therefore increasing the energy efficiency.
- In Air-Gap Membrane Distillation (AGMD), the permeate side is filled with a stagnant air film and one of its walls is a cooling plate. Here, the vapor diffuses into the air film, and condenses into the cooling plate to be collected at the bottom of the module. This configuration has the advantage diminishing the energy required to condense the water, as the previous configuration has to cool down enormous flows of air to achieve the same. However, the settled air gap is more propense to temperature polarization effects.
- In Vacuum Membrane Distillation (VMD), the permeate side is void: a vacuum pump connected to this side creates a vacuum, generating low vapor pressure (almost zero) and increasing the driving force for distillation. The extracted vapor is then captured and turn into liquid in a condenser. This technology is useful to erradicate traces of undesired byproducts/contaminants in a current, but it hasn't been the leading distillation method for desalination.

Since its not our purpose to give a detailed review of all systems, we will stick to one of them: DCMD.

4.2.1 Flow Diagram

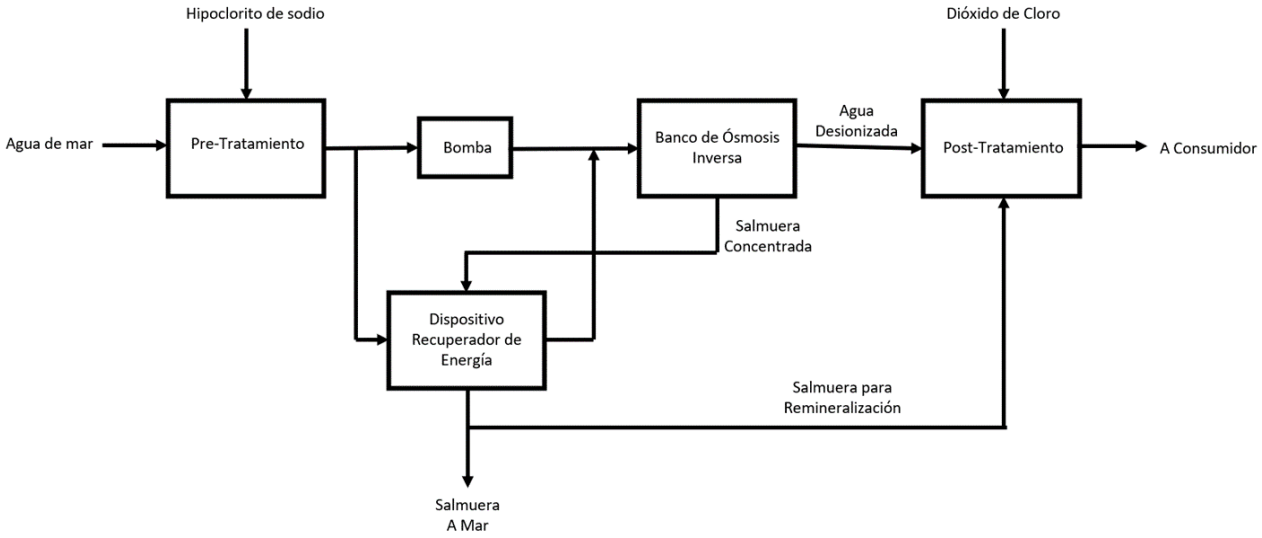

Figure 4.2: Block diagram of a DMCD desalination plant.

The desalination process can be broken down into three parts: pre-treatment, membrane distillation, and post-water treatment. Depending on the quality and type of water supplied to the plant (brackish water, gray water, sea water, etc.) and the requirements that the water must have at the outlet (irrigation water, drinking water, deionized water, etc.), the pre- and post treatment sub-stages will change, respectively. The stages for the desalination of seawater to produce drinking water are:

1. Sea water (with salinity $S = 35 - 40\, g\, salt/kg$ and temperature $T = 15 - 30°C$) enters the pre-treatment, which largely removes and/or eradicates organic matter, bacteria, viruses and macroscopic particles, in order to reduce the rate of fouling in the reverse osmosis membranes. Sodium hypochlorite is generally added to prevent bacterial proliferation, flocculants are used to precipitate colloidal particles, conventional filtration to remove particulates and sand, and occasionally filtration methods with larger pore sizes than reverse osmosis membranes such as ultrafiltration or nanofiltration are used, which they do not require a high pressure to work and prevent the passage of practically all contaminating agents in the water except dissolved salts.

2. Using a heat exchanger and a low-grade or renewable heat source, the pre-treated water is then heated to the target temperature ($T = 30 - 104°C$) and sent into the membrane module.

3. The water vapor condenses in the permeate flow in each module, and is then sent to a heat exchanger, where the current is cooled to normal temperature ($T = 15 - 30°C$). One part of the permeate is sent to post-treatment as product, and the other is recirculated into the process.

4. For the permeate stream consisting of practically deionized water sent to a post-treatment process, a small flow of concentrated brine is reincorporated until it reaches the appropriate concentration (deionized water is not suitable for human consumption), together with a amount of chlorine dioxide to disinfect the water and preserve it until consumption.

5. Part of the outlet brine is reintegrated to the feed, and the purge flow is cooled in a heat exchanger up to environmental law standards and then released.

Unlike RO systems, energy integration in MD systems is inefficient: as the heat sources used are low-grade heat and the temperature differences are also low, the efficiency of using for example, a current of hot concentrated brine to heat a current of entering seawater, are very low. Added to this, the heat exchanger used for this purpose would require higher contact area and residence time as the temperature difference between currents are less, ending up in unrealistically large and expensive exchangers. Still, one should investigate if this premise holds true for each individual case, as each plant operates under different temperatures.

For the operating configurations and cartridge types, the information given on the reverse osmosis chapter also holds true for this method. However, the permeate fluxes obtained for different cartridges are lower compared to MD systems.

4.2.2 Advantages and disadvantages

Table 4.1: Advantages and disadvantages of the MD desalination when compared to other desalination systems.

Advantages	Disadvantages
Versatile energy source use	High investment cost
High ERNC integration	High operating costs
Currently an intensely researched topic	Research is just recently taken off
Less fouling propensity than RO	Higher energy needs than RO
Can concentrate up to high salinity	
Works at low pressures	

4.2.3 Membranes

Membrane distillation works by forming an interface on the membrane pores and evaporating pure water on them, so then the vapor can transport to the other side. So, to achieve an optimum permeate flux and salt rejection for a MD membrane, we need a membrane that is highly porous so to span a large interfacial and increment the evaporation flux, is thin to reduce the water vapor mass transfer resistance, its active layer is highly hidrophobic to mantain the liquid-vapor interface on high porosities and avoid saltwater penetration, and is mechanical, thermal and chemically resistant.

The membrane must be as thin as possible to minimize the resistance to mass transport (remembering Fick's law for diffusion in a medium and taking it to the infinitesimal limit, we have: $J = -D\frac{\Delta c}{\Delta x}$ Therefore, the smaller the thickness Δx, the larger the flux J). As can be seen, these characteristics have opposite effects on the permeate flux and induce the manufacturer to optimize both amounts to achieve the desired specifications in a membrane. However, two types of membrane with similar characteristics have been developed to alleviate these effects: asymmetric membranes and composite membranes. Both membranes have a very thin and dense active layer where solution-diffusion occurs, and also have a thick and very porous substrate layer that acts as a support for the active layer, without hindering permeate transport (and thus, the "bottleneck" of matter transport is the active layer).

Asymmetric membranes are membranes made from a single material, and both layers are achieved by drying the membrane under different conditions. On the contrary, composite membranes are prepared by depositing a thin, dense layer on a substrate layer that is chemically fixed to the membrane. The most used materials to prepare them are vinyl-related plastic polymers.

Unlike RO membranes, the vapor transport mechanisms through the MD membranes are more than one, as the membrane is porous: it can experience viscous (poiseuille) flow, molecular diffusion or Knudsen diffusion. The predominant transport mechanism is given by pore size distribution. E.g. if a membrane whose mayority of pores are very narrow will have its vapor travel mostly by Knudsen diffusion.

The most influential physicochemical properties of a reverse osmosis membrane in the fluid dynamics of desalination are:

- The active and support layer thickness and porosity
- Pore size distribution
- Pore tortuosity

The scientific branch that studies the synthesis of membranes is another of the fundamental pillars in desalination technology, but the focus of this project is to study the optimization of the fluid dynamic conditions of the desalination modules throughout the process. Therefore, we will not delve further into this topic, since it is beyond the objectives of this work.

Chapter 5

Fouling

5.1 Definition

Sea water is not only salt water: several substances coexist in it, which, if not previously treated with them, one risks their progressive accumulation on the surface of the membrane, dirtying it. This mechanism is known as fouling. Fouling has two main effects on the reverse osmosis membrane:

- The operating pressure required for the same flow rate increases: the fouling layer forms an additional resistance to the transport of matter, so the water must pass through said additional resistance before passing through the membrane. For this, the fluid requires a higher pressure.
- Increases the pressure drop along the module: fouling increases the obstacles that the water flow has to cross to get from one end to the other, causing greater flow losses (and therefore axial pressure) associated with this extra resistance.

Both consequences are undesirable for the correct operation of the plant, since an increase in the operating pressure eventually leads to mechanical ruptures of the modules or to the occurrence of the telescope effect, as shown in figure 5.1. Fouling is exacerbated by high membrane permeate fluxes and low membrane tangential fluxes, since higher permeate flux brings more solute closer to the membrane, forming the concentration boundary layer much faster. With a low tangential velocity that is not capable of dragging all that solute, said boundary layer thickens, and resistance increases, increasing the residence time of the solutes and favoring their deposition on the membrane.

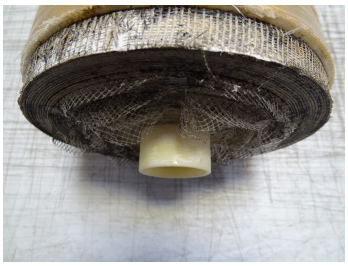

Figure 5.1: Telescopic effect in a spiral-wound module.

5.2 Mechanisms

Just as there are several substances present in the water, the types of fouling are varied. These can be categorized into:

- Colloidal fouling: solid particles (alumina, silica, iron silicates) with diameters between $10^{-9} and 10^{-5} m$ suspended in the water reach a critical concentration and begin to precipitate on the membrane, forming a gel layer on the surface.
- Biofouling: bacteria that survived the pre-treatment settle in the areas of lower flow on the surface of the membrane and begin to replicate by mitosis, using all the organic matter available

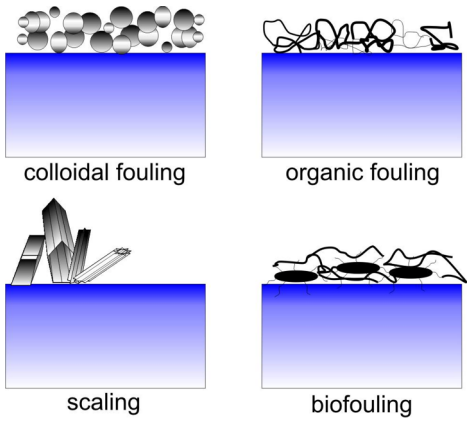

in the water as food. Bacterial proliferation can be catastrophic if left unchecked, due to the exponential growth of the bacterial population. Bacteria release proteins that, together with organic matter, generate additional resistance to the osmosis process.

- Scaling: as the concentration increases along the desalination product module, various salts naturally present in the water whose solubility is lower than that of common salt (NaCl) reach their solubility limit and begin to precipitate, forming crystals in the membrane. Sparingly soluble salts include divalent species (calcium carbonate, sulfate, fluoride, and phosphate), reactive silica, and sulfates of other divalent metals, such as barium and strontium.

5.3 Fouling Indicators

5.3.1 Silt Density Index (SDI)

Chapter 6

Numerical Modeling of Desalination Systems

In the case of reverse osmosis, there are several ways to represent a module using transport equations: models range from systems of empirical algebraic equations to represent the entire module (Jeong et al. (2021), Koutsou et al. (2020), Chen et al. al. (2020), Toh et al. (2020)) to a detailed three-dimensional modeling of the domain including the detail of the spacers (Picioreanu et al. (2009), Su et al. (2018), Luo et al. (2020)).

Due to the above, we will formulate various models which differ in complexity and considerations, based in observations from previous work made on the subject. These models will be presented starting from the most basic up to the most complete problem. Its important to notice that the most simple models can still capture the main aspects of reverse osmosis the whilst reducing the computational effort by making sensible asumptions, but more refined models allow to study certain phenomena with more detail, such as fouling aggregation.

In the case of membrane distillation, we will increase gradually the difficulty of the models considered. In the case of membrane distillation, the heat balance equation is added to account for temperature drop and polarization throughout the module. Also, thermodynamics and variable physical properties have to be accounted for, making the problem technically more difficult to model than reverse osmosis.

6.0.1 Model 1: Two dimensional filtrating channel with imperfect membrane and explicit spacers

This model is the simplest of all, and it captures the basic characteristics of the reverse osmosis mechanism: the boundary layer formation, the spacer effects on the concentration polarization reduction, and its effects (alongside changes in velocity and pressure) in the permeate flux and salt rejection. To achieve this, the following simplifications are applied:

1. We consider only the feed channel domain Ω_f for two reasons: first, as the membranes high salt rejection doesnt alter the concentration profile at the permeate channel as much as in the feed channel. Therefore, the osmotic effects on the permeate side on the feed side can be neglected. Second, the pressure drop across both channels due to fluid flow is four orders of magnitude less than the static pressure in each channel. This allows us to consider a constant pressure drop between the channels and discard the effects of the pressure drop on the permeate side, as the pressure drop in both domains is negligible when comparing to the static pressure difference.

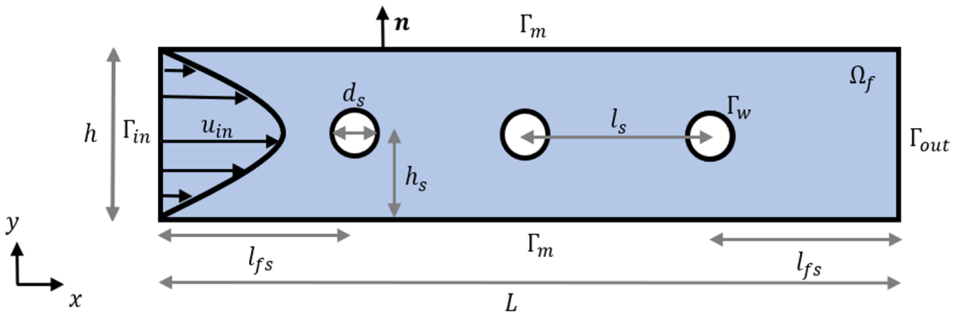

2. On the feed side enters saltwater, whose dissolved salt is only NaCl (to simplify the analysis), and whose salinity is that of seawater ($S = 35 - 40\, g/kg$). This approximation is sensible due to the high mass fraction of sodium chloride present in seawater with respect to other salts present, and it allow us to neglect several species transport equations that otherwise should be coupled with the system. However, this also impairs the fouling analysis, as the other components in seawater are responsible for it.

3. We'll model the spacers explicitly in the domain. This allow us to apply Navier-Stokes equations directly. For this study, we will consider all three spacer geometries that can be studied in two dimensions: cavity, zig-zag and submerged. These are presented in the following figure.

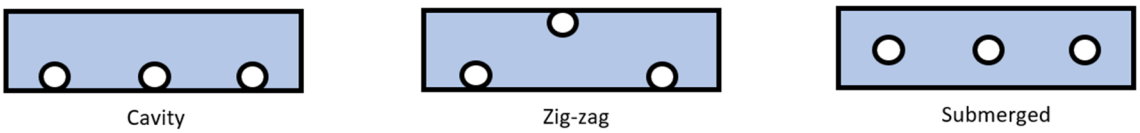

4. The domain simulated will be in two dimensions. This reduces de computation time required for the simulations, but it neglects the mixing effect that the spacers have on the velocity fields across the suppresed coordinate. The fluid regime is laminar, as the Reynolds number in the channels are reported to be less than 600 in practice (Luo, Li, & Heng, 2020).

5. We consider steady state, with developed velocity profile as an inlet boundary condition. The spacers are treated as walls, whilst the membranes have different boundary conditions based on specific models for reverse osmosis membranes.

6. Incompressible flow (ρ constant) will be considered, each one with its respective density. This approximation is based on the low deviation of the density with respect to its input value. If we consider that the salinity (concentration) of the feed water is $35 - 40\, g/kg$ and that of the permeate is $\sim 0\, g/kg$, that the maximum concentration at which the concentrated brine can be is $\frac{100\%}{TR} S$, where TR is the water recovery rate (typically 50% for seawater reverse osmosis), the amount of salt in the outlet permeate must not exceed 1% of the feed salts (Kucera, 2015), and that the system pressure ranges between $50 - 80\, bar$ ($0.5 - 0.8\, MPa$), the following density deviation curves are obtained:

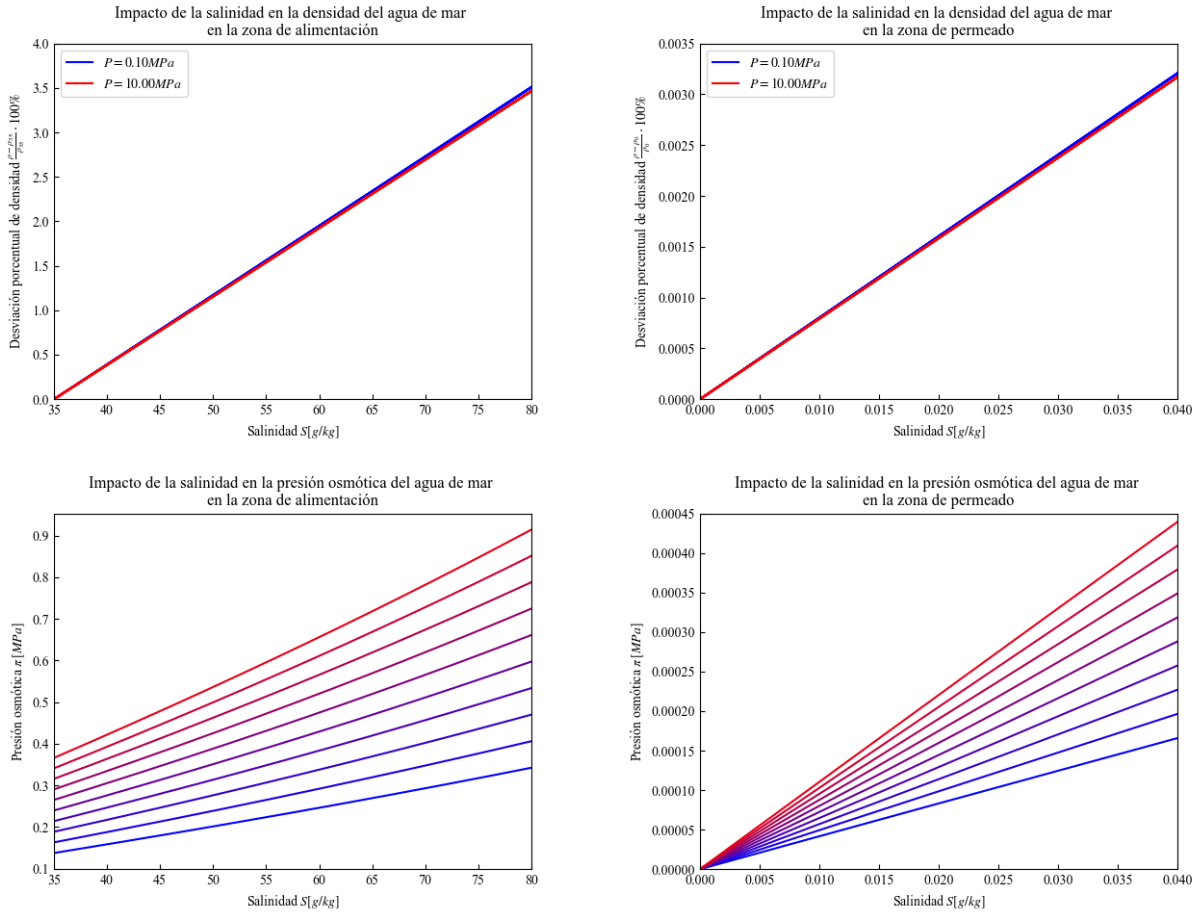

Figure 6.1: Density and osmotic pressure variation for feed and permeate channels.

Analyzing the density curves, it is observed that the deviation of the density with respect to the input value does not exceed 3.5% for the most concentrated system and at the highest pressure and temperature in the feeding zone. In the case of the permeate zone, the error does not exceed 0.004% (because the concentrations in the permeate zone are very low). Therefore, the incompressibility approximation is assumed to be valid for the ranges of variables used in both domains. Regarding the osmotic pressure, the curves in both zones present a linear behavior starting from the origin, thus confirming the possibility of parameterizing the osmotic pressure as $\pi(c) = ac$.

7. By performing an analysis similar to that for density, it can be determined that the dynamic viscosity μ and the diffusivity D can be considered approximately constant.

Defining the stress and strain tensors on domain Ω_f, $\boldsymbol{\tau}_f$ and $\boldsymbol{e}_f$, respectively:

$$\boldsymbol{\tau}_f(\boldsymbol{u}_f, p_f) = -p_f \boldsymbol{I} + 2\mu \boldsymbol{e}_f(\boldsymbol{u}_f) \tag{6.1}$$

$$\boldsymbol{e}_f(\boldsymbol{u}_f) = \frac{1}{2}\left(\nabla \boldsymbol{u}_f + \nabla \boldsymbol{u}_f^T\right) \tag{6.2}$$

Then, the problem can be stated as: find the field $\{\boldsymbol{u}_f, p_f, C_f\}$ that satisfies the following system,

$$
\begin{cases}
\rho \operatorname{div}\left(\boldsymbol{u}_f \otimes \boldsymbol{u}_f\right) - \operatorname{div}\left(\boldsymbol{\tau}_f\left(\boldsymbol{u}_f, p_f\right)\right) & = 0 & in\, \Omega_f \\
\operatorname{div}\left(\boldsymbol{u}_f\right) & = 0 & in\, \Omega_f \\
\operatorname{div}\left(C_f \boldsymbol{u}_f\right) - \operatorname{div}\left(D \nabla C_f\right) & = 0 & in\, \Omega_f \\
\boldsymbol{u}_f & = \boldsymbol{U}_{in}\left(\boldsymbol{r}\right) & in\, \Gamma_{in} \\
C_f & = C_{in} & in\, \Gamma_{in} \\
\left(-p_f \boldsymbol{I} + \mu\left(\nabla \boldsymbol{u}_f + \nabla \boldsymbol{u}_f^T\right)\right) \cdot \boldsymbol{n} & = -p_{out} \cdot \boldsymbol{n} & in\, \Gamma_{out} \\
\nabla C_f \cdot \boldsymbol{n} & = 0 & in\, \Gamma_{out} \\
\boldsymbol{u}_f & = \boldsymbol{0} & in\, \Gamma_w \\
\left(C_f \boldsymbol{u}_f - D \nabla C_f\right) \cdot \boldsymbol{n} & = 0 & in\, \Gamma_w \\
\boldsymbol{u}_f \cdot \boldsymbol{n} & = A\left(\Delta P - \pi\left(C_f\right)\right) & in\, \Gamma_m \\
\boldsymbol{u}_f \cdot \boldsymbol{t} & = 0 & in\, \Gamma_m \\
\pi\left(C_f\right) & = iRTC_f & \\
\left(C_f \boldsymbol{u}_f - D \nabla C_f\right) \cdot \boldsymbol{n} & = BC_f & in\, \Gamma_m
\end{cases}
\tag{6.3}
$$

The parameters for the simulation are given in the following table.

Parameter	Meaning	Value	Units
T	System temperature	298.0	K
R	Ideal gas constant	8.314×10^6	$kg\,mm^2 s^{-2} mol^{-1} K^{-1}$
i	Number of ions from salt solvation	2	$-$
$\boldsymbol{U}_{in}$	Inlet velocity profile	$\left[6\bar{u}_{in*}\frac{y}{h_*}\left(1-\frac{y}{h_*}\right), 0\right]$	$mm\,s^{-1}$
$\bar{u}_{in}$	Inlet mean fluid velocity	10.0	$mm\,s^{-1}$
C_{in}	Inlet salt molar concentration	600×10^{-9}	$mol\,mm^{-3}$
ΔP	Hydrostatic transmembrane pressure	5572.875	$kg\,mm^{-1} s^{-2}$
p_{out}	Outlet feed gauge pressure	0	$kg\,mm^{-1} s^{-2}$
L	Channel length	20	mm
d	Channel diameter	2.0	mm
N_{sp}	Number of spacers	3	$-$
h_s	Height of submerged spacers	1.0	mm
d_s	Spacer diameter	0.8	mm
l_{sf}	Distance between spacer centers	5.0	mm
l_{fs}	Inlet-first spacer distance	5.0	mm
ρ	Fluid density	1027.2×10^{-9}	$kg\,mm^{-3}$
D	Diffusivity of salt in water	1.611×10^{-3}	$mm^2 s^{-1}$
μ	Fluid dynamic viscosity	8.9×10^{-7}	$kg\,mm^{-1} s^{-1}$
A	Membrane water permeability	3.75×10^{-6}	$mm^2\, s^1 kg^{-1}$
B	Membrane salt permeability	5.56×10^{-6}	$mm\,s^{-1}$

6.0.2 Model 2: Two dimensional filtrating channel with imperfect membrane and spacers as porous media

The previous model requires coupling the domain with different boundary conditions for walls and obstacles, the introduction of more complex geometry which in turn may harden the finite element analysis, and the use of a high number of elements when simulating in three dimensions. Perfilov (Perfilov, 2018) stated that the domain could be simplified if the channel with spacers are treated as a porous media, as shown in the following figure. Although it only has been tested in membrane distillation configurations, the assumptions used are also applicable to reverse osmosis in principle (Kleffner, Braun, & Antonyuk, 2019).

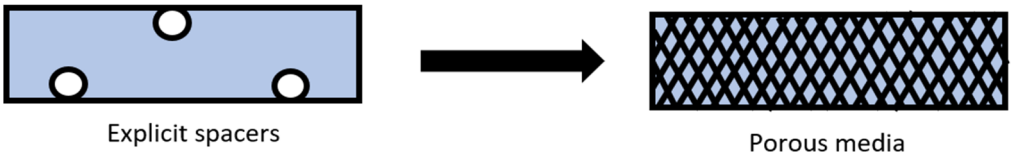

Then, the domain stays simple to analyze, and the numerical effort required to simulate the channel diminishes. This approximation is not out of reason: after all, a common spacer channel is less than a milimeter thick, and inside of it the spacer mesh is located, whose thickness is half that of the spacer. However, an additional constant is introduced, which is specific for each porous media: the permeability of the porous medium. Attempts have been done to approximate its value with theoretical and semi-empirical models, but the only true way of determining its exact value is though a experimental setup. In this work The following considerations are used in this model:

1. We will consider a steady state, two dimensional case. The domain will be a homogeoeus porous medium with porosity ε_f, and the fluid within fills up the entire channel. The fluid regime is laminar.

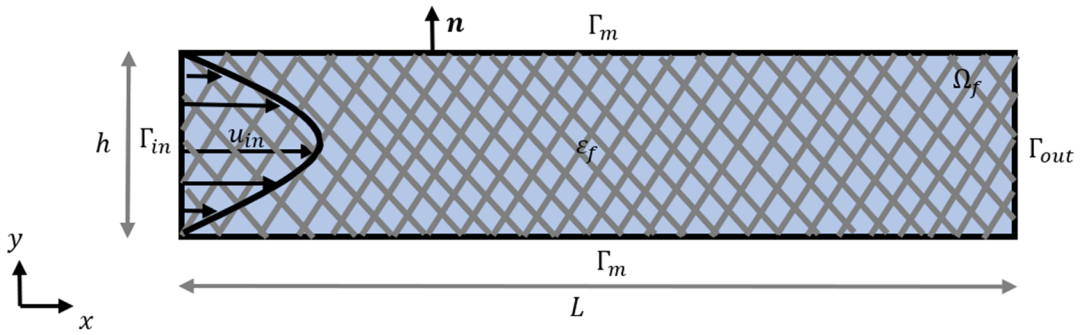

2. Membranes will have the same boundary conditions as the previous model, but for the apparent velocity $\boldsymbol{u}_m/\varepsilon_f$.

3. The fluid is considered incompressible, and its properties are constant.

4. The porosity of the medium is calculated based on its definition. To directly compare the results with the previous model, the spacer number and dimensions are used in this model:

$$\begin{aligned}\varepsilon_f &= \frac{\text{Void volume}}{\text{Total volume}} \\ &= \frac{\text{Total volume} - \text{Occupied volume}}{\text{Total volume}} \\ &= \frac{\text{Total area} - \text{Occupied area}}{\text{Total area}} \\ &= \frac{hL - N_{sp}\pi\frac{d_s^2}{4}}{hL} \qquad (6.4)\end{aligned}$$

(6.5)

5. The permeability coefficient will be obtained from theoretical expressions. Altough one can determine the permeability by analyzing the flow data of the previous model, it defeats the purpose of this one. Generally, the models to determine K are independent of fluid parameters, and dependent on the pore diameter, distribution and tortuosity. In conclusion, the permeability will be a constant in our system. As a first approach, we will use the Kozeny-Carman equation to determine permeability:

$$K = \Phi^2 \frac{\varepsilon_f^3 d_s^2}{150(1-\varepsilon_f)^2} \qquad (6.6)$$

Where Φ is the sphericity of the particle forming the porous media.In 2D, the spacers are seen as spherical particles, so $\Phi = 1$. It is worth noting that this expression original range validity is for creeping flow regime ($Re < 1$), after which the fluid begins to experiment friction losses.

Upon analyzing the previous equation, it is clear that the porosity model doesn't consider spacer distribution on the domain, so the prediction for all three configurations will be the same. Following these asumptions, the model is formulated as: find find the field $\{\boldsymbol{u}_f, p_f, C_f\}$ that satisfies the following system,

$$
\begin{cases}
\rho \operatorname{div}\left(\frac{\boldsymbol{u}_f}{\varepsilon_f} \otimes \frac{\boldsymbol{u}_f}{\varepsilon_f}\right) - \operatorname{div}\left(\boldsymbol{\tau}_f\left(\frac{\boldsymbol{u}_f}{\varepsilon_f}, p_f\right)\right) & = -\frac{\mu}{\rho K_f}\boldsymbol{u}_f - \frac{C_{frc}}{\sqrt{K_f}}|\boldsymbol{u}_f|\boldsymbol{u}_f & in\,\Omega_f \\
C_{frc} & = \frac{1.75\rho\varepsilon_f}{\sqrt{150\varepsilon_f^3}} & \\
\operatorname{div}\left(\frac{\boldsymbol{u}_f}{\varepsilon_f}\right) & = 0 & in\,\Omega_f \\
\operatorname{div}\left(C_f\frac{\boldsymbol{u}_f}{\varepsilon_f}\right) - \operatorname{div}\left(D\nabla C_f\right) & = 0 & in\,\Omega_f \\
\boldsymbol{u}_f & = \boldsymbol{U}_{in}(\boldsymbol{r}) & in\,\Gamma_{in} \\
C_f & = C_{in} & in\,\Gamma_{in} \\
\left(-p_f\boldsymbol{I} + \mu\left(\nabla\frac{\boldsymbol{u}_f}{\varepsilon_f} + \nabla\frac{\boldsymbol{u}_f}{\varepsilon_f}^T\right)\right)\cdot\boldsymbol{n} & = -p_{out}\cdot\boldsymbol{n} & in\,\Gamma_{out} \\
\nabla C_f\cdot\boldsymbol{n} & = 0 & in\,\Gamma_{out} \\
\frac{\boldsymbol{u}_f}{\varepsilon_f}\cdot\boldsymbol{n} & = A\left(\Delta P - \pi\left(C_f\right)\right) & in\,\Gamma_m \\
\pi\left(C_f\right) & = iRTC_f & \text{(van't Hoff equation for osmotic pressure)} \\
\left(C_f\frac{\boldsymbol{u}_f}{\varepsilon_f} - D\nabla C_f\right)\cdot\boldsymbol{n} & = BC_f & in\,\Gamma_m
\end{cases}
\tag{6.7}
$$

The parameters for the simulation are given in the following table.

Parameter	Meaning	Value	Units
T	System temperature	298.0	K
R	Ideal gas constant	8.314×10^6	$kg\,mm^2 s^{-2} mol^{-1} K^{-1}$
i	Number of ions from salt solvation	2	$-$
$\boldsymbol{U}_{in}$	Inlet velocity profile	$\left[6\bar{u}_{in*}\frac{y}{h_*}\left(1-\frac{y}{h_*}\right), 0\right]$	$mm\,s^{-1}$
$\bar{u}_{in}$	Inlet mean fluid velocity	10.0	$mm\,s^{-1}$
C_{in}	Inlet salt molar concentration	600×10^{-9}	$mol\,mm^{-3}$
ΔP	Hydrostatic transmembrane pressure	5572.875	$kg\,mm^{-1}s^{-2}$
p_{out}	Outlet feed gauge pressure	0	$kg\,mm^{-1}s^{-2}$
L	Channel length	20	mm
d	Channel diameter	2.0	mm
ϵ_f	Channel porosity	0.9174	$-$
ρ	Fluid density	1027.2×10^{-9}	$kg\,mm^{-3}$
D	Diffusivity of salt in water	1.611×10^{-3}	$mm^2 s^{-1}$
μ	Fluid dynamic viscosity	8.9×10^{-7}	$kg\,mm^{-1}s^{-1}$
A	Membrane water permeability	3.75×10^{-6}	$mm^2\,s^1 kg^{-1}$
B	Membrane salt permeability	5.56×10^{-6}	$mm\,s^{-1}$
K_f	Porous medium permeability	9.682×10^{-1}	mm^2

One must be careful, as the model will not predict the local effect of the spacers on the concentration and permeate velocity profiles in the membrane as the model considers the whole channel including the spacers as a homogeneous porous media, or it will not predict a difference in predictions between spacer configurations that give the same porosity. However, the porous model does require less elements to be calculated correctly as the explicit representation of the spacers needs a fine mesh refinement near its surface. In conclusion, tests need to be performed to see if the industrially relevant values (rejection factor and permeate flow) are well predicted by the model to see if the model has potential to represent the channel with spacers.

6.0.3 Model 3: Two dimensional coupled channels with explicit spacers

This coupled model considers the membrane as an interface between the feed and channel domains. Although the transport equations on this model are the same as model 1, the boundary conditions change to allow the interdependence between concentration and pressure changes between both channels (let's remember in model one we considered the permeate to be pure water. The schematic of this system is presented in the following figure.

The asumptions for this model are:

- Each channel has its own characteristic fluid properties, which are constants. For this, the stress tensor is defined as:

$$\boldsymbol{\tau}_*\left(\boldsymbol{u}_*, p_*\right) = -p_*\boldsymbol{I} + 2\mu_*\boldsymbol{e}_*\left(\boldsymbol{u}_*\right) \tag{6.8}$$

- We consider two dimensions, steady state and laminar flow in both channels. For the sake of completeness, we consider different trnasport and physical properties on both channels arising from the prominent concentration difference, although the model can be applied considering both sides properties as equal under the assumption that the concentration effect on the properties is negligible.

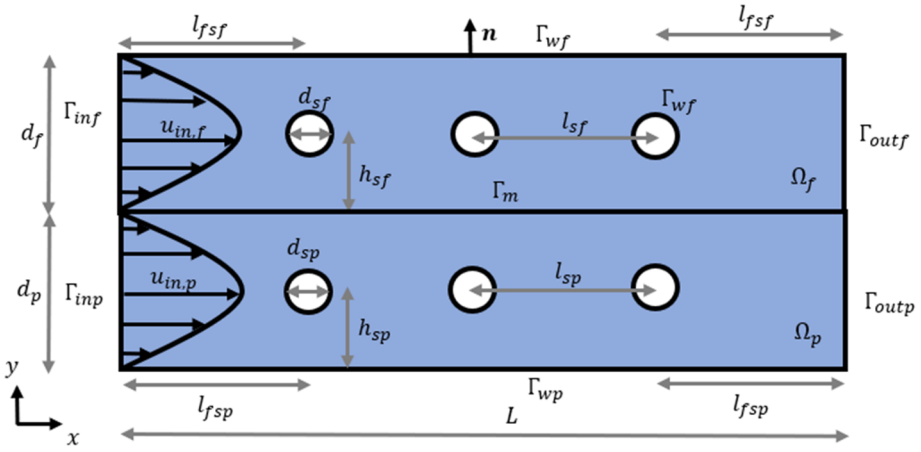

Following these asumptions, the model is formulated as: find the field $\{\boldsymbol{u}_f, p_f, C_f, \boldsymbol{u}_p, p_p, C_p\}$ that satisfies the following system,

$$
\begin{cases}
\rho_* \operatorname{div}(\boldsymbol{u}_* \otimes \boldsymbol{u}_*) - \operatorname{div}(\boldsymbol{\tau}_*(\boldsymbol{u}_*, p_*)) & = 0 & in\, \Omega_*, * = f, p \\
\operatorname{div}(\boldsymbol{u}_*) & = 0 & in\, \Omega_*, * = f, p \\
\operatorname{div}(C_* \boldsymbol{u}_*) - \operatorname{div}(D_* \nabla C_*) & = 0 & in\, \Omega_*, * = f, p \\
\boldsymbol{u}_* & = \boldsymbol{U}_{in*}(\boldsymbol{r}) & in\, \Gamma_{in*}, * = f, p \\
C_* & = C_{in*} & in\, \Gamma_{in*}, * = f, p \\
\left(-p_* \boldsymbol{I} + \mu_* \left(\nabla \boldsymbol{u}_* + \nabla \boldsymbol{u}_*^T\right)\right) \cdot \boldsymbol{n} & = -p_{out*} \cdot \boldsymbol{n} & in\, \Gamma_{out*}, * = f, p \\
\nabla C_* \cdot \boldsymbol{n} & = 0 & in\, \Gamma_{out*}, * = f, p \\
\boldsymbol{u}_* & = \boldsymbol{0} & in\, \Gamma_{w*}, * = f, p \\
(C_* \boldsymbol{u}_* - D_* \nabla C_*) \cdot \boldsymbol{n} & = 0 & in\, \Gamma_{w*}, * = f, p \\
\boldsymbol{u}_f \cdot \boldsymbol{n} & = \boldsymbol{u}_p \cdot \boldsymbol{n} & in\, \Gamma_m \\
\boldsymbol{u}_f \cdot \boldsymbol{n} - A(\Delta P - (\pi(C_f) - \pi(C_p))) & = 0 & in\, \Gamma_m \\
\pi(C_*) & = iRTC_* & * = f, p \\
(C_f \boldsymbol{u}_f - D_f \nabla C_f) \cdot \boldsymbol{n} & = (C_p \boldsymbol{u}_p - D_p \nabla C_p) \cdot \boldsymbol{n} & in\, \Gamma_m \\
(C_f \boldsymbol{u}_f - D_f \nabla C_f) \cdot \boldsymbol{n} & = B(C_f - C_p) & in\, \Gamma_m
\end{cases}
\tag{6.9}
$$

The parameters for the simulation are given in the following table.

Parameter	Meaning	Value	Units
T	System temperature	298.0	K
R	Ideal gas constant	8.314×10^6	$kg\,mm^2 s^{-2} mol^{-1} K^{-1}$
i	Number of ions from salt solvation	2	$-$
$\boldsymbol{U}_{in*}$	Inlet velocity profile	$\left[6\bar{u}_{in*}\frac{y}{h_*}\left(1-\frac{y}{h_*}\right), 0\right]$	$mm\,s^{-1}$
$\bar{u}_{inf}$	Inlet mean feed fluid velocity	10.0	$mm\,s^{-1}$
$\bar{u}_{inp}$	Inlet mean permeate fluid velocity	1.0	$mm\,s^{-1}$
C_{inf}	Inlet feed salt molar concentration	600×10^{-9}	$mol\,mm^{-3}$
C_{inp}	Inlet permeate salt molar concentration	6×10^{-9}	$mol\,mm^{-3}$
ΔP	Hydrostatic transmembrane pressure	5572.875	$kg\,mm^{-1} s^{-2}$
p_{outf}	Outlet feed gauge pressure	0	$kg\,mm^{-1} s^{-2}$
p_{outp}	Outlet permeate gauge pressure	0	$kg\,mm^{-1} s^{-2}$
L	Channel length	20	mm
d_f	Feed channel diameter	2.0	mm
d_p	Permeate channel diameter	2.0	mm
$N_{sp,f}$	Number of spacers in feed	3	$-$
$N_{sp,p}$	Number of spacers in permeate	3	$-$
h_{sf}	Height of submerged spacers in feed	1.0	mm
h_{sp}	Height of submerged spacers in permeate	1.0	mm
d_{sf}	Feed spacer diameter	0.8	mm
d_{sp}	Permeate spacer diameter	0.8	mm
l_{sf}	Distance between spacer centers in feed	5.0	mm
l_{sp}	Distance between spacer centers in permeate	5.0	mm
ϵ_f	Feed channel porosity	0.9174	$-$
ϵ_p	Permeate channel porosity	0.9174	$-$
l_{fsf}	Inlet-first spacer distance in feed	5.0	mm
l_{fsp}	Inlet-first spacer distance in permeate	5.0	mm
ρ_f	Feed fluid density	1027.2×10^{-9}	$kg\,mm^{-3}$
ρ_p	Permeate fluid density	1027.2×10^{-9}	$kg\,mm^{-3}$
D_f	Feed diffusivity of salt in water	1.611×10^{-3}	$mm^2 s^{-1}$
D_p	Permeate diffusivity of salt in water	1.611×10^{-3}	$mm^2 s^{-1}$
μ_f	Feed fluid dynamic viscosity	8.9×10^{-7}	$kg\,mm^{-1} s^{-1}$
μ_p	Permeate fluid dynamic viscosity	8.9×10^{-7}	$kg\,mm^{-1} s^{-1}$
A	Membrane water permeability	3.75×10^{-6}	$mm^2\, s^1 kg^{-1}$
B	Membrane salt permeability	5.56×10^{-6}	$mm\,s^{-1}$

6.0.4 Model 4: Two dimensional coupled channels with spacers as porous media

This model is an extension of model 2, as model 3 was of model 1. The following considerations are taken into account:

1. The coupled domains are two dimensional. The system is in steady state and its flow regime is laminar.

2. All the asumptions about the thermodynamic and transport properties made about model 2 are valid here. However, due to the difference of spacer materials and concentration in both channels, each domain has its own set of properties.

Following these asumptions, the model is formulated as: find find the field $\{\boldsymbol{u}_f, p_f, C_f, \boldsymbol{u}_p, p_p, C_p\}$ that satisfies the following system,

$$
\begin{cases}
\rho_* \operatorname{div}\left(\frac{\boldsymbol{u}_*}{\varepsilon_*} \otimes \frac{\boldsymbol{u}_*}{\varepsilon_*}\right) - \operatorname{div}\left(\boldsymbol{\tau}_*\left(\frac{\boldsymbol{u}_*}{\varepsilon_*}, p_*\right)\right) & = -\frac{\mu_*}{\rho * K_*}\boldsymbol{u}_* - \frac{C_{frc*}}{\sqrt{K_*}}|\boldsymbol{u}_*|\boldsymbol{u}_* & in\,\Omega_*, * = f,p \\
C_{frc*} & = \frac{1.75\rho_*\varepsilon_*}{\sqrt{150\varepsilon_*^3}} & \\
\operatorname{div}\left(\frac{\boldsymbol{u}_*}{\varepsilon_*}\right) & = 0 & in\,\Omega_*, * = f,p \\
\operatorname{div}\left(C_*\frac{\boldsymbol{u}_*}{\varepsilon_*}\right) - \operatorname{div}\left(D_*\nabla C_*\right) & = 0 & in\,\Omega_*, * = f,p \\
\boldsymbol{u}_* & = \boldsymbol{U}_{in*}(\boldsymbol{r}) & in\,\Gamma_{in*}, * = f,p \\
C_* & = C_{in*} & in\,\Gamma_{in*}, * = f,p \\
\left(-p_*\boldsymbol{I} + \mu_*\left(\nabla\frac{\boldsymbol{u}_*}{\varepsilon_*} + \nabla\frac{\boldsymbol{u}_*}{\varepsilon_*}^T\right)\right)\cdot\boldsymbol{n} & = -p_{out*}\cdot\boldsymbol{n} & in\,\Gamma_{out*}, * = f,p \\
\nabla C_*\cdot\boldsymbol{n} & = 0 & in\,\Gamma_{out*}, * = f,p \\
\boldsymbol{u}_* & = \boldsymbol{0} & in\,\Gamma_{w*}, * = f,p \\
\left(C_*\frac{\boldsymbol{u}_*}{\varepsilon_*} - D_*\nabla C_*\right)\cdot\boldsymbol{n} & = 0 & in\,\Gamma_{w*}, * = f,p \\
\frac{\boldsymbol{u}_f}{\varepsilon_f}\cdot\boldsymbol{n} & = \frac{\boldsymbol{u}_p}{\varepsilon_p}\cdot\boldsymbol{n} & in\,\Gamma_m \\
\frac{\boldsymbol{u}_f}{\varepsilon_f}\cdot\boldsymbol{n} - A\left(\Delta P - \left(\pi\left(C_f\right) - \pi\left(C_p\right)\right)\right) & = 0 & in\,\Gamma_m \\
\pi\left(C_*\right) & = iRTC_* & * = f,p \\
\left(C_f\frac{\boldsymbol{u}_f}{\varepsilon_f} - D_f\nabla C_f\right)\cdot\boldsymbol{n} & = \left(C_p\frac{\boldsymbol{u}_p}{\varepsilon_p} - D_p\nabla C_p\right)\cdot\boldsymbol{n} & in\,\Gamma_m \\
\left(C_f\frac{\boldsymbol{u}_f}{\varepsilon_f} - D_f\nabla C_f\right)\cdot\boldsymbol{n} & = B\left(C_f - C_p\right) & in\,\Gamma_m
\end{cases}
\tag{6.10}
$$

The parameters for the simulation are given in the following table.

Parameter	Meaning	Value	Units
T	System temperature	298.0	K
R	Ideal gas constant	8.314×10^6	$kg\,mm^2 s^{-2} mol^{-1} K^{-1}$
i	Number of ions from salt solvation	2	$-$
$\boldsymbol{U}_{in*}$	Inlet velocity profile	$\left[6\bar{u}_{in*}\frac{y}{h_*}\left(1-\frac{y}{h_*}\right), 0\right]$	$mm\,s^{-1}$
$\bar{u}_{inf}$	Inlet mean feed fluid velocity	10.0	$mm\,s^{-1}$
$\bar{u}_{inp}$	Inlet mean permeate fluid velocity	1.0	$mm\,s^{-1}$
C_{inf}	Inlet feed salt molar concentration	600×10^{-9}	$mol\,mm^{-3}$
C_{inp}	Inlet permeate salt molar concentration	6×10^{-9}	$mol\,mm^{-3}$
ΔP	Hydrostatic transmembrane pressure	5572.875	$kg\,mm^{-1}s^{-2}$
p_{outf}	Outlet feed gauge pressure	0	$kg\,mm^{-1}s^{-2}$
p_{outp}	Outlet permeate gauge pressure	0	$kg\,mm^{-1}s^{-2}$
L	Channel length	20	mm
d_f	Feed channel diameter	2.0	mm
d_p	Permeate channel diameter	2.0	mm
ρ_f	Feed fluid density	1027.2×10^{-9}	$kg\,mm^{-3}$
ρ_p	Permeate fluid density	1027.2×10^{-9}	$kg\,mm^{-3}$
D_f	Feed diffusivity of salt in water	1.611×10^{-3}	$mm^2 s^{-1}$
D_p	Permeate diffusivity of salt in water	1.611×10^{-3}	$mm^2 s^{-1}$
μ_f	Feed fluid dynamic viscosity	8.9×10^{-7}	$kg\,mm^{-1}s^{-1}$
μ_p	Permeate fluid dynamic viscosity	8.9×10^{-7}	$kg\,mm^{-1}s^{-1}$
A	Membrane water permeability	3.75×10^{-6}	$mm^2\,s^1 kg^{-1}$
B	Membrane salt permeability	5.56×10^{-6}	$mm\,s^{-1}$
K_f	Feed porous medium permeability	9.682×10^{-1}	mm^2
K_p	Permeate porous medium permeability	9.682×10^{-1}	mm^2

6.0.5 Model 5: Scaling in reverse osmosis channel

In this model, we focus on simulating the scaling process (cristallization of insoluble salts). This requires the introduction of a new variable representing the insoluble salt, C_X. As one incorporates more than one salt species into the mixture, the balances must be made for ions, as there are ions that can form various different salts. However, as the complexity of the multiple interactions between different ions would make the problem more difficult to analyze, we focus on the main substances responsible for fouling.

To consider the cristallization of salt in explicit parts of the membrane, the work of (Radu, Bergwerff, Van Loosdrecht, & Picioreanu, 2014) on gypsum fouling is the current best way to represent it. However, the complexity of the involved model and the further simplifications that would be necessary to apply on the model clashing with its fidelity to physics made the implementation of such model highly inconvenient. To that effect, some authors have analyzed the scaling factibility through postprocessing operations on a normal channel. A case for membrane distillation is (Amigo, Urtubia, & Suárez, 2018), that can readily be applied to the reverse osmosis transient channel case, corresponding to model 1 with the time-dependent terms. However, to extract the maximum information possible, it is recommended to perform the simulations in 3D.

6.0.6 Model 6: Colloidal fouling in reverse osmosis channel

In this model we study the effect of colloidal particle deposition on the reverse osmosis membrane performance. The multivariable dependence of thermodynamic and transport properties couples the equations even more than before, where coupling was included only at the boundaries. The second point turns the problem into a transient one, as accumulation of sediment is an intrinsically temporal phenomena.

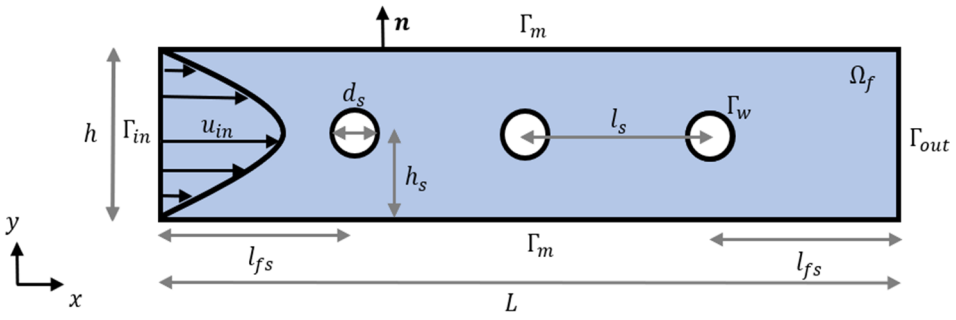

However, the weak compressibility allows us to relax the dependences: instead of using complex and highly nonlinear correlations for properties, we can interpolate them as linear functions, as the property fluctuations in the concentration range we work on is smooth and linear enough. The assumptions for this model are:

- We only model the feeding channel (the permeate channel doesn't foul, and the colloid doesn't penetrate the membrane).
- We consider the system in 2D (therefore neglecting the mixing effects in the omitted coordinate).
- The system is transient, and its regime is laminar.
- The system is isothermic (the heat equation is therefore omitted).
- The fluid is composed of water, NaCl S, and a colloidal substance X (in this case, colloidal silica).
- The fluid is newtonian and incompressible. The density is ρ_0, viscosity μ_0, diffusivity of NaCl D_S, and diffusivity of the colloid D_X.
- The membrane behaves following the sorption-diffusion model.
- The osmotic pressure is given by van't Hoff law.
- The deposition rate model is that of Su et al. (2019) (Su, Li, Palazzolo, & Ahmed, 2019). This model includes the increase in membrane resistance due to fouling as a flow through porous media.
- The fouling layer detachment rate from the mebrane is neglected.
- The flow through the cake layer is modelled with Brinkman equations. To use the same equation without an interface condition between two different porosity systems, a switch function $\psi(\varepsilon)$ is added. This function "turns off" the Darcy term on the momentum balance.

Following the previous assumptions, the problem is: find the field $\{\boldsymbol{u}_m, p_f, C_{S,f}, C_{X,f}\}$ that satisfies the following system,

$$\begin{cases}
\rho_0 \frac{\boldsymbol{u}_{f,t}}{\varepsilon} + \rho_0 \frac{\boldsymbol{u}_f}{\varepsilon} \cdot \nabla \frac{\boldsymbol{u}_f}{\varepsilon} - \operatorname{div}\left(-p_f \boldsymbol{I} + \mu_0(\nabla \frac{\boldsymbol{u}_f}{\varepsilon} + \nabla \frac{\boldsymbol{u}_f}{\varepsilon}^t)\right) + \psi(\varepsilon)\frac{\mu_0}{K}\boldsymbol{u}_f &= \boldsymbol{0} && in\,\Omega_f \\
\operatorname{div}\left(\frac{\boldsymbol{u}_f}{\varepsilon}\right) &= 0 && in\,\Omega_f \\
C_{S,f} + \operatorname{div}\left(C_{S,f}\frac{\boldsymbol{u}_f}{\varepsilon}\right) - \operatorname{div}\left(D_S(\boldsymbol{u}_f, p_f, C_{S,f})\nabla C_{S,f}\right) &= 0 && in\,\Omega_f \\
C_{X,f} + \operatorname{div}\left(C_{X,f}\frac{\boldsymbol{u}_f}{\varepsilon}\right) - \operatorname{div}\left(D_X(\boldsymbol{u}_f, p_f)\nabla C_{X,f}\right) - S_X(\boldsymbol{u}_f, p_f, C_{S,f}) &= 0 && in\,\Omega_f \\
\boldsymbol{u}_f &= \boldsymbol{U}_{in}(\boldsymbol{x}) && in\,\Gamma_{in} \\
C_{S,f} &= C_{S,in} && in\,\Gamma_{in} \\
C_{X,f} &= C_{X,in} && in\,\Gamma_{in} \\
\left(-p_f \boldsymbol{I} + \mu_0(\nabla \frac{\boldsymbol{u}_f}{\varepsilon} + \nabla \frac{\boldsymbol{u}_f}{\varepsilon}^t)\right)\cdot \boldsymbol{n} &= \boldsymbol{0} && in\,\Gamma_{out} \\
\nabla C_{S,f} \cdot \boldsymbol{n} &= 0 && in\,\Gamma_{out} \\
\nabla C_{X,f} \cdot \boldsymbol{n} &= 0 && in\,\Gamma_{out} \\
\boldsymbol{u}_f &= \boldsymbol{0} && in\,\Gamma_w \\
(C_{S,f}\boldsymbol{u}_f - D_S(\boldsymbol{u}_f, p_f, C_{S,f})\nabla C_{S,f})\cdot \boldsymbol{n} &= 0 && in\,\Gamma_w \\
(C_{X,f}\boldsymbol{u}_f - D_X(\boldsymbol{u}, p)\nabla C_{X,f})\cdot \boldsymbol{n} &= 0 && in\,\Gamma_w \\
\boldsymbol{u}_f &= A(\boldsymbol{u}_f, p_f, C_{S,f})\left(\Delta P - \pi\left(C_{S,f}\right)\right)\boldsymbol{n} && in\,\Gamma_m \\
\pi\left(C_S\right) &= iRTC_S && \\
(C_{S,f}\boldsymbol{u}_f - D_S(\boldsymbol{u}_f, p_f, C_{S,f})\nabla C_{S,f})\cdot \boldsymbol{n} &= BC_{S,f} && in\,\Gamma_m \\
(C_{X,f}\boldsymbol{u}_f - D_X(\boldsymbol{u}, p)\nabla C_{X,f})\cdot \boldsymbol{n} &= 0 && in\,\Gamma_m
\end{cases} \tag{6.11}$$

Complementing the previous system, the following relations need to be considered:

$$\begin{cases}
A(\boldsymbol{u}, p, C_S) &= (\mu_0(R_m + R_X(\boldsymbol{u}, p, C_S)))^{-1} \\
R_X(\boldsymbol{u}, p, C_S) &= \alpha_X(\boldsymbol{u}, p, C_S) m_X(\boldsymbol{u}, p, C_S) \\
\alpha_X(\boldsymbol{u}, p, C_S) &= \frac{45(1-\varepsilon(\boldsymbol{u},p,C_S))}{\rho_X a^2 \varepsilon^3(\boldsymbol{u},p,C_S)} \\
K(\boldsymbol{u}, p, C_S) &= \frac{a^2\varepsilon^3(\boldsymbol{u},p,C_S)}{150(1-\varepsilon(\boldsymbol{u},p,C_S))^2} \\
\varepsilon(\boldsymbol{u}, p, C_S) &= 1 - \frac{m_X(\boldsymbol{u},p,C_S)}{\rho_X A_X} \\
m_X(\boldsymbol{u}, p, C_S) &= \int_t^{t+dt} S_X(\boldsymbol{u}, p, C_S)dt \approx \bar{S}_X \Delta t \\
S_X(\boldsymbol{u}, p, C_S) &= \theta(\boldsymbol{u}, p) C_{X,in}(J(\boldsymbol{u}, p, C_S) - J_{crit}(\boldsymbol{u}, p)) \\
J(\boldsymbol{u}, p, C_S) &= A(\boldsymbol{u}, p, C_S)(\Delta P - iRTC_S) \\
J_{crit}(\boldsymbol{u}, p) &= \sqrt{J^2_{crit,br}(\boldsymbol{u}, p) + J^2_{crit,sh}(\boldsymbol{u}, p)} \\
J_{crit,br}(\boldsymbol{u}, p) &= 1.31\left(\frac{\gamma(\boldsymbol{u},p)D^2_{br}}{L}\right)^{1/3}\ln\left(\frac{\phi_{X,m}}{\phi_{X,in}}\right) \\
J_{crit,sh}(\boldsymbol{u}, p) &= 0.078\gamma(\boldsymbol{u}, p)\left(\frac{a^4}{L}\right)^{1/3}\ln\left(\frac{\phi_{X,m}}{\phi_{X,in}}\right) \\
D_X(\boldsymbol{u}, p) &= D_{br} + D_{sh}(\boldsymbol{u}, p) \\
D_{br} &= \frac{kT}{6\pi\mu_0 a} \\
D_{sh}(\boldsymbol{u}, p) &= 0.03\gamma(\boldsymbol{u}, p)a^2 \\
\theta(\boldsymbol{u}, p) &= \begin{cases} 1 & \gamma(\boldsymbol{u},p) < 214.29\,s^{-1} \\ 1.2502 - 1.1676\cdot 10^{-3}\gamma(\boldsymbol{u},p) & 214.29 < \gamma(\boldsymbol{u},p) < 985.71\,s^{-1} \\ 0.0993 & \gamma(\boldsymbol{u},p) > 985.71\,s^{-1} \end{cases} \\
\gamma(\boldsymbol{u}, p) &= \sqrt{\boldsymbol{\tau}(\boldsymbol{u},p) : \boldsymbol{\tau}(\boldsymbol{u},p)} \\
\boldsymbol{\tau}(\boldsymbol{u}, p) &= -p\boldsymbol{I} + \mu_0(\nabla \frac{\boldsymbol{u}}{\varepsilon} + \nabla \frac{\boldsymbol{u}}{\varepsilon}^t) \\
\psi(\varepsilon) &= \begin{cases} 0 & if\,\varepsilon = 1 \\ 1 & if\,\varepsilon \neq 1 \end{cases} \\
D_S(\boldsymbol{u}, p, C_S) &= D_{S0}\frac{\varepsilon(\boldsymbol{u},p,C_S)}{1-\ln\left(\varepsilon^2(\boldsymbol{u},p,C_S)\right)}
\end{cases} \tag{6.12}$$

In the previous equations, R_m corresponds to the membrane's intrinsic resistance, R_X is the hydraulic resistance of the membrane due to the fouling layer, α_X is the specific porous cake resistance (approximated by the Kozeny-Carman equation), ε is the local porosity of the fouling cake, ρ_X is the density of the colloidal particles, a is the radius of the colloidal particles, D_{S0} is the diffusivity of salt in water, $C_{X,in}$ is the inlet concentration of the colloidal substance, $J - J_{crit}$ is the local net permeate flux on the membrane, J is the total local permeate flux on the membrane, J_{crit} is the critical permeate flux through the porous cake, $J_{crit,br}$ is the critical permeate flux on a brownian diffusion dominated crossflow filtration, $J_{crit,sh}$ is the critical flux due to shear induced diffusion critical flux, θ is the deposition fraction, $\phi_{X,m}$ is the particle volumen fraction at the surface of the membrane,

$\phi_{X,in}$ is the particle volume fraction at inlet, L is the channel length, k is the Boltzmann constant, T is the absolute temperature, γ is the local shear rate, A_X is the cell bottom face area, m_X is the accumulated fouling mass in a cell, and S_X is the colloid deposition rate. Also, the multivariable dependence of the porosity and permeability as shown in the system of equations 6.12 was ommitted in equations 6.11 to shorten the notation.

6.0.7 Model 7: Biofouling in reverse osmosis channel

For the modelling of bacterial growth in the membrane, the most detailed model comes from the work of Picioreannu et al. (Picioreanu, Van Loosdrecht, & Heijnen, 1998; Picioreanu, van Loosdrecht, & Heijnen, 1998; Picioreanu, Van Loosdrecht, & Heijnen, 2001; Picioreanu, Vrouwenvelder, & Van Loosdrecht, 2009), who coupled the transport equations with a cellular automata to represent the bacterial growth criteria. In this case, we have three main concentrations with its own transport equation: the usual sodium chloride C_S, the bacterial substrate (i.e. the "food" for the bacteria) C_A and the bacterial colony C_X. Its worth noting that bacteria need a variety of substrates to live and proliferate, e.g. oxygen, organic matter, nitrogen organic compounds, etc. All of these species can be considered in a holistic model, but it may be cumbersome to parametrize all of the properties needed for each transport equation.
The assumptions for this model are:

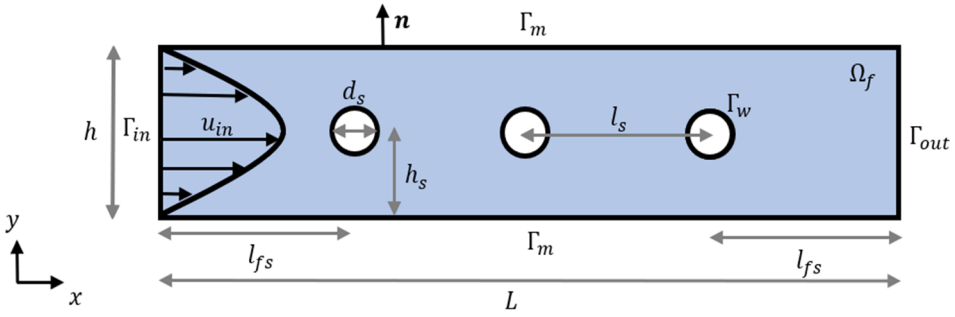

- The system only experiences biofouling.
- We only model one substrate in the system, as it is the limiting reactive in bacterial proliferation (Picioreanu et al., 2009).
- The biomass considered is a cumulae of different bacterial flora usually found on membranes, and their parameters are those of (Picioreanu et al., 2009), in order to validate the results. Different bacteria would require different parameters which need to be obtained empirically.
- The spacers are considered explicitly to study the effect of bacterial deposition and proliferation in them.
- Places in which C_X reaches a critical maximum value $C_{X,max}$ will experience bacterial proliferation.
- Other condition that must be satisfied for the bacteria to grow is that the modulus $\gamma = \sqrt{\boldsymbol{\tau} : \boldsymbol{\tau}}$ of the shear rate $\boldsymbol{\tau}$ is below the umbrale value γ_c.
- The bacteria that have deposited on the membrane are considered as a solid. Since the mesh modification on each iteration may introduce cumbersome steps to the algorithm, the solid condition of the newborn bacteria are considered through the use of an artificially high viscosity.
- The fluid is Newtonian and incompressible. The fluid density is ρ_0, the viscosity is $\mu_0(\boldsymbol{x}, C_X, \boldsymbol{\tau})$, the salt diffusivity is D_S and the substate diffusivity is D_A.
- The membrane behavior is represented with the sorption-diffusion model, with the additional simplification that the transmembrane pressure ΔP remains constant along the channel (i.e., the pressure drop along the channel effect is negligible to the membrane premeate flux).

- The bacterial growth rate is represented with the Law of Monod.
- To identify in which cells bacteria will proliferate, the cellular automata of (Picioreanu, van Loosdrecht, & Heijnen, 1998) will be considered. While not directly a partial differential equation, the cell mark-up of bacterial growth with the cellular automata must occur at each iterative step to have the updated viscosity field and bacterial concentrations available for the next iteration.
- The membrane behaves following the adsorption-diffusion model previously considered, with the corresponding simplifications.

Following the previous assumptions, the problem is: find the field $\{\boldsymbol{u}, p, C_S, C_A, C_X\}$ that satisfies the following system,

$$
\begin{cases}
\rho_0 \boldsymbol{u}_{f,t} + \rho_0 \boldsymbol{u}_f \cdot \nabla \boldsymbol{u}_f - \operatorname{div}\left(-p_f \boldsymbol{I} + \mu_0(C_X, \boldsymbol{u}, p)(\nabla \boldsymbol{u}_f + \nabla \boldsymbol{u}_f^t)\right) & = \boldsymbol{0} & in\, \Omega_f \\
\operatorname{div}(\boldsymbol{u}_f) & = 0 & in\, \Omega_f \\
(C_{S,f})_t + \operatorname{div}(C_{S,f}\boldsymbol{u}_f) - \operatorname{div}(D_S \nabla C_{S,f}) & = 0 & in\, \Omega_f \\
(C_{A,f})_t + \operatorname{div}(C_{A,f}\boldsymbol{u}_f) - \operatorname{div}(D_A(\gamma)\nabla C_{A,f}) + Y_{AX} S_{CX}(C_A, C_X) & = 0 & in\, \Omega_f \\
(C_{X,f})_t - S_{CX}(C_A, C_X) & = 0 & in\, \Omega_f \\
S_{CX}(C_A, C_X) & = \mu_m \frac{C_A}{K_A + C_A} C_X & \\
\boldsymbol{u}_f & = \boldsymbol{U}_{in}(\boldsymbol{x}) & in\, \Gamma_{in} \\
C_{S,f} & = C_{S,in} & in\, \Gamma_{in} \\
C_{A,f} & = C_{A,in} & in\, \Gamma_{in} \\
C_{X,f} & = C_{X,in} & in\, \Gamma_{in} \\
\left(-p_f \boldsymbol{I} + \mu_0(C_X, \boldsymbol{u}, p)(\nabla \boldsymbol{u}_f + \nabla \boldsymbol{u}_f^t)\right) \cdot \boldsymbol{n} & = \boldsymbol{0} & in\, \Gamma_{out} \\
\nabla C_{S,f} \cdot \boldsymbol{n} & = 0 & in\, \Gamma_{out} \\
\nabla C_{A,f} \cdot \boldsymbol{n} & = 0 & in\, \Gamma_{out} \\
\boldsymbol{u}_f & = \boldsymbol{0} & in\, \Gamma_w \\
(C_{S,f}\boldsymbol{u}_f - D_S \nabla C_{S,f}) \cdot \boldsymbol{n} & = 0 & in\, \Gamma_w \\
(C_{A,f}\boldsymbol{u}_f - D_A(\gamma)\nabla C_{A,f}) \cdot \boldsymbol{n} & = 0 & in\, \Gamma_w \\
\boldsymbol{u}_f \cdot \boldsymbol{n} & = A(\Delta P - \pi(C_f)) & in\, \Gamma_m \\
\pi(C_f) & = iRTC_f & \\
(C_{S,f}\boldsymbol{u}_f - D_S \nabla C_{S,f}) \cdot \boldsymbol{n} & = BC_{S,f} & in\, \Gamma_m \\
(C_{A,f}\boldsymbol{u}_f - D_A(\gamma)\nabla C_{A,f}) \cdot \boldsymbol{n} & = 0 & in\, \Gamma_m \\
\mu_0(C_X, \boldsymbol{u}, p) & = \begin{cases} 10^{-3} & si\, C_X < C_{X,c} \,\text{or}\, \gamma(C_X, \boldsymbol{u}, p) \geq \gamma_c \\ 10^4 & si\, C_X \geq C_{X,c} \,\text{and}\, \gamma(C_X, \boldsymbol{u}, p) < \gamma_c \end{cases} & \\
\boldsymbol{\tau}(C_X, \boldsymbol{u}, p) & = -p\boldsymbol{I} + \mu_0(C_X, \boldsymbol{u}, p)(\nabla \boldsymbol{u} + \nabla \boldsymbol{u}^t) & \\
\gamma(C_X, \boldsymbol{u}, p) & = \sqrt{\boldsymbol{\tau}(C_X, \boldsymbol{u}, p) : \boldsymbol{\tau}(C_X, \boldsymbol{u}, p)} &
\end{cases}
$$

Additionally to this, the cellular automata has to be implemented to update the bacteria occupancy (in this model, it means to update the viscosity μ_0) and expansion on the cells after each time iteration. To that effect, the rules of the automata for a given input concentration C_X^n and stress module γ^n, we have for each element:

If $C_X \geq C_0\, and\, \gamma < \gamma_c$, then

1. The mass is divided in two parts. Half of the mass remains in the current element, and half of it counts as a new biomass cell that needs to be placed in a different element. The viscosity μ_0 is updated to a high value (in this model, 10^4) and the concentration of the current cell is halved.
2. A search for a free element for the new biomass cell is initiated. This entails the following:
   (a) If there are more free neighbor cells around with $C_X = 0$, then put the new cell in one of them, randomly chosen with equal probability, the cell viscosity is updated to $\mu_0 = 10^4$, the concentration C_X of the new element is updated to equation INSERT, and the search ends.
   (b) Else, the new cell will displace one of its neighbor cells at a random. This displaced cell will start a search for a free space around it (beginning of this loop) and the search for the current cell will end.

6.0.8 Model 8: Membrane distillation membrane as a domain for given inlet-outlet profiles

As membranes are porous and have small scale pores, the velocity of vapor inside of the pores is small enough to consider as low Reynolds regime ($Re < 10$) and apply Darcy's law explicitly on the membrane instead of a simplified one dimensional model. This example is to study how the water vapor transports itself inside of the membrane, as well as the polarization effects on it. For this model, we will consider the following assumptions:

1. The domain Ω_m is a single channel with side walls Γ_w, an inlet which connects the membrane with the feed channel Γ_{in} and an outlet which connects the membrane with the permeate channel Γ_{out}.

2. The domain is seen in 2D (therefore the z-axis mixing effects are neglected).

3. The system is in steady state.

4. The fluid in the system is a dilute mixture of water vapor (1) in air (2).

5. The fluid is compressible (variable density ρ).

6. Based in the two previous points, the ideal gas mixture equation of state can be used to model the fluid.

7. The fluid mixture's diffusivity, heat capacity, viscosity and conductivity are given by correlations that are functions of temperature, pressure and concentration.

8. The domain's heat capacity and conductivity are approximated by a linear dependence between the fluid and the membrane properties and the porosity of the medium.

9. The membrane is approximated as a homogeneous porous media, characterized by a porosity ε and a permeability K.

10. The fluid regime is in low Reynolds regime ($Re < 20$), so the Darcy equation can be used.

11. The porosity of the medium can be calculated from geometrical considerations:

$$\varepsilon = \frac{\text{Void volume}}{\text{Total volume}} \tag{6.13}$$

12. The permeability of the channel should be determined experimentally, but for regular geometries as the ones used in this systems, a theoretical expression can be used. In this case, the Kozeny-Carman equation is used:

$$K = \Phi^2 \frac{\varepsilon^3 d_s^2}{150(1-\varepsilon)^2} \tag{6.14}$$

    Where Φ is the sphericity of the particle forming the porous media.In 2D, the spacers are seen as spherical particles, so $\Phi = 1$. It is worth noting that this expression original range validity is for creeping flow regime ($Re < 1$), after which the fluid begins to experiment friction losses. In this case, the equation is valid.

13. The fluid enters Ω_f with a known velocity and temperature profile. The inlet concentration is given by the thermodynamic equilibrium of the water vapor at Γ_{in}, which is determined by temperature.

14. The fluid leaves Ω_f with a known velocity and temperature profile. The outlet concentration is given by the thermodynamic equilibrium of the water vapor at Γ_{out}, which is determined by temperature.

Following the previous assumptions, the problem is: find the field $\{\boldsymbol{u}_m, p_m, T_m, C_m\}$ that satisfies the following system,

$$
\begin{cases}
\boldsymbol{u}_m & = -\frac{K}{\mu_m(p_m,T_m,C_m)}\left(\nabla p_m - \rho_m(p_m,T_m)\, g\right) & \\
\rho_m(p_m,T_m) & = \frac{p_m}{R(T_m+273.15)} & \\
\operatorname{div}\left(\rho_m(p_m,T_m)\frac{\boldsymbol{u}_m}{\varepsilon}\right) & = 0 & in\,\Omega_m \\
\boldsymbol{u}_m \rho_m(p_m,T_m)\hat{C}_{p,m}(p_m,T_m,C_m)\cdot\nabla T_m & = \operatorname{div}\left(k_{eff}(p_m,T_m,C_m)\nabla T_m\right) & in\,\Omega_m \\
k_{eff}(p_m,T_m,C_m) & = \left(\varepsilon k_m(p_m,T_m,C_m) + (1-\varepsilon)\, k_s(T_m)\right) & \\
\operatorname{div}\left(C_m\frac{\boldsymbol{u}_m}{\varepsilon}\right) + \operatorname{div}\left(\boldsymbol{J}_m(p_m,T_m)\right) & = 0 & in\,\Omega_m \\
\boldsymbol{J}_m(p_m,T_m) & = -\frac{R_{eff}(p_m,T_m)}{R(T_m+273.15)}\nabla\left(\frac{C_m}{\rho_m(p_m,T_m)}p_m\right) & in\,\Gamma_{in} \\
R_{eff}(p_m,T_m) & \left(\frac{1}{D_{Kn}^{eff}(T_m)} + \frac{1-\frac{C_m}{\rho_m(p_m,T_m)}}{D_{molec}^{eff}(p_m,T_m)}\right)^{-1} & in\,\Gamma_{in} \\
D_{molec}^{eff}(p_m,T_m) & = \frac{\varepsilon}{\tau}\left(\frac{0.0018583(T_m+273.15)^{1.5}\sqrt{\frac{1}{M_1}+\frac{1}{M_2}}}{p_m\sigma_{12}^2\Omega_{12}}\right) & in\,\Gamma_{in} \\
D_{Kn}^{eff}(T_m) & = \frac{d_p}{3\delta}\left(\frac{\varepsilon}{\tau}\right)^2\sqrt{\frac{8M_2}{\pi R(T_m+273.15)}} & in\,\Gamma_{in} \\
\tau & = \frac{(2-\varepsilon)^2}{\varepsilon} & in\,\Gamma_{in} \\
\mu_m(p_m,T_m,C_m) & = \frac{\mu_1(T_m)}{1+\frac{\rho_m(p_m,T_m)-C_m}{C_m}\phi_{12}(T_m)} + \frac{\mu_2(T_m)}{1+\frac{C_m}{\rho_m(p_m,T_m)-C_m}\phi_{21}(T_m)} & in\,\Gamma_{in} \\
\hat{C}_{p,m}(p_m,T_m,C_m) & = \frac{C_m}{\rho_m(p_m,T_m)}\hat{C}_{p\,1,m}(T_m) + \left(1-\frac{C_m}{\rho_m(p_m,T_m)}\right)\hat{C}_{p\,2,m}(T_m) & in\,\Omega_m \\
k_m(p_m,T_m,C_m) & = \frac{k_1(T_m)}{1+\frac{\rho_m(p_m,T_m)-C_m}{C_m}\phi_{12}(T_m)} + \frac{k_2(T_m)}{1+\frac{C_m}{\rho_m(p_m,T_m)-C_m}\phi_{21}(T_m)} & in\,\Gamma_{in} \\
\phi_{ij}(T_m) & = \frac{\left(1+\sqrt{\frac{\mu_i(T_m)}{\mu_j(T_m)}}\sqrt{\frac{M_j}{M_i}}\right)^2}{\sqrt{8\left(1+\frac{M_i}{M_j}\right)}} & in\,\Gamma_{in} \\
\mu_i(T_m) & = a_{\mu,i} + b_{\mu,i}T_m & \\
\hat{C}_{p\,i,m}(T_m) & = a_{cp,i} + b_{cp,i}T_m + c_{cp,i}T_m^2 + d_{cp,i}T_m^3 & in\,\Omega_m \\
k_i(T_m) & = a_{k,i} + b_{k,i}T_m & \\
k_s(T_m) & = a_{k,s} + b_{k,s}T_m & \\
T_m & = T_{in}(\boldsymbol{r}) & in\,\Gamma_{in} \\
C_m & = C_{in}(\boldsymbol{r}) & in\,\Gamma_{in} \\
p_m & = p_{in}(\boldsymbol{r}) & in\,\Gamma_{in} \\
T_m & = T_{out}(\boldsymbol{r}) & in\,\Gamma_{out} \\
C_m & = C_{out}(\boldsymbol{r}) & in\,\Gamma_{out} \\
p_m & = p_{out}(\boldsymbol{r}) & in\,\Gamma_{out} \\
-\left(\rho_m(p_m,T_m)\frac{K}{\mu_m(p_m,T_m,C_m)}\nabla p_m\right)\cdot\boldsymbol{n} & = 0 & in\,\Gamma_w \\
\left(-k_{eff}(p_m,T_m,C_m)\nabla T_m\right)\cdot\boldsymbol{n} & = 0 & in\,\Gamma_w \\
\left(C_m\boldsymbol{u}_m + \boldsymbol{J}_m(p_m,T_m)\right)\cdot\boldsymbol{n} & = 0 & in\,\Gamma_w
\end{cases}
\tag{6.15}
$$

6.0.9 Model 9: Membrane distillation coupled channels with membrane as a surface and explicit spacers

Unlike reverse osmosis, the effect of the permeate channel on the membrane distillation system is relevant for the process, as it can contribute to a major energy loss due to conduction, and an increase in permeate flux resistance because of the diminishing temperature gradient. For this reason, the effects of permeate channel width and inlet temperature an the efficiency of the process (both thermal and flux-wise) can be studied with this model. The model is based on both (El Kadi, Janajreh, & Hashaikeh, 2020) and (Lou, Vanneste, DeCaluwe, Cath, & Tilton, 2019)
The assumptions used in this model are:

- The modelled system consists of a feed and a permeate channel coupled by a membrane represented by a nonlinear set of equations for membrane distillation membranes.
- The system is in steady state, is two dimensional and has laminar flow.
- The configuration of the process is DCMD (both the feed and permeate domains are full of seawater and highly purified water, respectively).
- The influence of temperature and salinity on the fluid density is negligible in both domains. Therefore, the fluid in both channels can be treated as incompressible with the same density ρ_0. The same is considered for the viscosity μ_0.
- Both specific heat capacity and thermal conductivity are functions of temperature and salt concentration, given by equations INSERT ECS.
- The salinity S used in the previous items is derived from expression 2.2, considering there is only one salt species dissolved in the water.
- The membrane is represented with the dusty gas model (Perfilov, 2018).

- The fluid enters both channels with a known velocity profile, temperature and salt concentration.
- The fluid experiences free flow at the channel outlet.

Following the previous assumptions, the problem can be stated as: find the field $\{\boldsymbol{u}_*, p_*, T_*, C_*\}, * = f, p$ that satisfies the following system,

$$
\begin{cases}
\rho_* \boldsymbol{u}_{*,t} + \rho_* \operatorname{div}(\boldsymbol{u}_* \otimes \boldsymbol{u}_*) - \operatorname{div}(\boldsymbol{\tau}_*(\boldsymbol{u}_*, p_*)) &= 0 & in\ \Omega_*, * = f, p \\
\rho_* \hat{C}_p(T_*, C_*) T_{*,t} + \rho_* \hat{C}_{p,*} \boldsymbol{u}_* \cdot \nabla T_* &= \operatorname{div}(k_*(T_*, C_*)(T_*, C_*) \nabla T_*) & in\ \Omega_*, * = f, p \\
\operatorname{div}(\boldsymbol{u}_*) &= 0 & in\ \Omega_*, * = f, p \\
\operatorname{div}(C_* \boldsymbol{u}_*) - \operatorname{div}(D_* \nabla C_*) &= 0 & in\ \Omega_*, * = f, p \\
\boldsymbol{u}_* &= \boldsymbol{U}_{in*}(\boldsymbol{r}) & in\ \Gamma_{in*}, * = f, p \\
C_* &= C_{in*} & in\ \Gamma_{in*}, * = f, p \\
\left(-p_* \boldsymbol{I} + \mu_* \left(\nabla \boldsymbol{u}_* + \nabla \boldsymbol{u}_*^T\right)\right) \cdot \boldsymbol{n} &= -p_{out*} \cdot \boldsymbol{n} & in\ \Gamma_{out*}, * = f, p \\
\nabla C_* \cdot \boldsymbol{n} &= 0 & in\ \Gamma_{out*}, * = f, p \\
\boldsymbol{u}_* &= \boldsymbol{0} & in\ \Gamma_{w*}, * = f, p \\
(C_* \boldsymbol{u}_* - D_* \nabla C_*) \cdot \boldsymbol{n} &= 0 & in\ \Gamma_{w*}, * = f, p \\
\boldsymbol{u}_f \cdot \boldsymbol{n} &= \boldsymbol{u}_p \cdot \boldsymbol{n} & in\ \Gamma_m \\
\boldsymbol{u}_f \cdot \boldsymbol{n} - J_v(T_*, p_*, C_*) &= 0 & in\ \Gamma_m \\
J_v(T_f, p_f, C_f) &= \frac{\varepsilon}{\tau}\left(\frac{8 d_p}{3\delta}\sqrt{\frac{1}{2\pi R M W_{w,H2O} T_f}} + \frac{d_p^2}{16 \mu_v(T_f)\delta}\frac{P_f + P_p}{R T_f}\right)\left(P^0(T_f)\gamma(C_f)\left(1 - \frac{C_f}{\rho_0}\right) - p_p\right) & \\
\left(\hat{C}_p\left(T_f, C_f\right) T_f \boldsymbol{u}_f - k(T_f, C_f) \nabla T_f\right) \cdot \boldsymbol{n} &= \left(\hat{C}_p\left(T_p, C_p\right) T_p \boldsymbol{u}_p - k(T_p, C_p) \nabla T_p\right) \cdot \boldsymbol{n} & in\ \Gamma_m \\
\left(\hat{C}_p\left(T_f, C_f\right) T_f \boldsymbol{u}_f - k(T_f, C_f) \nabla T_f\right) \cdot \boldsymbol{n} &= J_v(T_f, p_f, C_f) \Delta \hat{H}_{vap}(T_f) + \frac{k_m(T_f)}{\delta}(T_f - T_p) & in\ \Gamma_m \quad (6.16) \\
\left(C_f \boldsymbol{u}_f - D_f \nabla C_f\right) \cdot \boldsymbol{n} &= \left(C_p \boldsymbol{u}_p - D_p \nabla C_p\right) \cdot \boldsymbol{n} & in\ \Gamma_m \\
\left(C_f \boldsymbol{u}_f - D_f \nabla C_f\right) \cdot \boldsymbol{n} &= 0 & in\ \Gamma_m \\
\mu_v\left(T_f\right) &= a_{\mu,v} + b_{\mu,v} T_f & \\
k_m(T_f) &= (1 - \varepsilon) k_s(T_f) + \varepsilon k_v(T_f) & \\
k_v\left(T_f\right) &= a_{k,v} + b_{k,v} T_f & \\
k_s\left(T_f\right) &= a_{k,s} + b_{k,s} T_f & \\
\hat{C}_p(T_*, C_*) &= a_{cp}(T_*) + b_{cp}(T_*) S(C_*) + c_{cp}(T_*) S(C_*)^2 & \\
a_{cp}(T_*) &= a_{cp1} + a_{cp2} T_* & \\
b_{cp}(T_*) &= b_{cp1} + b_{cp2} T_* & \\
c_{cp}(T_*) &= c_{cp1} + c_{cp2} T_* & \\
k(T_*, C_*) &= a_{k1} + a_{k2} T_* + (a_{k3} + a_{k4} T) S(C_*) & \\
\Delta \hat{H}_{vap}(T_f) &= a_{hv} + b_{hv} T_f & \\
S(C_*) &= \frac{M W_{NaCl}}{\rho_0} C_* &
\end{cases}
$$

6.0.10 Model 10: Vacuum Membrane Distillation hollow fiber axisymmetric model

In this model the case of a hollow fiber membrane distillation module is considered. Due to the diversity of scales involved in the problem, both a small scale transport inside and in the vicinities of a membrane fiber and a big scale on the module shell, the limiting length scale impedes modelling all of the module due to computational restrictions. However, some approximations allow for the representation of the fibers through the modelling of a single fiber. In this part, we develop a model of a single hollow fiber, which can be subsequently used to represent the whole module.
The assumptions of the model are the following:

- The modelled system consists of a feed and a permeate channel coupled by a membrane represented by a nonlinear set of equations for membrane distillation membranes.
- The system is in steady state, is two dimensional and has laminar flow.
- The configuration of the process is DCMD (both the feed and permeate domains are full of seawater and highly purified water, respectively).
- The influence of temperature and salinity on the fluid density is negligible in both domains. Therefore, the fluid in both channels can be treated as incompressible with the same density ρ_0. The same is considered for the viscosity μ_0.
- Both specific heat capacity and thermal conductivity are functions of temperature and salt concentration, given by equations INSERT ECS.
- The salinity S used in the previous items is derived from expression 2.2, considering there is only one salt species dissolved in the water.
- The membrane is represented with the dusty gas model (Perfilov, 2018).
- The fluid enters both channels with a known velocity profile, temperature and salt concentration.
- The fluid experiences free flow at the channel outlet.

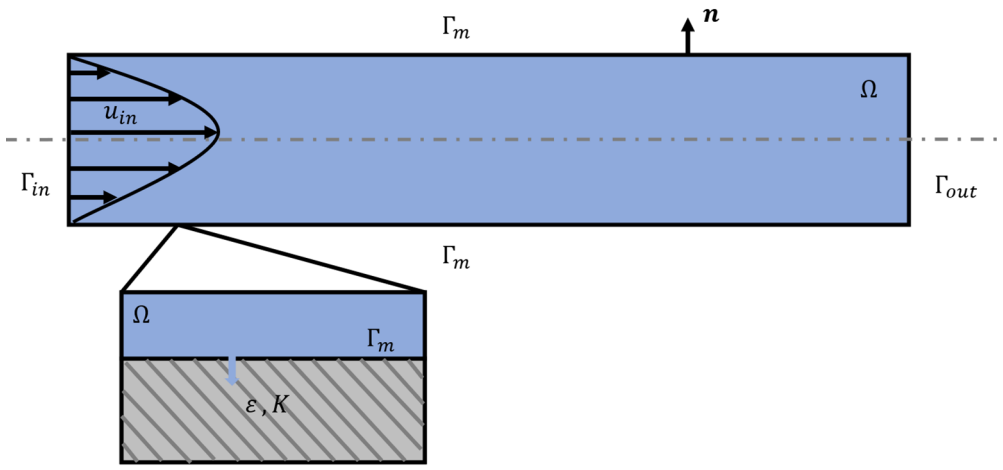

The assumptions for this model are:

1. The feed solution is composed of sodium chloride and water, and is introduced on the lumen (inner part) of the fibers. The fibers are encased in a shell which is subject of a vacuum, drawing the permeate from the membrane to outside as a vapor, to then be condense outside of the module. The reverse configuration can be also used, but the chosen here has the highest permeate flux (Schofield, 1989).

2. The module inlet distributes the feed solution to each fiber uniformly.

3. The vacuum pressure along the module is constant and unaffected by the number of fibers in the module.

4. The heat loss of the vacuum to the environment is negligible. Therefore, summed up with the previous assumption, the inmediate outer environment of each fiber is homogeneous and constant (both the permeate side pressure and temperatures P_p and T_p, respectively) .

5. The membrane is porous and highly hydrophobic, and its transport is modeled by a combination of viscous and Knudsen transport (Schofield, 1989). The molecular diffusion is not present, as in the VMD all air was extracted from the membrane pores, leaving only the water vapor inside it.

6. The system has a laminar flow, and is in steady state.

7. The fluid is incompressible with density ρ_0 and constant viscosity μ_0.

8. The outlet condition for all variables is an outflow boundary condition ("free" flow).

9. The heat capacity of the fluid $\hat{C}_{p,f}$ is given by expression 2.30.

10. The thermal conductivity of the saltwater is given by expression 2.22.

11. The salinity S used in the previous items is derived from expression 2.2, considering there is only one salt species dissolved in the water.

Then, the problem can be stated as: find the field $\{\boldsymbol{u}_f, p_f, T_f, C_f\}$ that satisfies the following

system,

$$
\begin{cases}
\rho_0 \operatorname{div}(\boldsymbol{u}_f \otimes \boldsymbol{u}_f) - \operatorname{div}(\boldsymbol{\tau}_f(\boldsymbol{u}_f, p_f)) & = 0 & in\ \Omega_f \\
\boldsymbol{\tau}_f(\boldsymbol{u}_f, p_f) & = -p_f \boldsymbol{I} + 2\mu_0 \boldsymbol{e}_f(\boldsymbol{u}_f) & \\
\boldsymbol{e}_f(\boldsymbol{u}_f) & = \frac{1}{2}\left(\nabla \boldsymbol{u}_f + \nabla \boldsymbol{u}_f^T\right) & \\
\operatorname{div}(\boldsymbol{u}_f) & = 0 & in\ \Omega_f \\
\boldsymbol{u}_f \rho_0 C_{p,f} \cdot \nabla T_f - \operatorname{div}(k_f \nabla T_f) & = 0 & in\ \Omega_f \\
\operatorname{div}(C_f \boldsymbol{u}_f) - \operatorname{div}(D \nabla C_f) & = 0 & in\ \Omega_f \\
\boldsymbol{u}_f & = \boldsymbol{U}_{in}(\boldsymbol{r}) & in\ \Gamma_{in} \\
T_f & = T_{in} & in\ \Gamma_{in} \\
C_f & = C_{in} & in\ \Gamma_{in} \\
\left(-p_f \boldsymbol{I} + \mu_0\left(\nabla \boldsymbol{u}_f + \nabla \boldsymbol{u}_f^T\right)\right) \cdot \boldsymbol{n} & = -p_{out} \boldsymbol{n} & in\ \Gamma_{out} \\
\nabla T_f \cdot \boldsymbol{n} & = 0 & in\ \Gamma_{out} \\
\nabla C_f \cdot \boldsymbol{n} & = 0 & in\ \Gamma_{out} \\
\rho_0 \boldsymbol{u}_f \cdot \boldsymbol{n} & = J_v^1(T_f) & in\ \Gamma_m \\
\boldsymbol{u}_f \cdot \boldsymbol{t} & = 0 & in\ \Gamma_m \\
\left(\hat{C}_{p,f} T_f \boldsymbol{u}_f - k_f \nabla T_f\right) \cdot \boldsymbol{n} & = J_v^2(T_f) & in\ \Gamma_m \\
(C_f \boldsymbol{u}_f - D \nabla C_f) \cdot \boldsymbol{n} & = 0 & in\ \Gamma_m \\
J_v^1(T_f) & = \frac{\varepsilon}{\tau}\left(\frac{8 r_p}{3\delta}\sqrt{\frac{1}{2\pi R M_w T_f}} + \frac{r_p^2}{8\mu_v(T_f)\delta}\frac{P_m}{RT_f}\right)\left(\left(P^0(T_f) - P_p\right) M_w\right) & \\
J_v^2(T_f) & = J_v^1(T_f)\Delta \hat{H}_{vap}(T_f) + \frac{k_m}{\delta}(T_f - T_p) & \\
\mu_v(T_f) & = a_1 + \dfrac{1}{a_2 + a_3 T_{in} + a_4 T_{in}^2} \quad \text{or} \quad A_1 + A_2 T_{in} + A_3 T_{in}^2 + A_4 T_{in}^3 & \\
P^0(T) & = \exp\left(a_{p0} - \frac{b_{p0}}{T_{fm} + c_{p0}}\right) \text{ or } \quad b_1 + b_2 T_{fm} + b_3 T_{fm}^2 + b_4 T_{fm}^3 & \\
k_m(T_f) & = (1-\varepsilon) k_s(T_f) + \varepsilon k_v(T_f) & \\
\tau & = \frac{1}{\varepsilon} & \\
\Delta H(T) & = a_{hv1} + a_{hv2}(T_{fm} + 273.15) & \\
\frac{k_m}{\delta}(T_{fm} - T_{pm}) & = 0.1\, J_v^2(T) &
\end{cases}
$$

Here, J_v is the vapor flux that goes through the membrane, $\Delta \hat{H}_{vap}$ is the vaporization enthalpy, δ is the membrane thickness, T_p and P_p are the permeate side temperature and pressure respectively, d_p is the pore radius, μ_v is the water vapor viscosity, γ is the activity coefficient of the feed solution P^0 is the vapor pressure of water, ε is the porosity of the membrane, τ is the tortuosity of the pore, MW_i is the molar weight of component i, k_m is the membrane thermal conductivity, k_s is the membrane material conductivity and k_v is the water vapor conductivity.

In the above, $\boldsymbol{u} = (u_x, u_y), p, \theta$ and T represent the fluid velocity, pressure, molar concentration profile and fluid temperature, respectively. The velocity at the inlet is considered to be of the *Berman type* (Berman, 1953) in the sense that for $x = 0$ and for all $y \in [-d/2, d/2]$, we have a minimum salt concentration, maximum temperature at the border and maximum membrane permeability. More precisely, we define $\boldsymbol{u}_{in}$ as:

$$
\begin{aligned}
\boldsymbol{u}_{in} \cdot \boldsymbol{n} &= \left(u_0 - v_w \frac{2x}{d}\right)\left(\frac{3}{2}(1-\lambda^2)\right)\left[1 - \frac{\mathrm{Re}}{420}\left(2 - 7\lambda^2 - 7\lambda^4\right)\right], \\
\boldsymbol{u}_{in} \cdot \boldsymbol{t} &= v_w\left[\frac{\lambda}{2}(3-\lambda^2) - \frac{Re}{280}\lambda(2 - 3\lambda^2 + \lambda^6)\right], \\
&\text{where } Re = \frac{v_w(d/2)}{\mu_f/\rho_f}, v_w = J_v^1(T_{fm})\big|_{x=0} \text{ and } \lambda = 2y/d.
\end{aligned}
$$

The parameters for the simulation are given in the following table(Sharqawy, Lienhard, & Zubair, 2010; Zhang, Peng, Ji, & Wang, 2016; Carro, Mora, & Vellojin, 2022).

Table 6.1: Parameters for the vacuum membrane distillation model

Parameters	Meaning	Values	Units
u_{in}	Inlet mean fluid velocity	0.73	ms^{-1}
k_v	Vapor conductivity	0.026	$Wm^{-1}K^{-1}$
θ_{in}	Inlet mean salt concentration	35	kgm^{-3}
T_{in}	Inlet mean fluid temperature	50	°C
D_f	Salt diffusivity	$1.5 \cdot 10^{-9}$	m^2s^{-1}
τ	Pores tortuosity	2.0	$-$
ρ_f	Fluid density	998.2	$kg\,m^{-3}$
r_p	Mean pore radius	$0.2 \cdot 10^{-6}$	m
$\hat{C}_{p,f}$	Water specific heat	4182	$J\,kg^{-1}K^{-1}$
δ	Membrane thickness	$0.45 \cdot 10^{-3}$	m
ϵ	Membrane porosity	0.5	$-$
R	Gas ideal constant	8.31	$Jmol^{-1}K^{-1}$
k_s	Membrane conductivity	0.256	$Wm^{-1}K^{-1}$
M_w	Water molecular weight	$18 \cdot 10^{-3}$	$kg\,mol^{-1}$
μ_v	Water viscosity	$1.13 \cdot 10^{-5}$	$Pa\,s$
p_p	Permeate pressure	3000	Pa
L	Channel length	0.25	m
k	Water conductivity	0.600	$Wm^{-1}K^{-1}$
k_m	Mean conductivity	0.141	$Wm^{-1}K^{-1}$
d	Channel diameter	$0.7 \cdot 10^{-3}$	m

6.1 Considerations for the further formulation of models

Although the previous models cover with detail the majority of the modelling proposed by the CFD community in the last thirty years, there are always new areas of study that hasn't been covered yet, and also many simplifications that in a close future may vanish and be considered in new problems. For these reasons, the following list contains some of the remaining main ideas that in my judgement are relevant on the creation of new models.

References

Amigo, J., Urtubia, R., & Suárez, F. (2018). Exploring the interactions between hydrodynamics and fouling in membrane distillation systems–a multiscale approach using cfd. *Desalination*, *444*, 63–74.

Beavers, G. S., & Joseph, D. D. (1967). Boundary conditions at a naturally permeable wall. *Journal of fluid mechanics*, *30*(1), 197–207.

Berman, A. S. (1953). Laminar flow in channels with porous walls. *Journal of Applied physics*, *24*(9), 1232–1235.

Bird, L., Stewart. (1960). *Transport phenomena*. John Wiley & Sons.

Carro, N., Mora, D., & Vellojin, J. (2022). A finite element model for concentration polarization and osmotic effects in a membrane channel. *arXiv preprint arXiv:2212.08140*.

El Kadi, K., Janajreh, I., & Hashaikeh, R. (2020). Numerical simulation and evaluation of spacer-filled direct contact membrane distillation module. *Applied Water Science*, *10*(7), 1–17.

Geraldes, V., Semião, V., & De Pinho, M. N. (2001). Flow and mass transfer modelling of nanofiltration. *Journal of membrane science*, *191*(1-2), 109–128.

Incropera, F. P., & DeWitt, D. P. (1999). *Fundamentos de transferencia de calor*. Pearson Educación.

Kleffner, C., Braun, G., & Antonyuk, S. (2019). Influence of memrane intrusion on permeate-sided pressure drop during high-pressure reverse osmosis. *Chemie Ingenieur Technik*, *91*(4), 443–454.

Kucera, J. (2015). *Reverse osmosis: industrial processes and applications*. John Wiley & Sons.

Lewis, E. L., & Perkin, R. (1978). Salinity: Its definition and calculation. *Journal of Geophysical Research: Oceans*, *83*(C1), 466–478.

Lin, W., Lei, J., Wang, Q., Wang, X.-m., & Huang, X. (2022). Performance enhancement of spiral-wound reverse osmosis membrane elements with novel diagonal-flow feed channels. *Desalination*, *523*, 115447.

Lou, J., Vanneste, J., DeCaluwe, S. C., Cath, T. Y., & Tilton, N. (2019). Computational fluid dynamics simulations of polarization phenomena in direct contact membrane distillation. *Journal of Membrane Science*, *591*, 117150.

Luo, J., Li, M., & Heng, Y. (2020). A hybrid modeling approach for optimal design of non-woven membrane channels in brackish water reverse osmosis process with high-throughput computation. *Desalination*, *489*, 114463.

Mangi, S. A., Makhija, A., Raza, M. S., Khahro, S. H., & Jhatial, A. A. (2021). A comprehensive review on effects of seawater on engineering properties of concrete. *Silicon*, 1–8.

Millero, F. J., Feistel, R., Wright, D. G., & McDougall, T. J. (2008). The composition of standard seawater and the definition of the reference-composition salinity scale. *Deep Sea Research Part I: Oceanographic Research Papers*, *55*(1), 50–72.

Nayar, K. G., Sharqawy, M. H., Banchik, L. D., et al. (2016). Thermophysical properties of seawater: A review and new correlations that include pressure dependence. *Desalination*, *390*, 1–24.

Perfilov, V. (2018). Mathematical modelling of membrane separation processes.

Picioreanu, C., Van Loosdrecht, M. C., & Heijnen, J. J. (1998). Mathematical modeling of biofilm structure with a hybrid differential-discrete cellular automaton approach. *Biotechnology and bioengineering*, *58*(1), 101–116.

Picioreanu, C., van Loosdrecht, M. C., & Heijnen, J. J. (1998). A new combined differential-discrete cellular automaton approach for biofilm modeling: Application for growth in gel beads. *Biotechnology and bioengineering*, *57*(6), 718–731.

Picioreanu, C., Van Loosdrecht, M. C., & Heijnen, J. J. (2001). Two-dimensional model of biofilm detachment caused by internal stress from liquid flow. *Biotechnology and bioengineering*, *72*(2), 205–218.

Picioreanu, C., Vrouwenvelder, J., & Van Loosdrecht, M. (2009). Three-dimensional modeling of biofouling and fluid dynamics in feed spacer channels of membrane devices. *Journal of Membrane Science*, *345*(1-2), 340–354.

Radu, A., Bergwerff, L., Van Loosdrecht, M., & Picioreanu, C. (2014). A two-dimensional mechanistic model for scaling in spiral wound membrane systems. *Chemical Engineering Journal*, *241*, 77–91.

Schofield, R. W. (1989). *Membrane distillation*. University of New South Wales Australia.

Sharqawy, M., Lienhard, V., & Zubair, S. (2010). The thermophysical properties of seawater: a review of existing correlations and data accessed thermophysical properties of seawater: a review of existing correlations and data. *Desalin. Water Treat*, *16*, 354–380.

Su, X., Li, W., Palazzolo, A., & Ahmed, S. (2019). Permeate flux increase by colloidal fouling control in a vibration enhanced reverse osmosis membrane desalination system. *Desalination*, *453*, 22–36.

Zhang, Y., Peng, Y., Ji, S., & Wang, S. (2016). Numerical simulation of 3d hollow-fiber vacuum membrane distillation by computational fluid dynamics. *Chemical Engineering Science*, *152*, 172–185.